

# SIMULATION AND PERFORMANCE INVESTIGATION OF Z-SOURCE INVERTER FOR ELECTRIC VEHICLES

## A DISSERTATION

*Submitted in partial fulfillment of the  
requirements for the award of the degree*

*of*

MASTER OF TECHNOLOGY

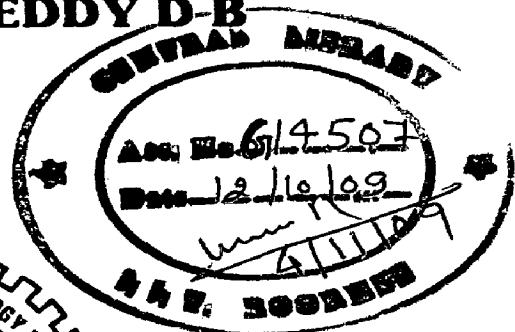
*in*

ELECTRICAL ENGINEERING

(With Specialization in Electric Drives and Power Electronics)

*By*

**PRASHAANTH REDDY D-B**



DEPARTMENT OF ELECTRICAL ENGINEERING  
INDIAN INSTITUTE OF TECHNOLOGY ROORKEE  
ROORKEE - 247 667 (INDIA)

JUNE, 2009

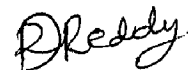
## CANDIDATE'S DECLARATION

I hereby declare that the work that is being presented in this dissertation report entitled "SIMULATION AND PERFORMANCE INVESTIGATION OF Z-SOURCE INVERTER FOR ELECTRIC VEHICLES" submitted in the partial fulfillment of the requirements of the award of the degree of MASTER OF TECHNOLOGY in ELECTRICAL ENGINEERING with specialization in ELECTRIC DRIVES AND POWER ELECTRONICS, submitted in the Department of Electrical Engineering, Indian Institute of Technology, Roorkee, is an authentic record of my own work carried out under the guidance of Dr.S.P.Dubey, Assistant Professor, Department of Electrical Engineering.

The matter embodied in this dissertation report has not been submitted by me for the award of any other degree or diploma.

Date: 30-06-09

Place: Roorkee



(PRASHAANTH REDDY D B)

---

This is to certify that the above statement made by the candidate is correct to the best of my knowledge.



(DR. S.P. DUBEY)  
Assistant Professor,  
Department of Electrical Engineering,  
IIT Roorkee.

## ACKNOWLEDGEMENTS

---

It is my proud privilege to express my sincere thanks to my dissertation supervisor, **Dr S. P. Dubey, Assistant Professor, Department of Electrical Engineering**, for valuable guidance and constant encouragement throughout the duration of the dissertation. And I am very thankful for his encouragement and for giving me the chance to work on DSP Technology and also for his encouragement to do the hardware.

My sincere thanks to **Dr. J. D. Sharma, Professor**, Department of Electrical Engineering, for providing the eZdsp kit throughout the duration of my work.

My sincere thanks to **Dr. A.Pramod Agarwal, Professor**, Department of Electrical Engineering, for providing the ICs and support during the work.

And also my sincere thanks to **Dr.S.P.Gupta, Dr S.P.Srivatsava**, Department of Electrical Engineering, for providing constant support and encouragement during my work.

I am also sincerely grateful to research scholars **Mr Dheeraj P**, Mr Jatin Patel, Lab Assistants Sadiram, Dinesh Mohan, Gautham Singh and my friends Vikash M, Raghavender, Meeravali Shaik, Rahul T, Sai Krishana Reddy, Ch Mohan Krishna, Vadhiraj.

Finally, my heartiest gratitude goes to **my Parents and my Brother**, for their encouragement and support. They have always been a great role model and lead me to greater success in pursuit of higher knowledge. *Finally I am dedicating all my work to my brother.*

# ABSTRACT

---

With the increasing demand for environmentally friendlier and higher fuel economy vehicles, automotive companies are focusing on electric vehicles, hybrid electric vehicles (HEVs), plug-in hybrid electric vehicles (PHEVs), and fuel-cell vehicles. The sources in these vehicles are storage device such as battery or fuel cells. These devices give the DC Voltages. But for the traction drive of Vehicle AC Motors will be used. For this Inverters must be used. The traditional inverters can be used for this purpose. But the devices like battery, fuel cell, photovoltaic cells give less amount of DC Voltages but the AC drive requires higher voltages. But VSI and CSI can't boost the voltages in wide range. So additional stage of DC-DC conversion is required which increases cost and decreases efficiency.

The Z-Source Inverter can Boost the voltages without additional stage, which increase the system efficiency and reduces the cost. The Voltage Boost operation is possible because of the Impedance network present in the Z-Source Inverter. Different controlling methods are given like Boost Control, Constant Boost Control. The SVM technique has to be modified to use for the Z-Source Inverter. Closed loop voltage control is used in this work. Both the Capacitor voltage and AC Voltage, AC output Currents are taken as reference.

The Modified Space Vector Modulation is simulated in closed loop control with various sources like Photo Voltaic Cell, Fuel Cell. The FFT analysis of output voltages and currents is carried out.

Hardware is developed in the laboratory. The control scheme is implemented on TMS320F2812 DSP processor based eZdsp.



## List of Figures

<u>Figure No.</u>	<u>Figure description</u>	<u>Page No.</u>
Fig 2.1	Voltage Source Inverter	7
Fig 2.2	Traditional I-source converter	8
Fig 2.3	VSI fed by additional DC/DC conversion state	10
Fig 2.4	Block diagram of the power schematic	11
Fig 2.5	4-phase bi-directional fly-back converter	11
Fig 2.6	Switching Pulses During Forward Power Flow	11
	Switching Pulses During Reverse Power Flow	11
Fig 2.7	ZSI System configuration	12
Fig 2.8	Bidirectional ZSI	13
Fig 2.9	Z-source inverter for fuel-cell applications	14
Fig 2.10	Equivalent circuit of the Z-source inverter viewed from the dc link	15
Fig 2.11	Equivalent circuit of the Z-source inverter viewed from the dc link when the inverter bridge is in the shoot-through zero state	15
Fig 2.12	Equivalent circuit of the Z-source inverter viewed from the dc link when the inverter bridge is in one of the eight nonshoot-through switching states	15
Fig 2.13	Traditional carrier-based PWM control without shoot-through zero states, where the traditional zero states (vectors) $V_{111}$ and $V_{000}$ are generated determined by the references	15
Fig 2.14	Modified carrier-based PWM control with shoot-through zero states that are evenly distributed among the three phase legs, while the equivalent active vectors are unchanged	17
Fig 3.1	Sketch map of simple control	19
Fig 3.2	Maximum Boost Control	20
Fig 3.3	Maximum Constant Boost Control	21
Fig 3.4	Space vector diagram for the inverter	23
Fig 3.5	Synthesis of $V_{ref}$ by $V_1, V_2$ and $V_0$	26
Fig 3.6	Modified SVPWM implementation. Sector 1	28

Fig 3.7	Modified SVPWM implementation. Sector 2	29
Fig 3.8	Modified SVPWM implementation. Sector 3	29
Fig 3.9	Modified SVPWM implementation. Sector 4	30
Fig 3.10	Modified SVPWM implementation. Sector 5	30
Fig 3.11	Modified SVPWM implementation. Sector 6	31
Fig 4.1	Maximum Boost Control	32
Fig 4.2	Maximum Boost Control Technique Simulation	33
Fig 4.3	DC Voltage, DC Link Voltage, Inductor Current, Inverter output Voltage, Terminal Voltage	33
Fig 4.4	Inverter output Voltage under No Load	34
Fig 4.5	No Load Capacitor Voltages	35
Fig 4.6	DC Voltage, Voltage Stress, Inductor Current, Voltage across Load	35
Fig 4.7	Line Voltages	35
Fig 4.8	Voltage THD 2.0	35
Fig 4.9	Simulink Model of Maximum Boost Control with third Harmonic Injection	36
Fig 4.10	Inverter Output Voltages	36
Fig 4.11	DC Voltage, DC Link Voltage	37
Fig 4.12	Capacitor Voltage	37
Fig 4.13	Closed Loop MSVM Simulink Model	39
Fig 4.14	DC Source Voltage, DC Link Voltage, Inverter output, Load Voltage, Load Current at Steady state	39
Fig 4.15	DC Source Voltage, DC Link Voltage, Inverter output, Load Voltage, Load Current when reference capacitor AC output voltage is changed	40
Fig 4.16	Shoot through Time and Capacitor Voltage	40
Fig 4.17	The FFT analysis of the load voltage THD 1.32	41
Fig 4.18	The FFT analysis of the load current THD 0.46	41
Fig 4.19	Photo Voltaic Cell Model	42
Fig 4.20	Image of Solar Car	42
Fig 4.21	Closed Loop MSVM with Photo Voltaic Cell	43

Fig 4.22	Photovoltaic Cell Output, DC Link Voltage, Inverter Output, Load Voltage, Load Current	43
Fig 4.23	The FFT analysis of the load current THD 0.89	44
Fig 4.24	Shoot Through Time and Capacitor Voltage	44
Fig 4.25	Image of Fuel Cell	45
Fig 4.26	MSVM Simulation of ZSI with Fuel Cell	45
Fig 4.27	Fuel Cell Voltage; DC Link Voltage, Inverter Voltage, Load Line Voltages, Load Currents	45
Fig 5.1	The Z-Source Inverter Developed	48
Fig 5.2	Pulse amplification and isolation Circuit	50
Fig 5.3	Pulse amplification and isolation Circuit	51
Fig 5.4	+12V Power Supply	51
Fig 5.5	+5V Power Supply	52
Fig 5.6	IGBT Switch	53
Fig 5.7	Snubber Circuit	54
Fig 5.8	Snubber Circuit	58
Fig 5.9	Block Diagram of eZdsp F2812	58
Fig 5.10	(a) eZdsp board (b) Parallel port (c) Power supply	59
Fig 5.11	Simulink Tool for Development of Simulink Model	62
Fig 5.12	Simulink Model of Open Loop Control of Z-Source Inverter	62
Fig 5.13	Simulink Model of Open Loop Control of Z-Source Inverter.	63
Fig 5.14	The Pulses Generated	63
Fig 5.15	eZdsp kit	63
Fig 5.16	Pulses Generated (a) and (b)	64
Fig 5.17	Power Circuit	65
Fig 5.18	Impedance Network	65
Fig 5.19	Hardware setup	66

# CONTENTS

---

*CANDIDATE'S DECLARATION*

*ACKNOWLEDGEMENT*

*ABSTRACT*

*LIST OF FIGURES*

<b>1. Introduction</b>	1
1.1. Introduction	1
1.2. Power Converter Technologies In Electric Vehicle Traction Drive	2
1.3. Literature Review	3
<b>2. Z-Source Inverter</b>	7
2.1. Introduction	7
2.2. Traditional inverters VSI and CSI	8
2.2.1 VSI	8
2.2.2CSI	8
2.3. The dc/dc boosted PWM inverter topology	10
2.4. Z-Source Inverter	12
2.5. Conclusion	18
<b>3. Control Methods for Z-Source Inverter</b>	21
3.1. Simple Control	19
3.2. Maximum Boot Control	20
3.3. Maximum Constant Boost control	20
3.4. Space Vector Modulation	21
3.4.1. Switching States of the Inverter	21
3.4.2. Space vectors	22
3.4.3. Synthesis of the reference vector using space vectors	24
3.4.4. Calculation of dwell times	25
3.5. Modified Space Vector Modulation	27
3.6. Conclusion	31
<b>4. Simulation</b>	32
4.1. Introduction.	32
4.2. Maximum Boot Control.	32
4.2.1. No load.	33
4.2.2. With RL Load.	35

4.3. Maximum Boost Control With Third Harmonic Injection.	36
4.4. Modified Space Vector Modulation.	38
4.4.1. MSVM With DC Supply.	39
4.4.2. MSVM With Photo Voltaic Cell.	42
4.4.3. MSVM With Fuel Cell.	45
4.5 Conclusion.	46
<b>5. Hardware and Development.</b>	<b>47</b>
5.1. Power Circuit.	47
5.1.1. Inductor Design.	48
5.1.2. Capacitor Selection.	49
5.2. Pulse Amplification and Isolation Circuit.	49
5.3. Power Supplies.	51
5.4. Snubber Circuit.	53
5.5. Switching Devices.	55
5.5.1. IGBT.	55
5.5.2. Fast Recovery Diode across the IGBT.	55
5.6. Digital Control.	56
5.6.1. Overview of the eZdsp F2812.	56
5.6.2. Key Features of the eZdsp F2812.	57
5.6.3. Functional Overview of the eZdsp F2812.	57
5.6.4. Code Composer Studio.	59
5.6.5. Link for Code Composer Studio.	60
5.7. Conclusion.	66
<b>6. Conclusion and Scope for Future Work.</b>	<b>67</b>
<b><i>REFERENCES</i></b>	<b>68</b>
<b><i>BIBLIOGRAPHY</i></b>	<b>70</b>
<b><i>APPENDIX</i></b>	<b>71</b>

## Introduction and Literature Review

---

### 1.1 Introduction

With the increasing demand for environmentally friendlier and higher fuel economy vehicles, automotive companies are focusing on electric vehicles, hybrid electric vehicles (HEVs), plug-in hybrid electric vehicles (PHEVs), and fuel-cell vehicles. These vehicles would also enable meeting the demands for electrical power due to the increasing use of the electronic features to improve vehicle performance, fuel economy, emissions, passenger comfort, and safety. In electric vehicles, HEVs, PHEVs, and fuel-cell vehicles, the challenges are to achieve high efficiency, ruggedness, small sizes, and low costs in power converters and electric machines, as well as in associated electronics. In particular, in fuel-cell vehicles, a power-conditioning unit such as a dc–dc converter for matching the fuel-cell voltage with the battery pack may also be necessary. In Electric vehicles, a fast-response motor, inverter, and control system are essential and must be able to operate in adverse environmental conditions. Furthermore, the integration of actuators with power electronics not only improves the overall system reliability but also reduces the cost, size, etc. In addition to power electronics, the technology of the electric motor plays a major role in the vehicle's dynamics and the type of power converter for controlling the vehicle operating characteristics.

### 1.2 Power Converter Technologies In Electric Vehicle Traction Drive

There are two types of converter configurations for the traction of the EV.

- 1) Traditional Inverters
- 2) The dc/dc boosted PWM inverter topology

#### **Voltage Source Inverter**

In traditional three-phase voltage-source converter dc voltage source supported by a relatively large capacitor feeds the main converter circuit, a three-phase bridge. The dc voltage source can be a battery, fuel-cell stack, diode rectifier, and/or capacitor. The V-source converter is widely used. It, however, has the following conceptual and theoretical barriers and limitations.

- The ac output voltage is limited below and cannot exceed the dc voltage. Therefore, the V-source inverter is a buck (step-down) inverter for dc-to-ac power conversion.
- The upper and lower devices of each phase leg cannot be gated on simultaneously either by purpose or by EMI noise.

### **Current Source Inverter**

The traditional three-phase current-source converter structure. A dc current source feeds the main converter circuit, a three-phase bridge. the I-source converter has the following conceptual and theoretical barriers and limitations [1]

- The ac output voltage has to be greater than the original dc voltage that feeds the dc inductor or the dc voltage produced is always smaller than the ac input voltage. Therefore, the I-source inverter is a boost inverter for dc-to-ac power conversion
- At least one of the upper devices and one of the lower devices have to be gated on and maintained on at any time. Otherwise, an open circuit of the dc inductor would occur and destroy the devices.

Both the V-source converter and the I-source converter have the following common problems[1].

- They are either a boost or a buck converter and cannot be a buck–boost converter. That is, their obtainable output voltage range is limited to either greater or smaller than the input voltage.
- They are vulnerable to EMI noise in terms of reliability.

### **Z-Source Inverter**

The Z-source inverter is one of quite new ideas designated to renewable energy system, mainly fuel cell and photovoltaics. To the-same-as VSI switches topology a special Z-network is introduced and shoot-through states may be used in similar manner as in Current Source Inverter[1].

ZSI employs a unique impedance network (or circuit) to couple the converter main circuit to the power source, load, or another converter, for providing unique features that cannot be observed in the traditional V- and I-source converters where a capacitor and inductor are used respectively. The Z-source converter overcomes the above-mentioned conceptual and

theoretical barriers and limitations of the traditional V-source converter and I-source converter and provides a novel power conversion concept.

**The Z-source inverter has following features[1]:**

1. It is able to boost output voltage to higher than the input voltage or buck the voltage, it is very suitable for motor drive application.
2. It is able to handle shoot through state, thus increases the system reliability.
3. It can reduce the output harmonic compared to traditional inverter because the elimination of dead time.

### **1.3 Literature Review**

In the year 2002 Fang. Z. Peng proposed “Z-source inverter” this paper gives the basic idea about the Z-Source inverter. This paper focused on an example—a Z-source inverter for fuel-cell applications. Through the example, the paper described the operating principle, analyzed the circuit characteristics, and demonstrated its concept and superiority. Analytical, simulation, and experimental results have been presented. The Z-source inverter can boost–buck voltage, minimize component count, increase efficiency, and reduce cost.

In 2004 Fang. Z. Peng proposed a new control technique in the paper , “Maximum boost control of the Z-source inverter ”.This paper discusses about the advantages of the Maximum boost control Over the simple control technique. In this technique this control method maintains the six active states unchanged and turns all zero states into shoot-through zero states. Thus maximum gain is obtained for any given modulation index without distorting the output waveform

In the year 2004 Miaosen Shen, Alan Joseph, Jin Wang, Fang Z. Peng, and Donald J. Adams in the paper “Comparison of traditional inverter and Z-Source inverter for fuel cell vehicles” the ZSI is compared with the traditional inverters and the advantages of Z-Source inverter are discussed in detail in many aspects such as switching device power.



In 2004 Fang. Z. Peng, Miaosen Shen, and Zhaoming Qian proposed another control method in their paper “Maximum Constant Boost Control of Z-Source Inverter”. The paper presented two control methods to obtain maximum voltage gain of the Z-source inverter. The methods maximize the shoot through period without affecting the active states by turning all zero states into the shoot through zero state, thus maximum output voltage can be obtained for a given modulation index. In turn, maximum modulation index can be used to obtain any desired output voltage, thus, minimizing the voltage stress across the switches.

In 2004 Fang. Z. Peng, in the paper “Z-source inverter for adjustable speed drives” This paper presents a Z- Source inverter system and control for general-purpose motor drives. Paper explained how Z -source inverter system provides ride-through capability under voltage sags, reduces line harmonics, improves power factor and reliability, and extends output voltage range.

In 2004 M.Shen, J.Wang, F.Z.Peng, L.M.Tolbert, and D.J.Adams, “Comparison of Traditional Inverters and Z-Source Inverter for Fuel Cell Vehicles” three different inverters: traditional PWM inverter, dc/dc boosted PWM inverter, and Zsource inverter for fuel cell vehicles were investigated. Total switching device power of each of these inverters was calculated. For purposes of comparison and shown the superiority of ZSI.

In 2006 Miaosen Shen, Alan Joseph, Yi Huang, Fang Z. Peng, Zhaoming Qian ”Design and Development of a 50kW Z-Source Inverter for Fuel Cell Vehicles”. A detailed design process of the Z-source inverter is presented in this paper. A dc rail clamp circuit is used to reduce the overshoot of the device during turn off. Experimental results confirmed the design process and demonstrated the high efficiency characteristic of the Z-source inverter.

In 2007 Xinping Ding, Zhaoming Qian, Shuitao Yang, Bin Cuil, Fangzheng Peng in paper “A High-Performance Z-Source Inverter Operating with Small Inductor at Wide-Range Load” presented a high-performance Z-source inverter, which can overcome limitations of traditional Z-source inverter. The proposed Z-source inverter can operate at wide range load (even no-load) with small inductor, eliminate the possibility of the dc-link voltage drops, and simplify the inductor and controller design.

In 2004 Poh Chiang Loh, D. Mahinda Vilathgamuwa, Yue Sen Lai, Geok Tin Chua and Yunwei Li “In the paper Pulse-Width Modulation of Z-Source Inverters” presented a detailed analysis, showing how various conventional pulse-width modulation strategies can be modified to switch a voltage-type Z-Source inverter either continuously or discontinuously, while retaining all the unique harmonic performance features of these conventional modulation strategies.

In 2005 Tran-Quang Vinh, Tae-Won Chun, Jung-Ryol Ahn, and Hong-Hee Lee “Algorithms for Controlling Both the DC Boost and AC Output Voltage of the Z-Source Inverter” the peak dc-link voltage direct sensing & scaling method, and modified modulation strategy have been described, which simplifies the controller design, improves the transient response and decrease the voltage stress across the switches.

In 2007 Xinping Ding , Zhaoming Qian , Shuitao Yang , Bin Cuil, Fangzheng Peng in paper “A PID Control Strategy for DC-link Boost Voltage in Z-source Inverter ” This paper presents a PID controller for dc-link boost voltage in Z-source inverter. With this technique a constant capacitor voltage can be achieved with an excellent transient performance which enhances the rejection of disturbance, including the input voltage ripple and load current variation, and have good ride-through for voltage-sags.

In 2007 Xinping Ding , Zhaoming Qian , Shuitao Yang , Bin Cuil, Fangzheng Peng in paper “A Direct Peak DC-link Boost Voltage Control Strategy in Z-Source Inverter” a PID controller for direct peak dc-link boost voltage in Z-source inverter has been introduced. With this technique a high-performance inverter output voltage can be achieved with an excellent transient performance which enhances the rejection of disturbance, including the input voltage ripple and load current variation.

## **Organization of the dissertation**

**Chapter 1:** Gives the Introduction about z-Source Inverter. It provides the literature review.

**Chapter 2:** The Z-Source is compared with traditional inverters and detailed analysis of Z-Source inverter and its working principles explained.

**Chapter 3:** Various control methods of Z-Source inverter explained and Modified Space Vector Modulation for Z-Source Inverter is explained in detail.

**Chapter 4:** Simulation of Maximum Boost control of Z-Source inverter is done under no load and RL Load. Closed Loop Voltage Control along with Modified Space Vector Modulation is presented with DC Supply, Photovoltaic Cell, Fuel Cell as sources. The FFT analysis is carried out.

**Chapter 5:** Various stages of hardware development explained and Digital implementation of control scheme is presented

### 2.1 Introduction

There are two types of converter configurations for the traction of the EV.

- 1) Traditional Inverters
- 2) The dc/dc boosted PWM inverter topology

### 2.2 Traditional inverters VSI and CSI

There exist two traditional converters: voltage-source (or voltage-fed) and current-source (or current-fed) converters (or inverters depending on power flow directions).

#### 2.2.1 VSI

Fig. 2.1 shows the traditional three-phase voltage-source converter (abbreviated as V-source converter) structure.

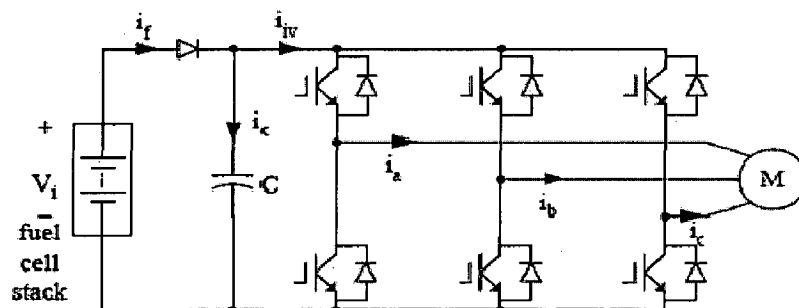


**Fig .2.1. Voltage Source Inverter**

A dc voltage source supported by a relatively large capacitor feeds the main converter circuit, a three-phase bridge. The dc voltage source can be a battery, fuel-cell stack, diode rectifier, and/or capacitor. Six switches are used in the main circuit; each is traditionally composed of a power transistor and an anti parallel (or freewheeling) diode to provide bidirectional current flow and unidirectional voltage blocking capability. The V-source converter is widely used. It, however, has the following conceptual and theoretical barriers and limitations [1]

The VSI however, has the following conceptual and theoretical barriers and limitations [1]

- The ac output voltage is limited below and cannot exceed the dc-link voltage or the dc-link voltage has to be greater than the ac input voltage. Therefore, the V-source inverter is a buck (step-down) inverter for dc-to-ac power conversion and the V-source converter is a boost (step-up) rectifier (or boost converter) for ac-to-dc power conversion. For applications where over drive is desirable and the available dc voltage is limited, an additional dc-dc boost converter is needed to obtain a desired ac output. The additional power converter stage increases system cost and lowers efficiency.
- The upper and lower devices of each phase leg cannot be gated on simultaneously either by purpose or by EMI noise. Otherwise, a shoot-through would occur and destroy the devices. The shoot-through problem by electromagnetic interference (EMI) noise's misgating-on is a major killer to the converter's reliability. Dead time to block both upper and lower devices has to be provided in the V-source converter, which causes waveform distortion, etc.
- An output *LC* filter is needed for providing a sinusoidal voltage compared with the current-source inverter, which causes additional power loss and control complexity.

## CONCLUSION

In Electric Vehicles, the battery voltage changes in a wide range for different state of charge, the voltage variation could be as large as 50% depends on the battery type. With this voltage range, the traditional PWM inverter has to be oversized to handle full voltage and twice the current at 50% of the battery voltage to output full power. Thus increases the cost of the inverter [1].

### 2.2.2 CSI

Fig. 2.2 shows the traditional three-phase current-source converter structure. A dc current source feeds the main converter circuit, a three-phase bridge

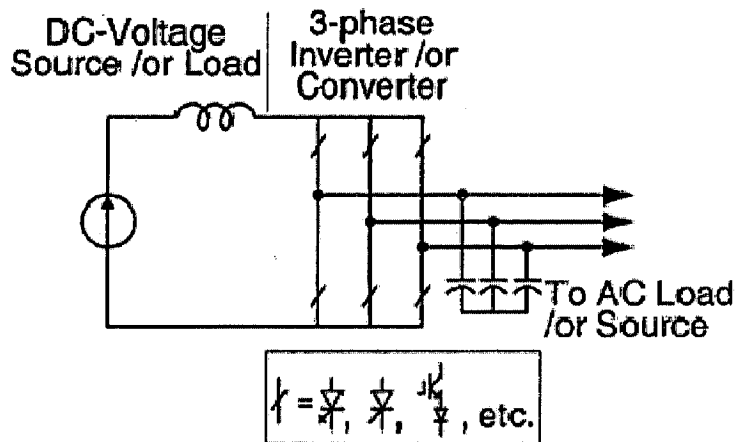


**Fig. 2.2. Traditional I-source converter.**

The dc current source can be a relatively large dc inductor fed by a voltage source such as a battery, fuel-cell stack, diode rectifier, or thyristor converter. Six switches are used in the main circuit, each is traditionally composed of a semiconductor switching device with reverse block capability such as a gate-turn-off thyristor (GTO) and SCR or a power transistor with a series diode to provide unidirectional current flow and bidirectional voltage blocking [1].

However, the I-source converter has the following conceptual and theoretical barriers and limitations [1]

- The ac output voltage has to be greater than the original dc voltage that feeds the dc inductor or the dc voltage produced is always smaller than the ac input voltage. Therefore, the I-source inverter is a boost inverter for dc-to-ac power conversion and the I-source converter is a buck rectifier (or buck converter) for ac-to-dc power conversion. For applications where a wide voltage range is desirable, an additional dc-dc buck (or boost) converter is needed. The additional power conversion stage increases system cost and lowers efficiency.
- At least one of the upper devices and one of the lower devices have to be gated on and maintained on at any time. Otherwise, an open circuit of the dc inductor would occur and destroy the devices. The open-circuit problem by EMI noise's misgating-off is a major concern of the converter's reliability. Overlap time for safe current commutation is needed in the I-source converter, which also causes waveform distortion, etc.

- The main switches of the I-source converter have to block reverse voltage that requires a series diode to be used in combination with high-speed and high-performance transistors such as insulated gate bipolar transistors (IGBTs). This prevents the direct use of low-cost and high-performance IGBT modules and intelligent power modules (IPMs).

## CONCLUSION

In addition, both the V-source converter and the I-source converter have the following common problems[1].

- They are either a boost or a buck converter and cannot be a buck–boost converter. That is, their obtainable output voltage range is limited to either greater or smaller than the input voltage.
- Their main circuits cannot be interchangeable. In other words, neither the V-source converter main circuit can be used for the I-source converter, nor vice versa.
- They are vulnerable to EMI noise in terms of reliability.

### 2.3 The dc/dc boosted PWM inverter topology

Anyway, energy from source or storage must be converted by power electronics equipment. Usually they electrical characteristic is represented by DC voltage source, therefore review of applications shows that Voltage Source Inverter (VSI) is most popular topology. In result, power electronics interface based on VSI, which is step-down converter, is usually supported by another conversion stage.

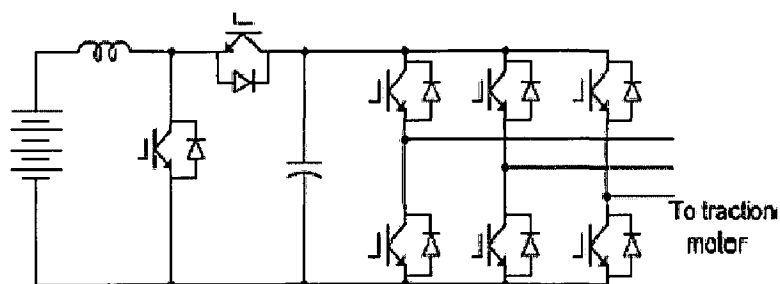


Fig.2.3. VSI fed by additional DC/DC conversion state

The basic block diagram of the prototype of the Multi Power Port (MPP) which is built for the hybrid-electric vehicle application is shown in Fig. 2.4. The heart of the circuit is the bidirectional fly-back DC-DC converter. A four phase converter is constructed. The power schematic of the bi-

directional DC/DC converter is shown in Fig. 2.5. It has got four identical bidirectional fly-back DC-DC converters. Each converter has got an individual battery and all the converters are connected to the common DC bus. If we consider the first converter then during the forward power flow S1 and D2 are active and during reverse power flow S2 and D1 are active. During forward power flow the active switches S1, S3, S5 and S7 get switching pulses of 75% duty cycle with 90 degree phase difference between subsequent phases as shown in figure 2.6(a). During reverse power flow the active switches S2, S4, S6 and S8 get switching pulses of 25% duty cycle which are 90 degree phase shifted to each other as shown in figure 2.6(b). So when the traction motor is operated in the motoring mode then the power is transferred from the battery and the converter works in the forward mode. During regenerative braking or battery charging from mains, the converter operates in the reverse mode and charges the battery.

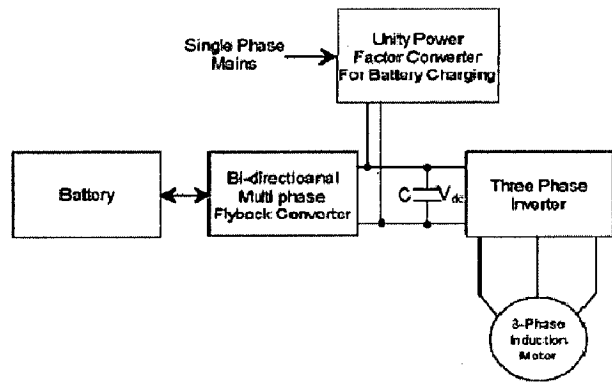


Fig. 2.4. Block diagram of the power schematic

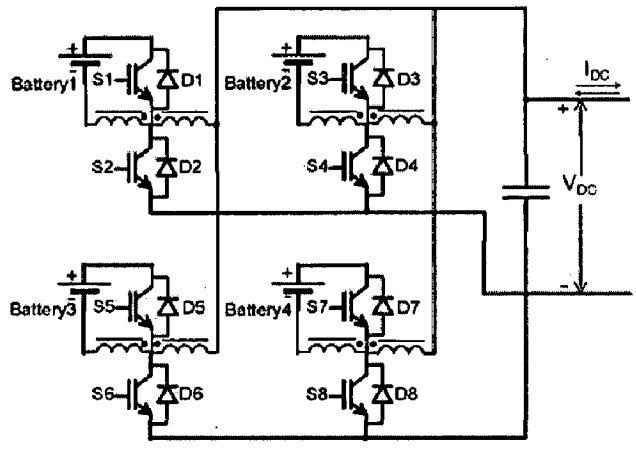
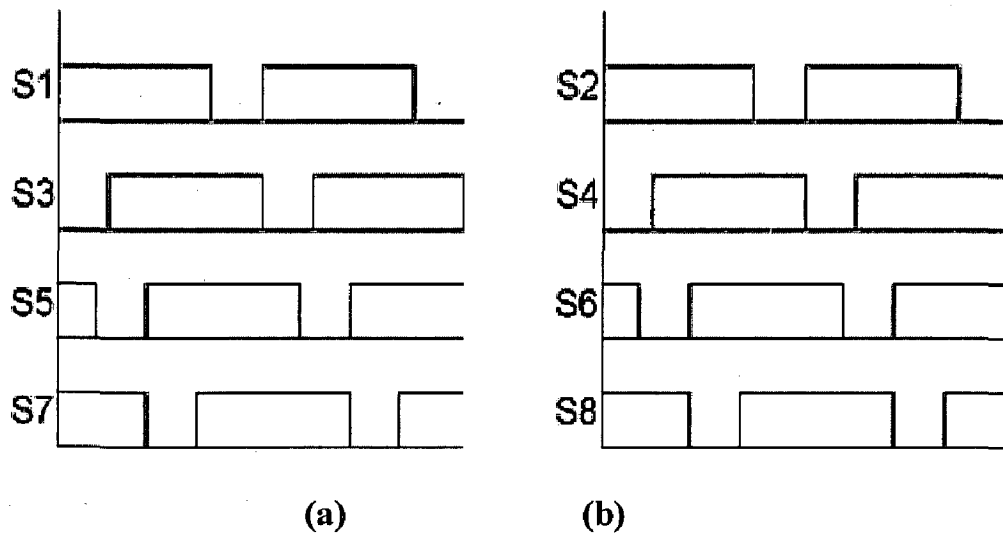


Fig. 2.5. 4-phase bi-directional fly-back converter





**Fig. 2.6. (a) Switching pulses during forward power flow (b) Switching pulses During reverse power flow**

### Conclusion

Because of the wide voltage range and limited voltage level of fuel cell stack/battery, the conventional PWM inverter topology imposes high stresses to the switching devices and motor, and limits the motor's constant power speed ratio. The dc/dc boosted PWM inverter topology can alleviate the stresses and limitations, however, suffers problems such as high cost and complexity associated with the two-stage power conversion

### 2.4 Z-Source Inverter

The Z-source inverter is one of quite new ideas designated to renewable energy system, mainly fuel cell and photovoltaic's. To the same as VSI switches topology a special Z-network is introduced and shoot-through states may be used in similar manner as in Current Source Inverter.

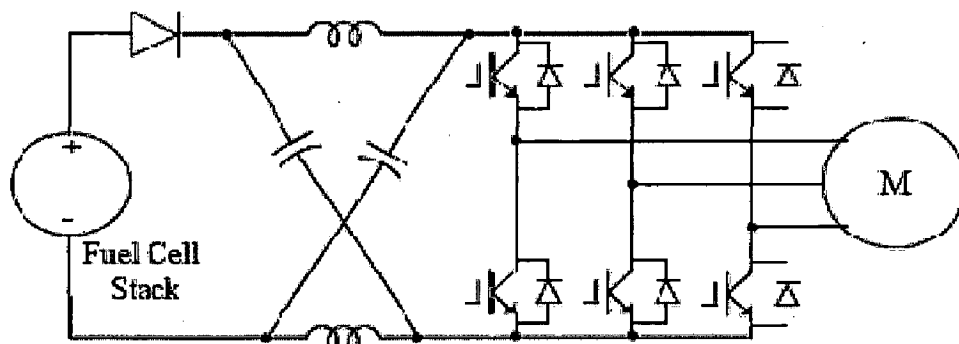


**Fig. 2.7. ZSI System configuration**

But the basic topology of Z-Source inverter [1] as shown in Fig 2.7 is useless because of only one direction of energy transfer from DC to AC side. Obviously three-phase bridge is able to change energy (current) direction but limitation is caused by input diode  $D_0$ , which plays very important role in DC voltage boost operation. While diode cannot be removed, only method to change Z-source inverter into bidirectional system is addition of anti-parallel transistor see Fig.2.8..

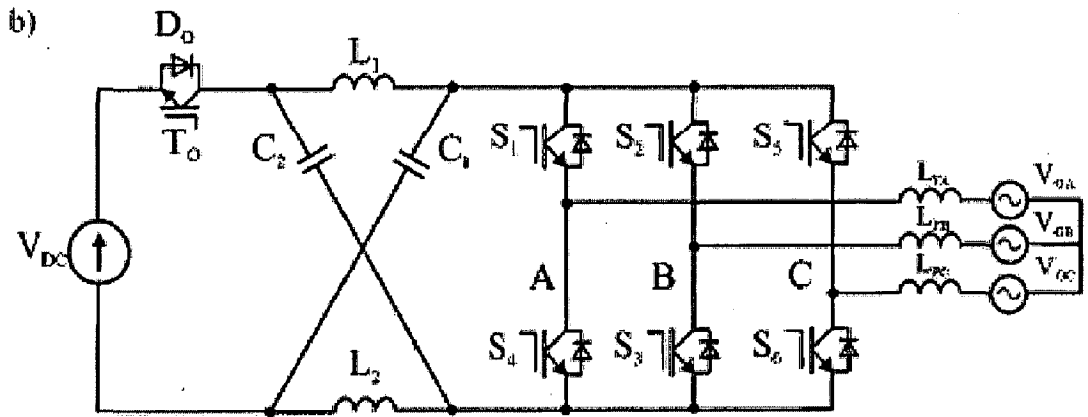


**Fig.2.8. Bidirectional ZSI.**

ZSI employs a unique impedance network (or circuit) to couple the converter main circuit to the power source, load, or another converter, for providing unique features that cannot be observed in the traditional V- and I-source converters where a capacitor and inductor are used respectively. The Z-source converter overcomes the above-mentioned conceptual and theoretical barriers and limitations of the traditional V-source converter and I-source converter and provides a novel power conversion concept.

In Fig.2.8 a two-port network that consists of a split-inductor  $L_1$  and  $L_2$  and capacitors  $C_1$  and  $C_2$  connected in X shape is employed to provide an impedance source (Z-source) coupling the converter (or inverter) to the dc source, load, or another converter. The dc source/or load can be either a voltage or a current source/or load. Therefore, the dc source can be a battery, diode rectifier, thyristor converter, fuel cell, an inductor, a capacitor, or a combination of those. Switches used in the converter can be a combination of switching devices and diodes such as the antiparallel combination as shown in Fig.2.7. The inductance  $L_1$  and  $L_2$  can be provided through a split inductor or two separate inductors.

The Z-source concept can be applied to all dc-to-ac, ac-to-dc, ac-to-ac, and dc-to-dc power conversion. To describe the operating principle and control, this paper focuses on an application example of the Z-source converter: a Z-source inverter for dc-ac power conversion needed for fuel-cell applications. Fig.2.8 shows a Z-source inverter for fuel-cell applications. The diode in series with the fuel cell in Figures is usually needed for preventing reverse current flow.

### Operation, And Control [1]

The unique feature of the Z-source inverter is that the output ac voltage can be any value between zero and infinity regardless of the fuel-cell/battery voltage. That is, the Z-source inverter is a buck–boost inverter that has a wide range of obtainable voltage. The traditional V- and I-source inverters cannot provide such feature.

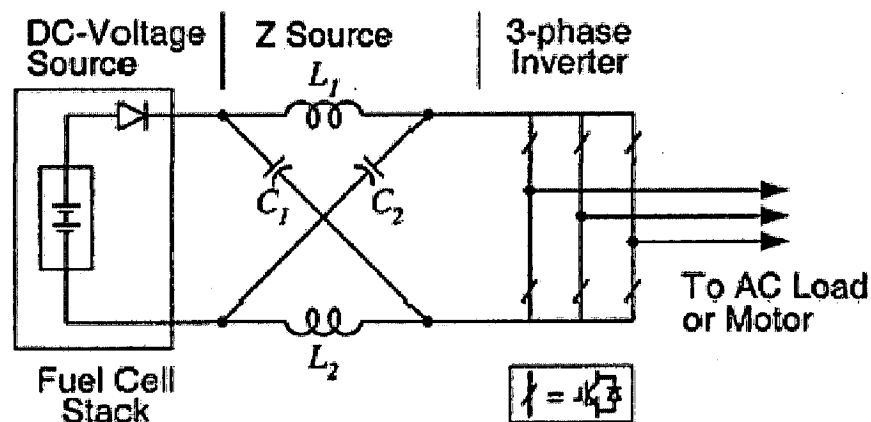


Fig .2.9 Z-source inverter for fuel-cell applications.

To describe the operating principle and control of the Z-source inverter in Fig. 2.8, let us briefly examine the Z-source inverter structure. In Fig. 2.8, the three-phase Z-source inverter bridge has nine permissible switching states (vectors) unlike the traditional three-phase V-source inverter that has eight. The traditional three-phase V-source inverter has six active vectors when the dc voltage is impressed across the load and two zero vectors when the load terminals are shorted through either the lower or upper three devices, respectively.

However, the three-phase Z-source inverter bridge has one extra zero state(or vector) when the load terminals are shorted through both the upper and lower devices of any one phase

leg (i.e., both devices are gated on), any two phase legs, or all three phase legs. This shoot-through zero state (or vector) is forbidden in the traditional V-source inverter, because it would cause a shoot-through. We call this third zero state (vector) the shoot-through zero state (or vector), which can be generated by seven different ways: shoot-through via any one phase leg, combinations of any two phase legs, and all three phase legs. The Z-source network makes the shoot-through zero state possible. This shoot-through zero state provides the unique buck-boost feature to the inverter.

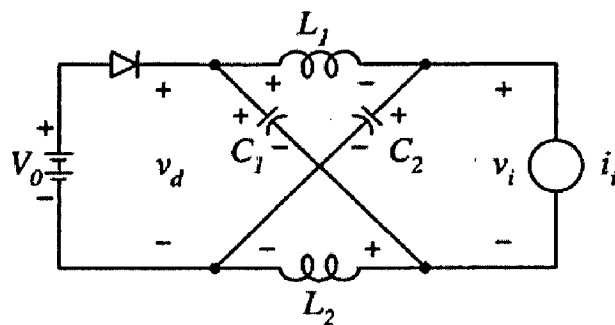


Fig. 2.10. Equivalent circuit of the Z-source inverter viewed from the dc link.

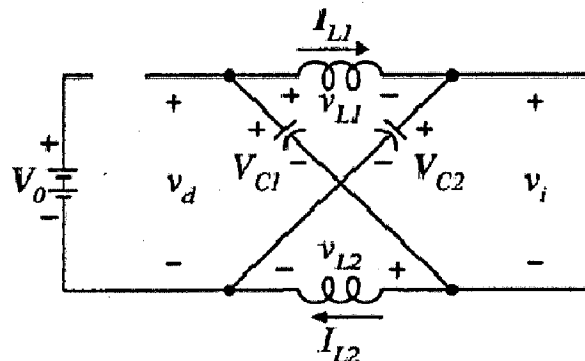


Fig. 2.11. Equivalent circuit of the Z-source inverter viewed from the dc link when the inverter bridge is in the shoot-through zero state.

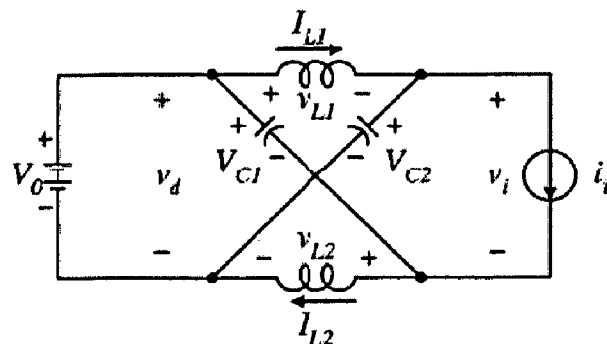
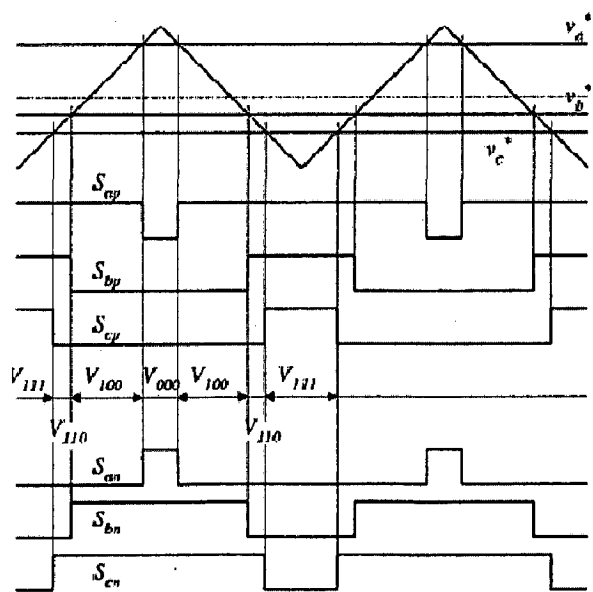


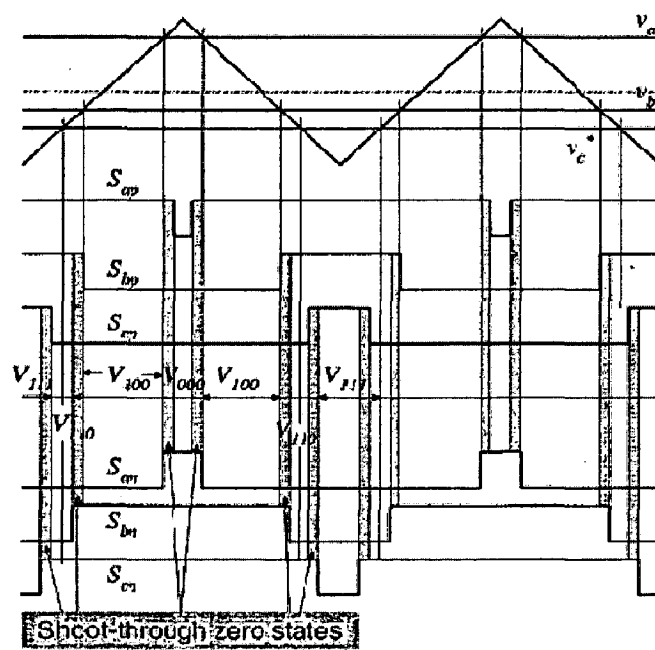
Fig. 2.12. Equivalent circuit of the Z-source inverter viewed from the dc link when the inverter bridge is in one of the eight nonshoot-through switching states

Fig. 2.10 shows the equivalent circuit of the Z-source inverter shown in Fig.2.8 when viewed from the dc link. The inverter bridge is equivalent to a short circuit when the inverter bridge is in the shoot-through zero state, as shown in Fig. 2.11, whereas the inverter bridge becomes an equivalent current source as shown in Fig. 2.12 when in one of the six active states. Note that the inverter bridge can be also represented by a current source with zero value (i.e., an open circuit) when it is in one of the two traditional zero states. Therefore, Fig. 2.12 shows the equivalent circuit of the Z-source inverter viewed from the dc link when the inverter bridge is in one of the eight non shoot-through switching states.

All the traditional pulse width-modulation (PWM) schemes can be used to control the Z-source inverter and their theoretical input–output relationships still hold. In every switching cycle, the two non shoot-through zero states are used along with two adjacent active states to synthesize the desired voltage. When the dc voltage is high enough to generate the desired ac voltage, the traditional PWM of Fig. 2.13 is used. While the dc voltage is not enough to directly generate a desired output voltage, a modified PWM with shoot-through zero states will be used as shown in Fig. 2.14 to boost voltage.



**Fig. 2.13. Traditional carrier-based PWM control without shoot-through zero states, where the traditional zero states (vectors)  $V_{111}$  and  $V_{000}$  are generated every switching cycle and determined by the references.**



**Fig. 2.14. Modified carrier-based PWM control with shoot-through zero states that are evenly distributed among the three phase legs, while the equivalent active vectors are unchanged.**

It should be noted that each phase leg still switches on and off once per switching cycle. Without change the total zero-state time interval, shoot-through zero states are evenly allocated into each phase. That is, the active states are unchanged. However, the equivalent dc-link voltage to the inverter is boosted because of the shoot-through states. The detailed relationship will be analyzed in the next section. It is noticeable here that the equivalent switching frequency viewed from the Z-source network is six times the switching frequency of the main inverter, which greatly reduces the required inductance of the Z-source network.

With the Z-Source inverter, there are two control freedoms: modulation index and shoot through duty ratio. The configuration in Fig.2.8 introduces another control freedom: the shift of the PWM reference signals. In both cases, one is able to control the fuel cell, traction motor, and the state of charge of the battery without using any extra dc/dc converters

**The Z-source inverter has following features:**

1. It is able to boost output voltage to higher than the input voltage or buck the voltage, it is very suitable for motor drive application.

2. It is able to handle shoot through state, thus increases the system reliability.
3. It can reduce the output harmonic compared to traditional inverter because the elimination of dead time.

## **2.5 CONCLUSION**

In Electric Vehicles , the battery voltage changes in a wide range for different state of charge, the voltage variation could be as large as 50% depends on the battery type. With this voltage range, the traditional PWM inverter has to be oversized to handle full voltage and twice the current at 50% of the battery voltage to output full power. Thus increases the cost of the inverter. The dc/dc boosted PWM inverter can minimize the stress of the inverter with an extra dc/dc stage, thus increases the system cost, complexity, and reduces the reliability.

But ZSI is able to boost output voltage to higher than the input voltage or buck the voltage, thus it is very suitable for motor drive application. It increases the system reliability because of its ability to handle shoot through states and it can reduce the output harmonic compared to traditional inverter because the elimination of dead time.

## Control Methods for Z-Source Inverter

Compared with a traditional voltage source inverter, the Z-source inverter has an extra switching state: shoot-through. During the shoot-through state, the output voltage to the load terminals is zero, the same as traditional zero states. Therefore, to maintain sinusoidal output voltage, the active-state duty ratio has to be maintained and some or all of the zero states turned into shoot-through state

Several control methods have been proposed: simple control [1], maximum boost control [7], and maximum constant boost control [11].

### 3.1 Simple Control

The simple control [1] uses two straight lines to control the shoot-through states, as shown in Fig. 3.1. When the triangular waveform is greater than the upper envelope,  $V_p$ , or lower than the bottom envelope,  $V_n$ , the circuit turns into shoot-through state. Otherwise it operates just as traditional carrier-based PWM. This method is very straightforward; however, the resulting voltage stress across the device is relatively high because some traditional zero states are not utilized.

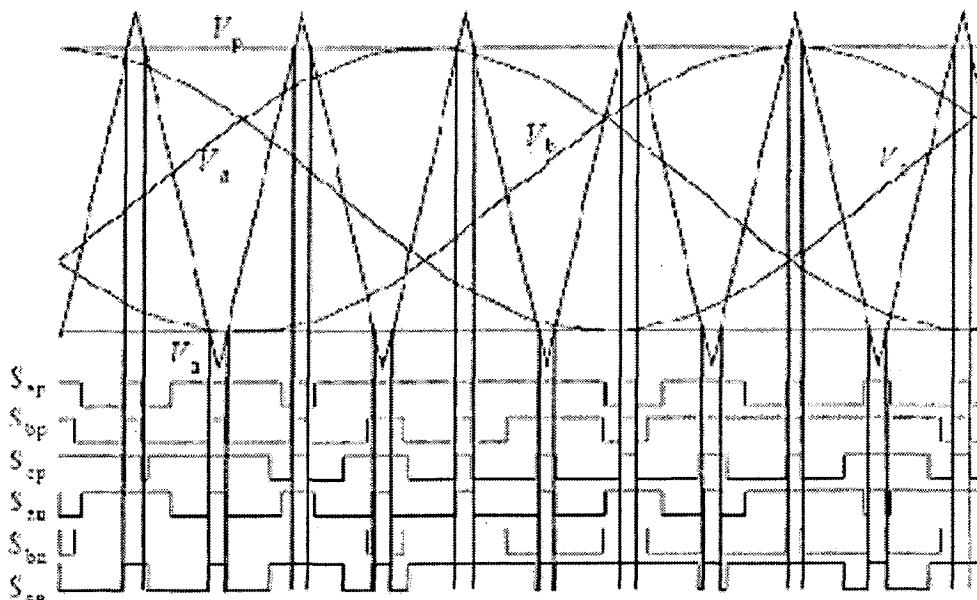


Fig. 3.1. Sketch map of simple control



### 3.2 Maximum Boost Control

To fully utilize the zero states so as to minimize the voltage stress across the device, maximum boost control [7] turns all traditional zero states into shoot-through state, as shown in Fig. 3.2.

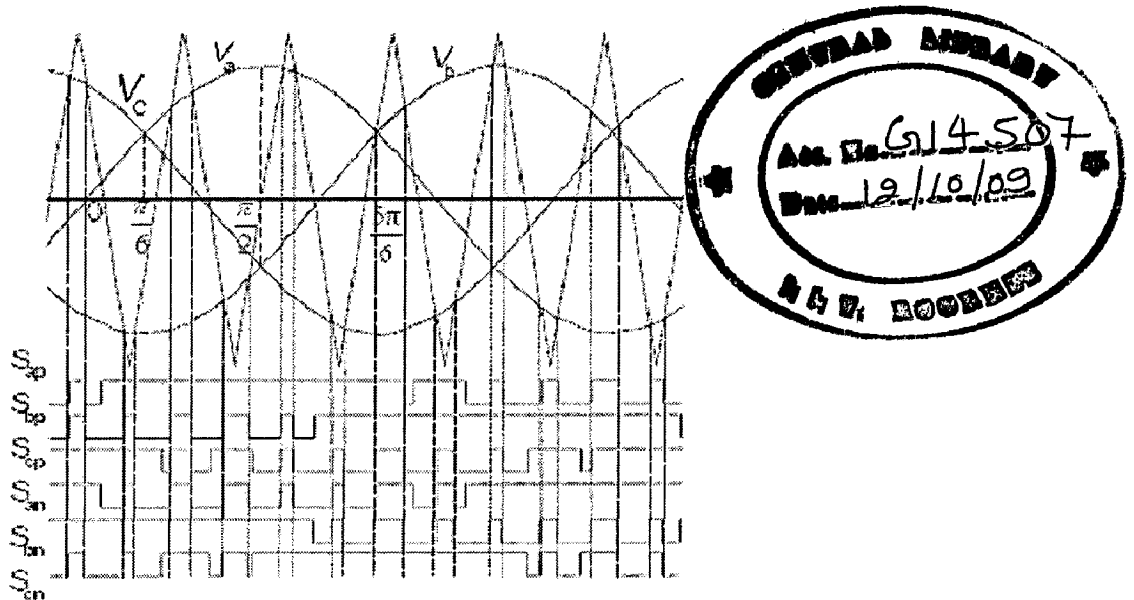
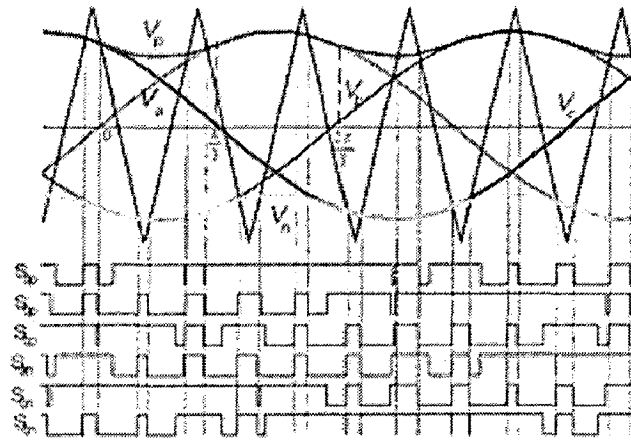


Fig.3.2 Maximum Boost Control

Indeed, turning all zero states into shoot-through state can minimize the voltage stress; however, doing so also causes a shoot-through duty ratio varying in a line cycle, which causes inductor current ripple. This will require high inductance for low-frequency or variable-frequency applications.

### 3.3 Maximum Constant Boost Control

The sketch map of maximum constant boost control [11] is shown in Fig. 3.3. This method achieves maximum boost while keeping the shoot-through duty ratio always constant; thus it results in no line frequency current ripple through the inductors with the maximum constant boost control with third harmonic injection method, the inverter can buck and boost the voltage from zero to any desired value smoothly within the limit of the device voltage.



**Fig.3.3 maximum Constant Boost Control**

### 3.4. Space vector modulation

Space vector modulation (SVPWM) is one of the preferred real-time modulation techniques and is widely used for the digital control of Voltage source inverters. It is an advanced, computation intensive PWM and possibly the best among all the PWM techniques for variable frequency drive applications.

#### 3.4.1. Switching states of the inverter:

Switching states represent the operating status of switches in the two-level inverter. State 'P' denotes that upper switch in an inverter leg is ON, where as 'O' denotes that the lower switch is ON. With 'P' the inverter terminal voltage is  $+V_{dc}$ , where as with 'O' it is 0.

The definition of switching states for the three legs of the inverter as follows:

Switching State	Leg A			Leg B			Leg C		
	S1	S4	$V_{AN}$	S3	S6	$V_{BN}$	S5	S2	$V_{CN}$
P	On	Off	Vd	On	Off	Vd	On	Off	Vd
0	Off	On	0	Off	On	0	Off	On	0

**Table – 3.1**

There are eight possible combinations of switching states in two level inverter. They are listed in the table 2.2. The switching state (POO), for example corresponds to the conduction of  $S_1$ ,  $S_6$  and  $S_2$  in the inverter legs A,B and C respectively. Among the eight switching states, (PPP)

Space Vector	Switching State (Three Phases)	On-State Switch	Vector Definition	
Zero Vector $\vec{V}_0$	[ P P P ]	$S_1, S_3, S_5$	$V_0 = 0$	
	[ O O O ]	$S_2, S_4, S_6$		
Active Vector $\vec{V}_1$	[ P O O ]	$S_1, S_6, S_2$	$\vec{V}_1 = \frac{2}{3} V_d e^{j0}$	
	$\vec{V}_2$	[ P P O ]	$S_1, S_3, S_2$	$\vec{V}_2 = \frac{2}{3} V_d e^{j\frac{\pi}{3}}$
	$\vec{V}_3$	[ O P O ]	$S_4, S_3, S_2$	$\vec{V}_3 = \frac{2}{3} V_d e^{j\frac{2\pi}{3}}$
	$\vec{V}_4$	[ O P P ]	$S_4, S_3, S_5$	$\vec{V}_4 = \frac{2}{3} V_d e^{j\frac{3\pi}{3}}$
	$\vec{V}_5$	[ O O P ]	$S_4, S_6, S_5$	$\vec{V}_5 = \frac{2}{3} V_d e^{j\frac{4\pi}{3}}$
	$\vec{V}_6$	[ O O P ]	$S_4, S_6, S_5$	$\vec{V}_6 = \frac{2}{3} V_d e^{j\frac{5\pi}{3}}$

Table – 3.2

### 3.4.2. Space vectors:

Each switching state in the inverter corresponds to a space vector. A typical space vector diagram for a two-level inverter is shown below, where the six active vectors  $V_1$  to  $V_6$  form a regular hexagon with six equal sectors ( I to VI) and the zero vectors  $V_0, V_7$  lying on the centre of the hexagon.

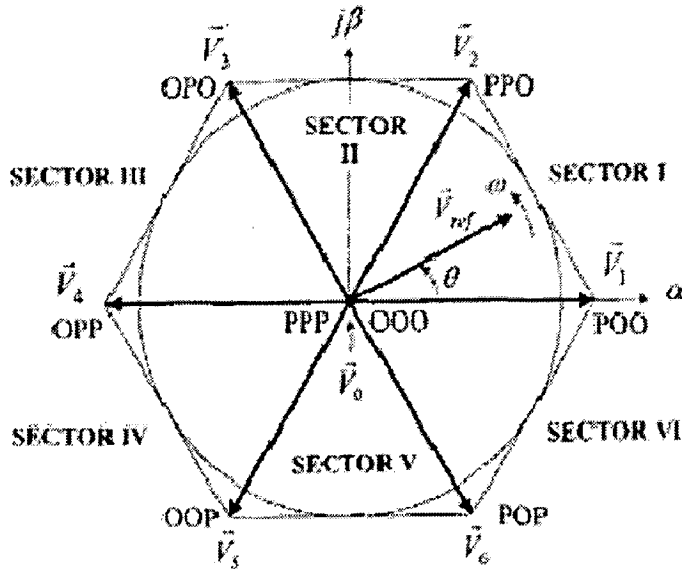


**Fig 3.4 Space vector diagram for the inverter**

The relationship between the switching states and space vectors as shown in the table 3.2 can be obtained as follows:

Assuming the operation of the inverter to be three-phase balanced, we have,

$$V_{AO}(t) + V_{BO}(t) + V_{CO}(t) = 0 \quad \dots\dots\dots (3.1)$$

Where,  $V_{AO}$ ,  $V_{BO}$ ,  $V_{CO}$  are the instantaneous load phase voltages.

It is possible to transform the balanced three-phase variables to the equivalent two-phase variables using the following relation [11]:

$$\begin{bmatrix} v_{\alpha}(t) \\ v_{\beta}(t) \end{bmatrix} = \frac{2}{3} \begin{bmatrix} 1 & \frac{1}{2} & \frac{1}{2} \\ 0 & \frac{\sqrt{3}}{2} & -\frac{\sqrt{3}}{2} \end{bmatrix} \begin{bmatrix} v_{ao}(t) \\ v_{bo}(t) \\ v_{co}(t) \end{bmatrix} \quad \dots\dots\dots (3.2)$$

A space vector can be generally expressed in the  $\alpha$ - $\beta$  plane using the two phase voltages obtained by the relation above as,

$$\vec{V}(t) = V_{\alpha}(t) + jV_{\beta}(t) \quad \dots\dots\dots (3.3)$$

Substituting (3.2) in (3.3), we get,

$$V(t) = \frac{2}{3}V_{AO}(t)e^{j0} + V_{BO}(t)e^{j(2\pi/3)} + V_{CO}(t)e^{j(4\pi/3)} \quad -(3.4)$$

For example, the space vector  $V_1$  corresponding to active switching state (POO) can be derived as follows:

For switching state (POO), the generated load phase voltages are,

$$V_{AO}(t) = (2/3)V_d, V_{BO}(t) = -(1/3)V_d, V_{CO}(t) = -(1/3)V_d \quad -(3.5)$$

Corresponding space vector  $V_1$  can be obtained by substituting above values into (3.4), which will yield,

$$\vec{V}_1 = \left(\frac{2}{3}\right)V_d e^{j0}$$

Following the same procedure for the other switching states, the other active space vectors can also be obtained.

In general, the six active space vectors can be expressed as,

$$\vec{V}_k = \frac{2}{3}V_d e^{j(k-1)} \quad \text{where } k = 1,2,3,\dots,6 \quad -(3.6)$$

Zero vector  $V_0$  has two switching states (PPP) and (OOO), one of which seems redundant. The redundant switching state can however be utilised to minimize the switching frequency of the inverter as will be discussed later.

### 3.4.3.Synthesis of the reference vector using space vectors:

If three-phase sinusoidal and balanced voltages given by the equations

$$V_a = V_m \cos \omega t$$

$$V_b = V_m \cos\left(\omega t - \frac{2\pi}{3}\right)$$

$$V_c = V_m \cos\left(\omega t - \frac{4\pi}{3}\right)$$

- (3.7)

are applied to a three-phase induction motor, a space vector  $V_{ref}$  with a magnitude  $V_m$  rotates in a circular orbit at angular velocity  $\omega$ , given by,

$$\omega = 2\pi f \quad \text{-(3.8)}$$

Where,  $f_1$  is the fundamental frequency of the inverter output voltage.

The angular displacement between  $V_{ref}$  and  $\alpha$ -axis of the  $\alpha$ - $\beta$  plane can be obtained by,

$$\theta(t) = \int \omega(t)dt + \theta(0) \quad \text{-(3.9)}$$

For a given magnitude and phase of the reference voltage vector  $V_{ref}$ , it can be synthesized by three nearby stationary vectors, generally two active vectors and a zero vector, based on which the switching states of the inverter can be selected and gate signals for the active switches can be generated.

#### **3.4.4. Calculation of dwell times:**

The dwell time for the stationary vectors essentially represents the duty-cycle time i.e., ON-time(or OFF-time) of the chosen switches during a sampling period  $T_s$  of the modulation scheme. The dwell time calculation is based on 'Volt-second balancing principle', i.e., the product of the reference voltage  $V_{ref}$  and sampling period  $T_s$  equals the sum of the voltage multiplied by the time interval of the chosen space vectors.

Assuming  $T_s$  to be very small so that  $V_{ref}$  remains constant during that period,  $V_{ref}$  can be synthesized by two adjacent active vectors and one zero vector.

For instance, synthesis of  $V_{ref}$  when it falls in sector I, can be done using space vectors  $V_1, V_2$  and  $V_0$  as shown in the figure

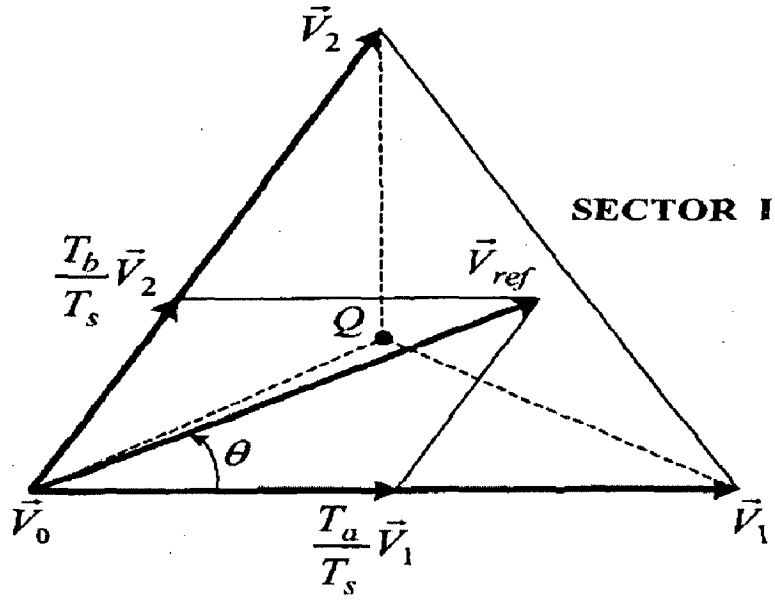


Fig 3.5: Synthesis of  $V_{ref}$  by  $V_1, V_2$  and  $V_0$

Using the Volt-second balance principle,

$$\begin{aligned} \vec{V}_{ref} T_s &= \vec{V}_1 T_a + \vec{V}_2 T_b + \vec{V}_0 T_0 \\ T_s &= T_a + T_b + T_0 \end{aligned} \quad - (3.10)$$

Where,  $T_a, T_b$  and  $T_0$  being the dwell times of the space vectors  $V_1, V_2$  and  $V_0$  respectively.

We know,

$$V_{ref} = v_{ref} e^{j\theta}, \quad V_1 = (2/3)v_d, \quad V_2 = (2/3)v_d e^{j(\pi/3)} \quad \text{and} \quad V_0 = 0.$$

Substituting these values in the relations given by 3.10 and splitting these relations into real( $\alpha$ -axis) component and imaginary( $\beta$ -axis) component, we have:

$$\begin{aligned} V_{ref} (\cos \theta) T_s &= \frac{2}{3} V_d T_a + \frac{1}{3} V_d T_b \\ V_{ref} (\sin \theta) T_s &= \frac{1}{\sqrt{3}} V_d T_b \end{aligned} \quad - (3.11)$$

Solving above equation along with the relation  $T_s = T_a + T_b + T_0$  simultaneously, we get dwell times  $T_a, T_b$  and  $T_0$  for sector I as given below:

$$\begin{aligned}
T_a &= \frac{\sqrt{3}T_s V_{ref}}{V_d} \sin\left(\frac{\pi}{3} - \theta\right) \\
T_b &= \frac{\sqrt{3}T_s V_{ref}}{V_d} \sin\theta \quad \text{for } 0 \leq \theta \leq (\pi/3) \\
T_0 &= T_s - T_a - T_b
\end{aligned} \quad - (3.12)$$

Set of equations (2.12), which apply to sector I, can also be used when  $V_{ref}$  lies in other sectors provided that a multiple of  $\pi/3$  is subtracted from the actual angular displacement  $\theta$  such that the modified angle  $\theta'$  falls into the range between zero and  $\pi/3$  for use in the equation,

$$\theta' = \theta - (k-1)\pi/3 \quad \text{for } 0 \leq \theta' < \pi/3 \quad - (3.13)$$

where,  $k = 1, 2, \dots, 6$  for sectors I, II, ..., VI

### 3.5 Modified Space Vector Modulation

For realization of the Z-source converter to utilize the shoot through, the conventional SVPWM technique should be modified. Fig. 8 shows both the conventional and modified switching patterns for the Z-source converter at each sector. In this figure, a new duration ( $T$ ) should be added to the switching time ( $T_1$ ,  $T_2$ , and  $T_0$ ) of the traditional SVPWM in order to boost the dc-link voltage of the Z-source converter and to generate the sinusoid ac output voltage. For implementation of the modified space vector PWM, the switching time of the upper switches and lower switches in a three-phase inverter is summarized in Table I below

In the Z-source converter, the peak value of phase-a inverter output voltage can be written as [1]

$$V_{a-p} = M \frac{V_{p-dc}}{2} = MK \frac{V_{in}}{2}$$

Where

$$K = \frac{T_z}{T_b - T_a} = \frac{1}{1 - 2\frac{T_0}{T_z}} \geq 1$$

$K$  is called a boost factor and  $M$  and  $V_p$  dc denote the modulation index and the peak dc-link voltage, respectively,

$T_z = T_a + T_b$ :  $T_z$  is the switching period,  $T_a$  is the total duration of shoot-through zero vectors during  $T_z$ , and  $T_b$  is the total duration of non shoot-through switching vectors during  $T_z$



Above equation, the peak value of inverter output voltage ( $V_{a-p}$ ) definitely depends on both the modulation index ( $M$ ) and the boost factor ( $K$ ), and the boost factor ( $K$ ) is determined by a ratio  $T_a/T_z$ . Moreover, sum of the modulation index ( $M = T_b/T_z$ ) and the ratio  $T_a/T_z$  is always equal to unity.

Thus, the boosted rate of the dc-link voltage is dependent on the total duration ( $T_a = 3T$ ) of shoot-through zero vectors that simultaneously turn on both power switches in a leg. In Fig. 8.3.6, each phase still switches on and off once per switching cycle ( $T_z$ ), and has only one shoot-through zero state ( $T$ ) over one period ( $T_z$ ) in any sector without the change of total zero vectors ( $V_0$ ,  $V_7$ , and  $T$ ) and total nonzero switching vectors ( $V_1$ –  $V_6$ ). Even if the output voltage of inverter and dc-link voltage can be controlled by adjusting  $T_a$ , the maximum available shoot through interval ( $T_a$ ) to boost the dc-link voltage ( $v_i$ ) is limited by the zero vector duration ( $T_0/2$ ) which is determined by the modulation index.

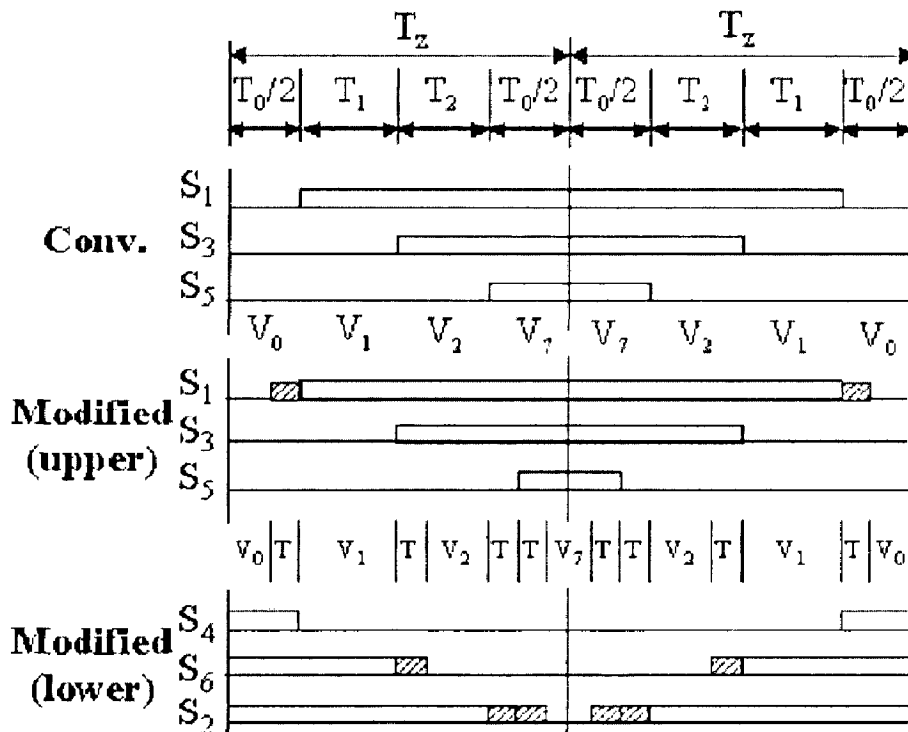


Fig. 3.6. Modified SVPWM implementation. (a) Sector 1.

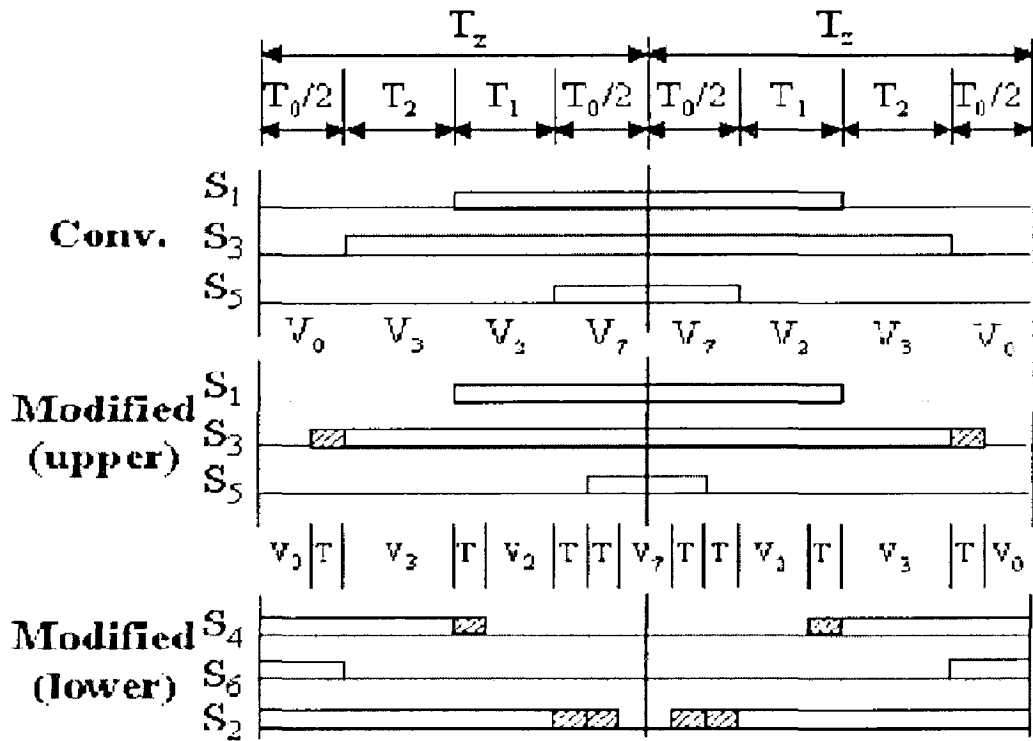


Fig. 3.7. Modified SVPWM implementation . Sector 2

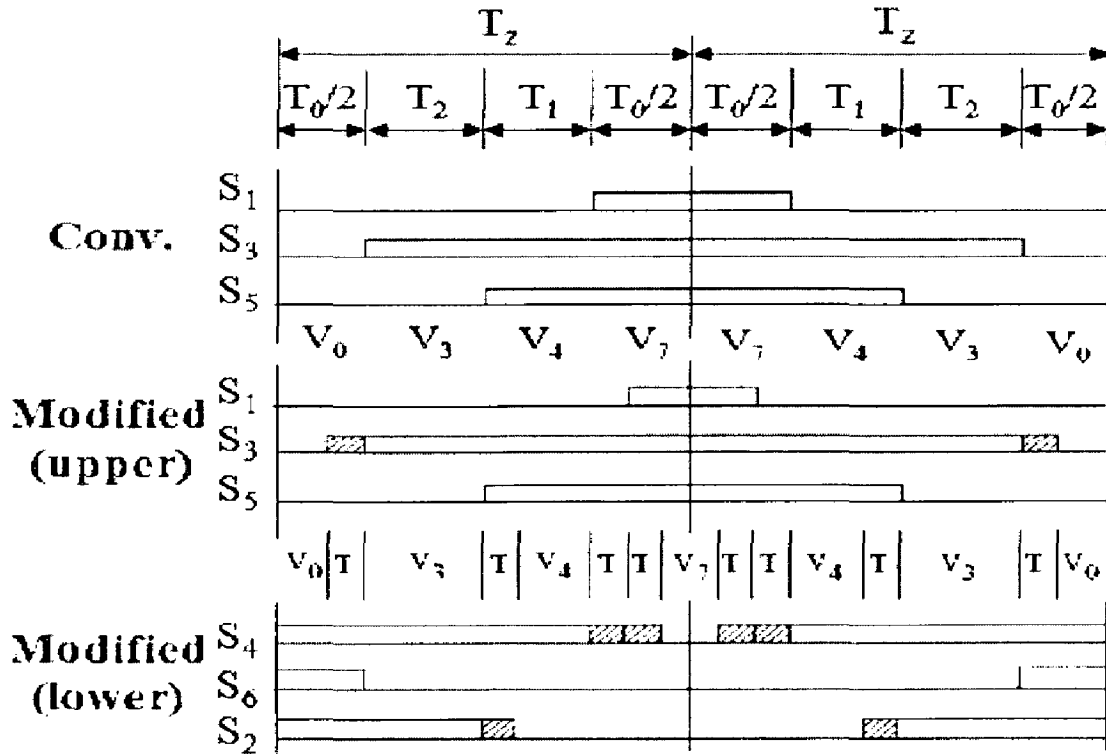


Fig. 3.8. Modified SVPWM implementation . Sector 3

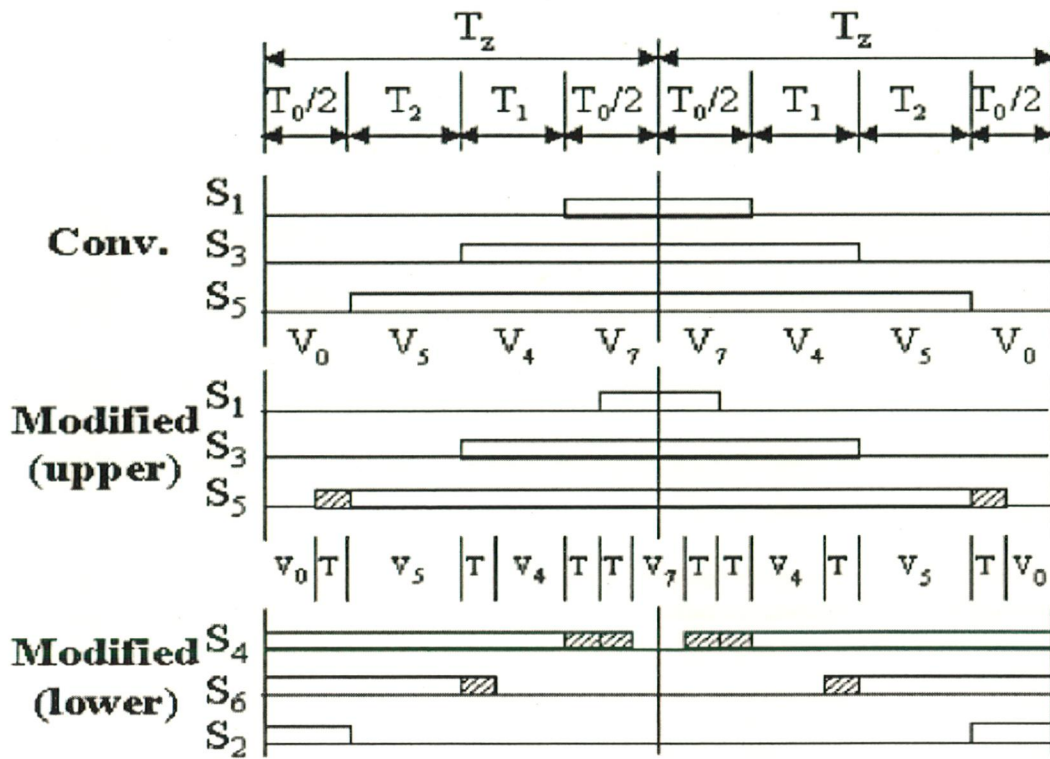


Fig. 3.9. Modified SVPWM implementation . Sector 4

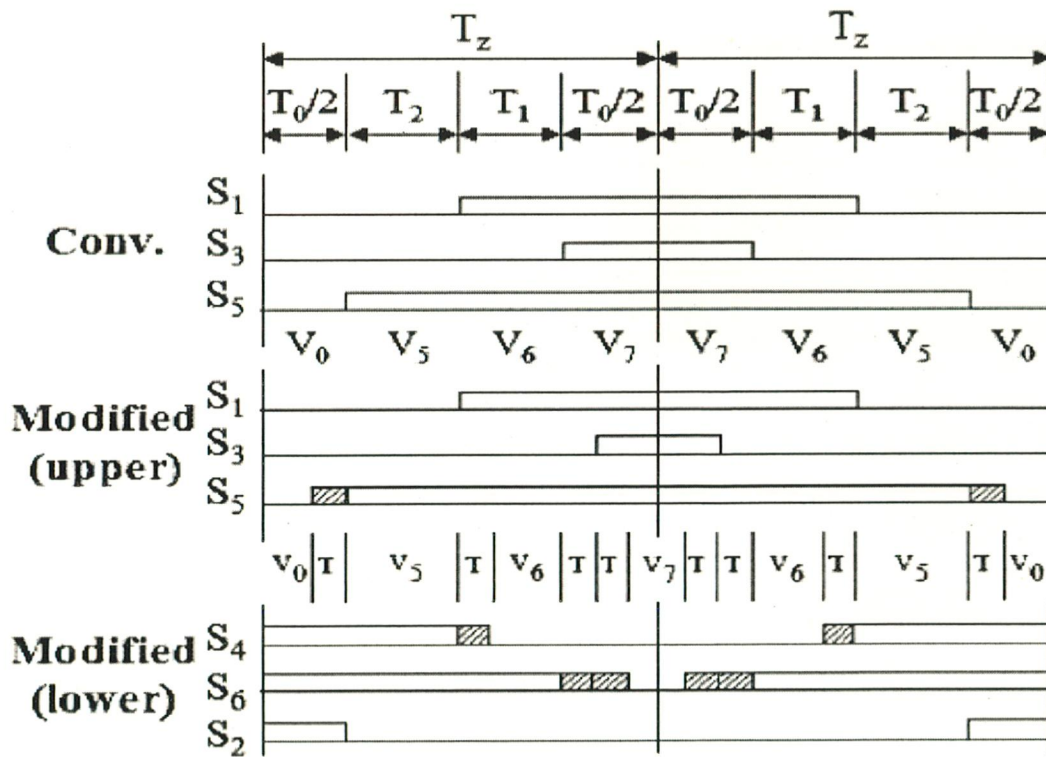


Fig. 3.10. Modified SVPWM implementation. Sector 5

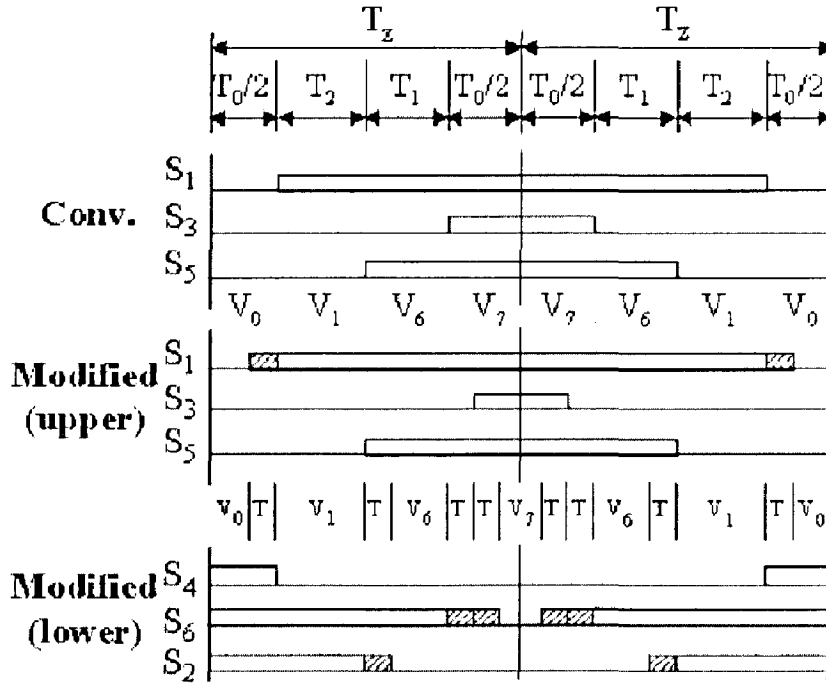


Fig. 3.11. Modified SVPWM implementation . Sector 6

Sector	Upper (S1, S3, S5)	Lower (S4, S6, S2)
1	$S1 = T1 + T2 + T0/2 + T$ $S3 = T2 + T0/2$ $S5 = T0/2 - T$	$S4 = T0/2$ $S6 = T1 + T0/2 + T$ $S2 = T1 + T2 + T0/2 + 2T$
2	$S1 = T1 + T0/2$ $S3 = T1 + T2 + T0/2 + T$ $S5 = T0/2 - T$	$S4 = T2 + T0/2 + T$ $S6 = T0/2$ $S2 = T1 + T2 + T0/2 + 2T$
3	$S1 = T0/2 - T$ $S3 = T1 + T2 + T0/2 + T$ $S5 = T2 + T0/2$	$S4 = T1 + T2 + T0/2 + 2T$ $S6 = T0/2$ $S2 = T1 + T0/2 + T$
4	$S1 = T0/2 - T$ $S3 = T1 + T0/2$ $S5 = T1 + T2 + T0/2 + T$	$S4 = T1 + T2 + T0/2 + 2T$ $S6 = T2 + T0/2 + T$ $S2 = T0/2$
5	$S1 = T2 + T0/2$ $S3 = T0/2 - T$ $S5 = T1 + T2 + T0/2 + T$	$S4 = T1 + T0/2 + T$ $S6 = T1 + T2 + T0/2 + 2T$ $S2 = T0/2$
6	$S1 = T1 + T2 + T0/2 + T$ $S3 = T0/2 - T$ $S5 = T1 + T0/2$	$S4 = T0/2$ $S6 = T1 + T2 + T0/2 + 2T$ $S2 = T2 + T0/2 + T$

TABLE 3.3: SWITCHING TIME DURATION AT EACH SECTOR

### 3.6 Conclusion

Simple control, Boost Control, Maximum Boost Control Techniques are discussed. The SVM has advantages over the PWM techniques. SVM is modifications discussed

# Chapter 4

## Simulation

### 4.1 Introduction

In this chapter the Maximum Boost Control of Z-Source Inverter is simulated at no load and load. The use the advantages of SVM for Z-Source Inverter the SVM technique have to be modified in order to boost the capacitor voltage. Closed loop Voltage control is used along with the Modified Space Vector Modulation.

### 4.2 Maximum Boost Control

To fully utilize the zero states so as to minimize the voltage stress across the device, maximum boost control [7] turns all traditional zero states into shoot-through state, as shown in Fig. 4.1.

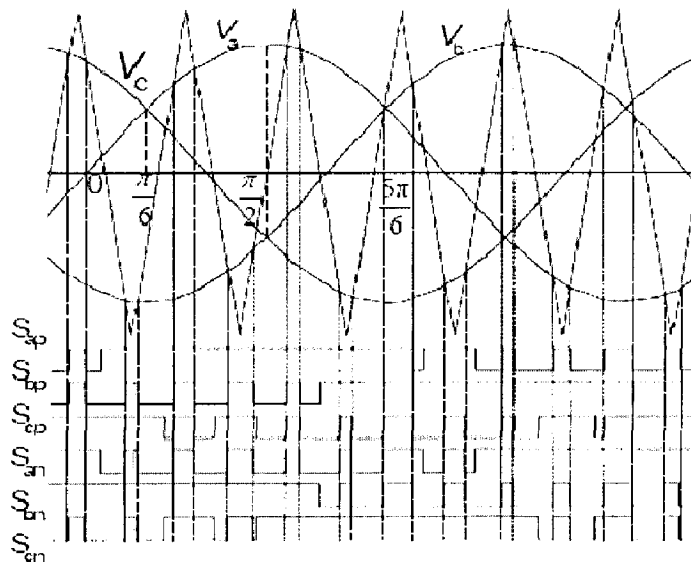


**Fig.4.1 Maximum Boost Control**

Indeed, turning all zero states into shoot-through state can minimize the voltage stress; however, doing so also causes a shoot-through duty ratio varying in a line cycle, which causes inductor current ripple, this will require high inductance for low-frequency or variable-frequency applications.

MAX.BOOST CONTROL Z-SOURCE INVERTER

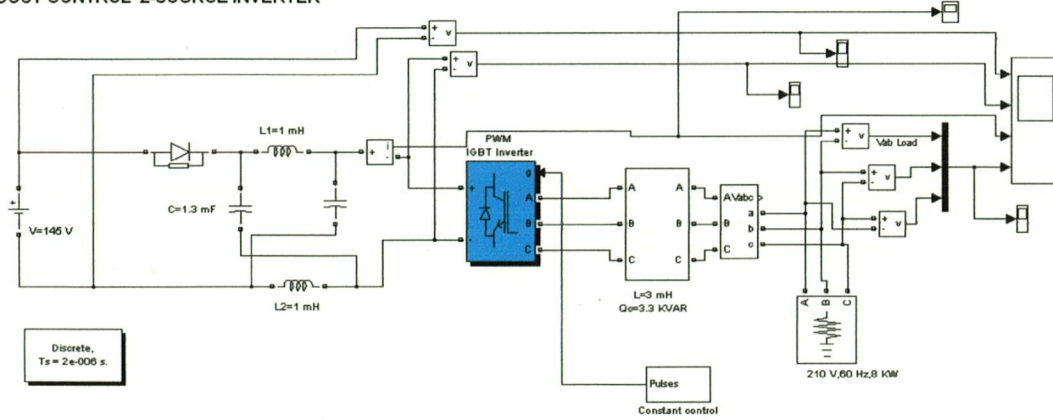


Fig4.2 Maximum Boost Control Technique Simulation

4.2. 1 No Load

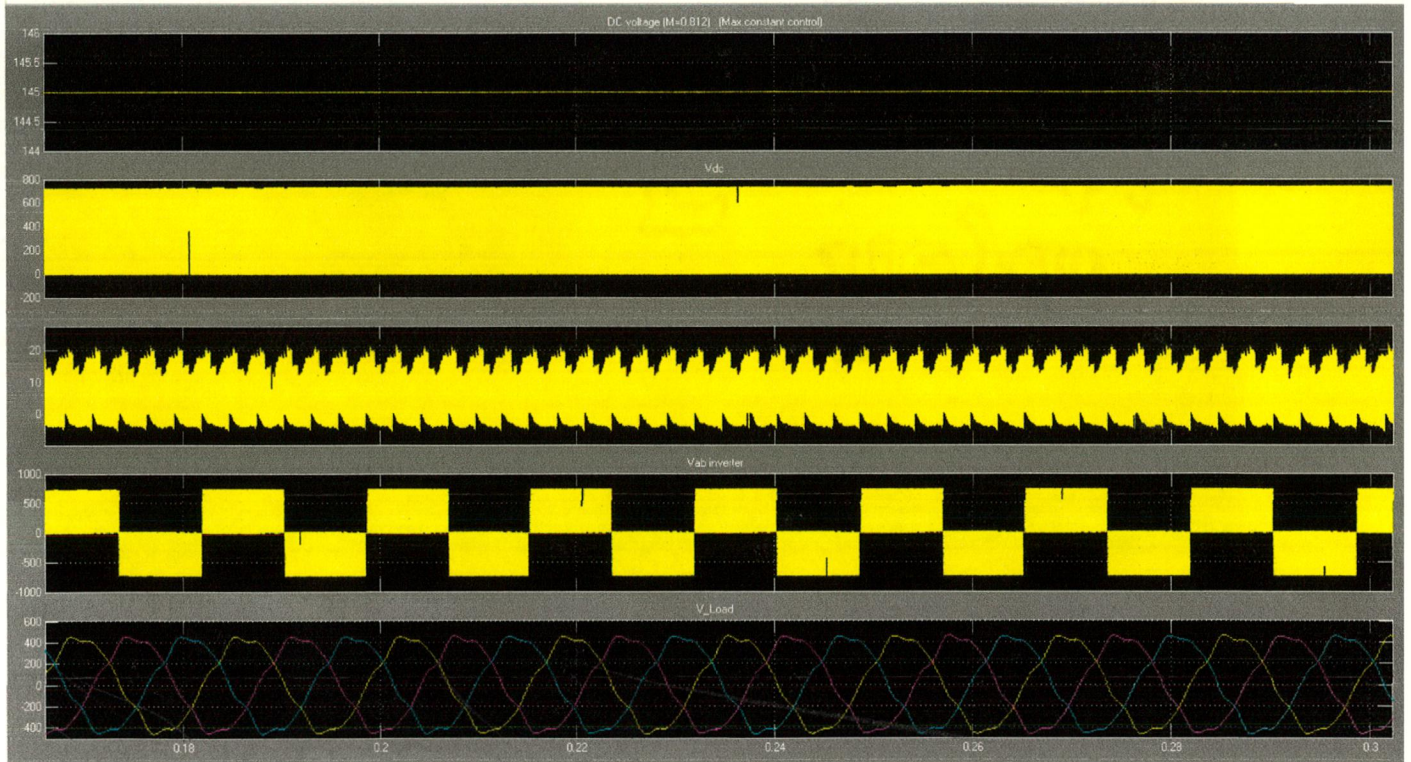
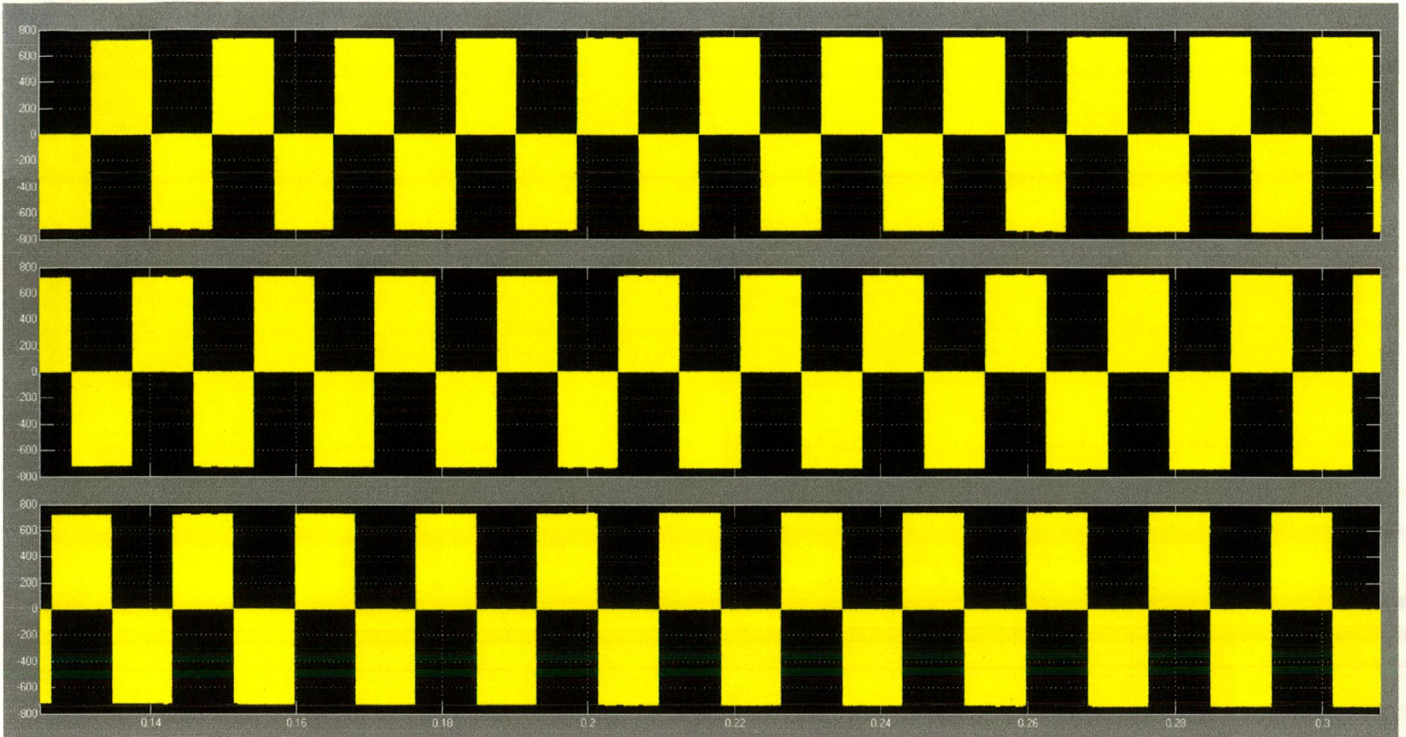
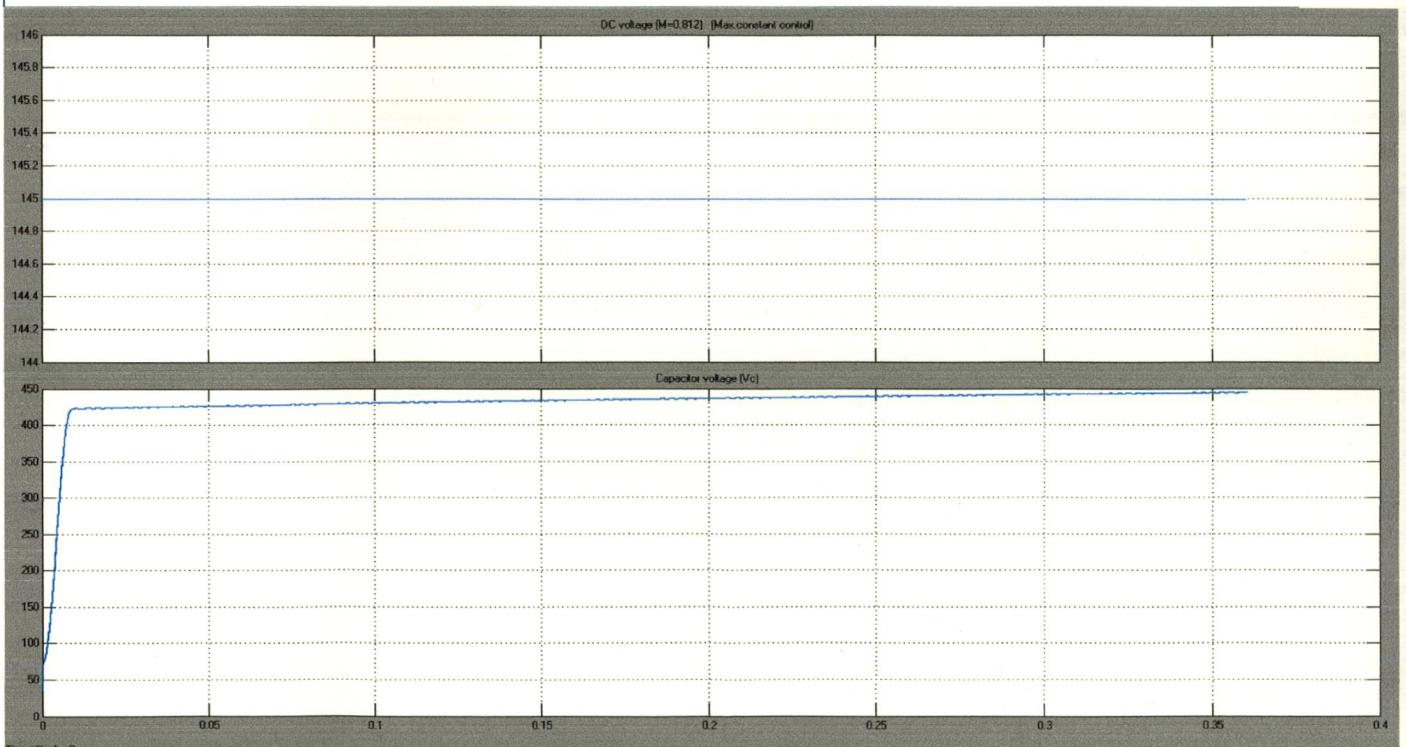


Fig 4.3 DC Voltage, DC Link Voltage, Inductor Current, Inverter output Voltage, Terminal Voltage





**Fig4.4 Inverter output Voltage under No Load**



**Fig4.5 No Load Capacitor Voltages**



## 4.2.2 With RL Load

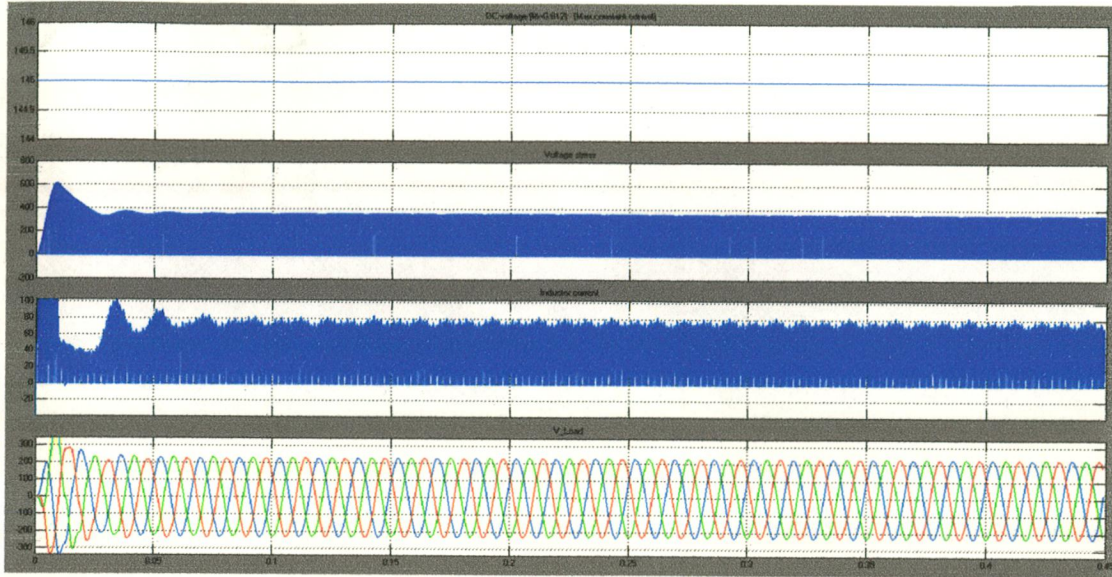


**Fig.4.6. DC Voltage, Voltage Stress, Inductor Current, Voltage across Load.**

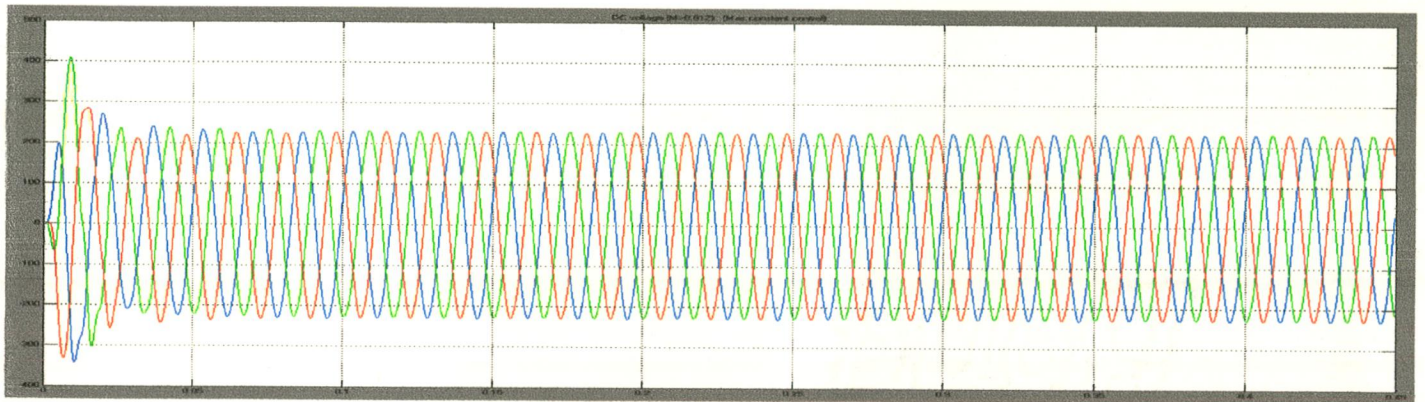


**Fig.4.7. Line Voltages**

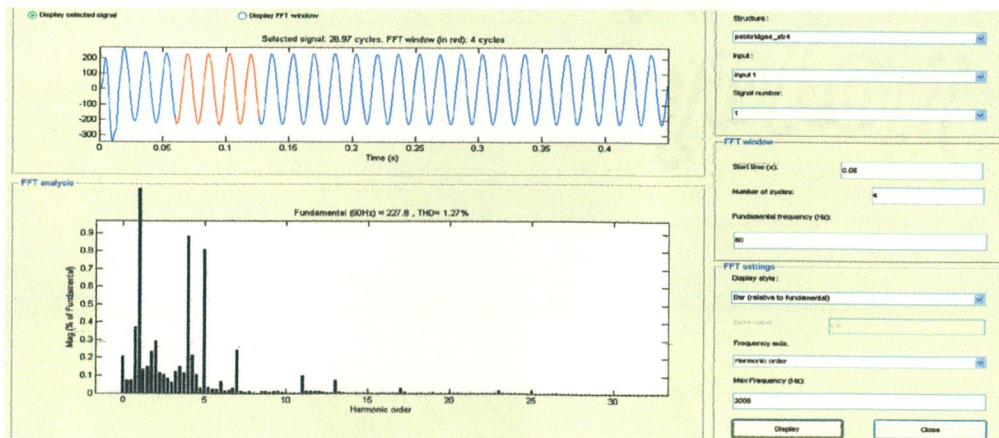


**Fig.4.8. Voltage THD 1.27.**



### 4.3 Maximum Boost Control with Third Harmonic Injection

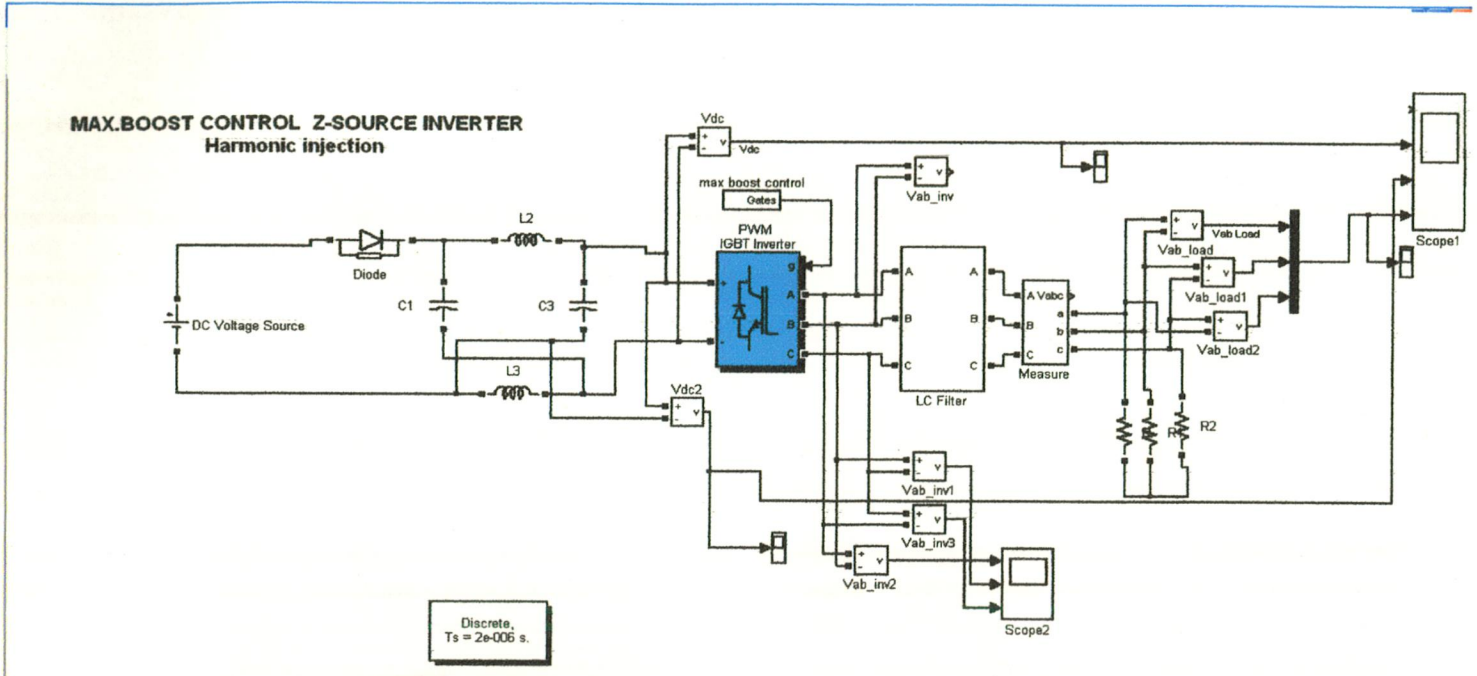


Fig4.9 Simulink Model of Maximum Boost Control with third Harmonic Injection

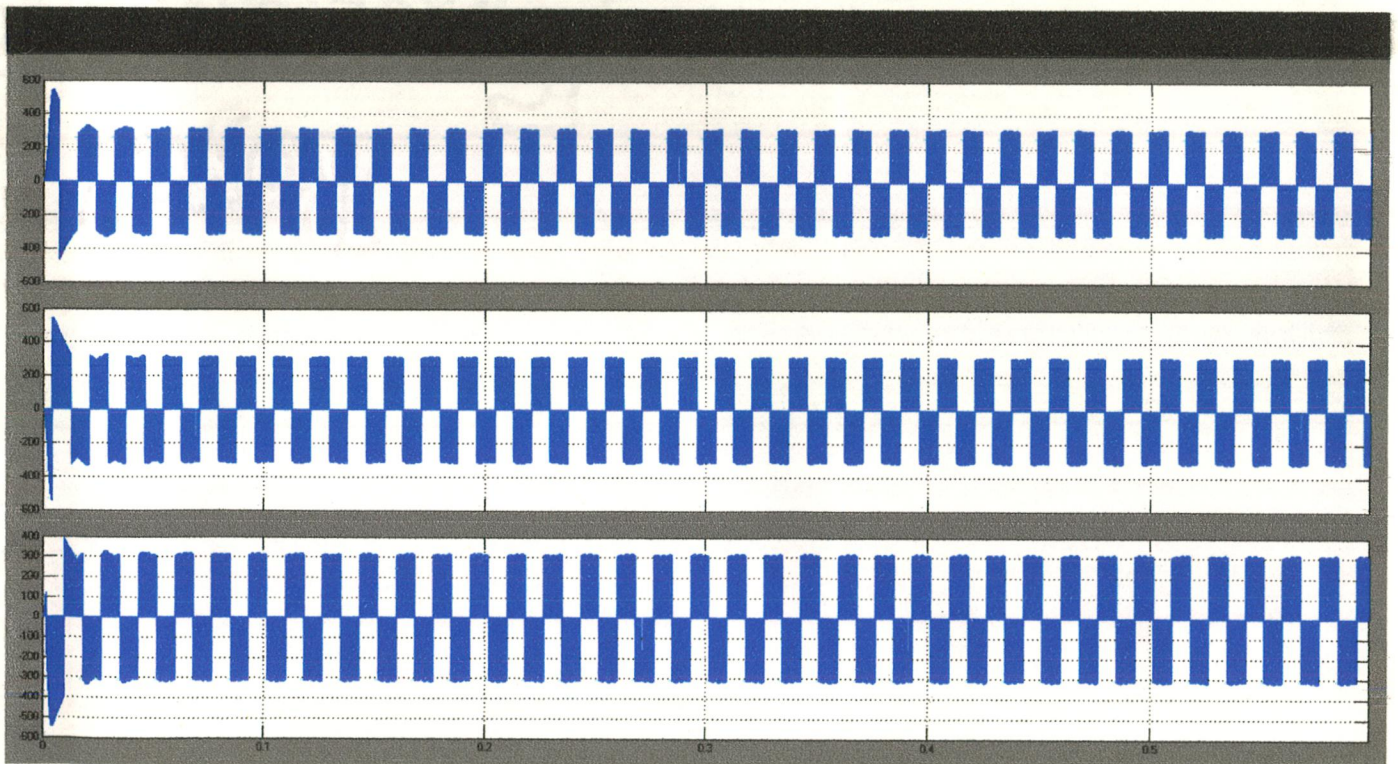
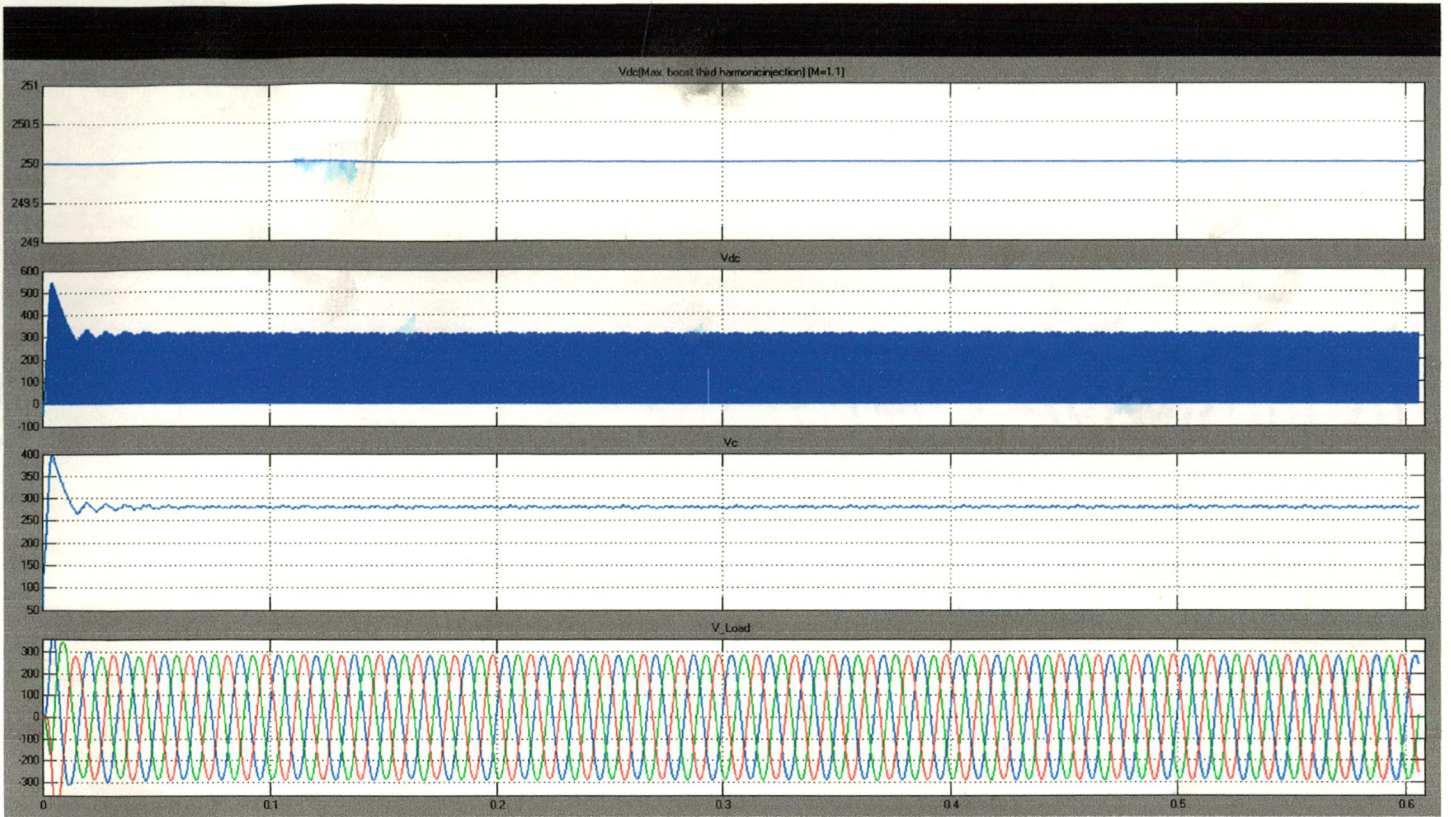
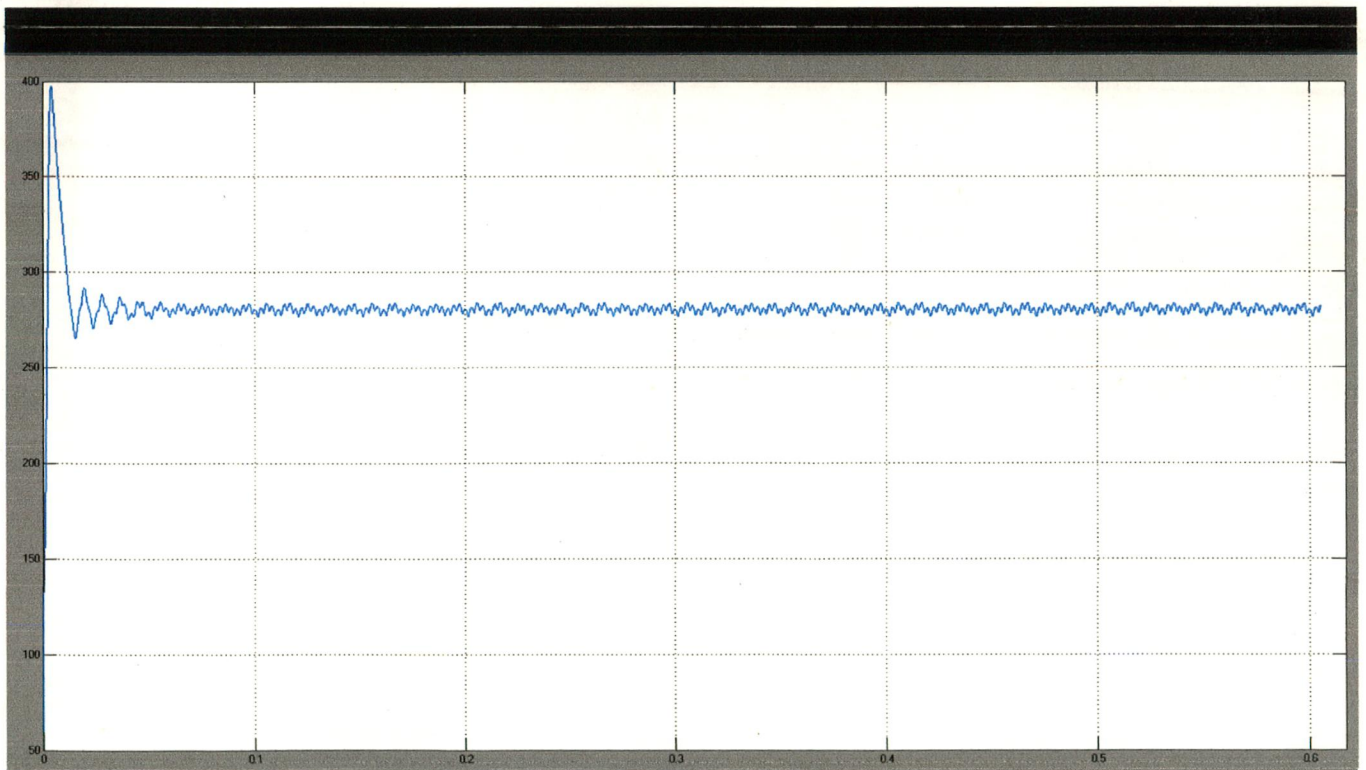


Fig4.10 Inverter Output Voltages





**Fig 4.11 DC Voltage, DC Link Voltage, Inductor Current, Inverter output Voltage, Terminal Voltage**



**Fig.4.12 Capacitor Voltage**

#### 4.4 Modified Space Vector Modulation

Space vector modulation (SVPWM) is one of the preferred real-time modulation techniques and is widely used for the digital control of Voltage source inverters. It is an advanced, computation intensive PWM and possibly the best among all the PWM techniques for variable frequency drive applications [17, 20].

For realization of the Z-source converter to utilize the shoot through, the conventional SVPWM technique should be modified. A new duration ( $T_2$ ) should be added to the switching time ( $T_1$ ,  $T_2$ , and  $T_0$ ) of the traditional SVPWM in order to boost the dc-link voltage of the Z-source converter and to generate the sinusoid ac output voltage. Thus, the boosted rate of the dc-link voltage is dependent on the total duration of shoot-through zero vectors that simultaneously turn on both power switches in a leg.

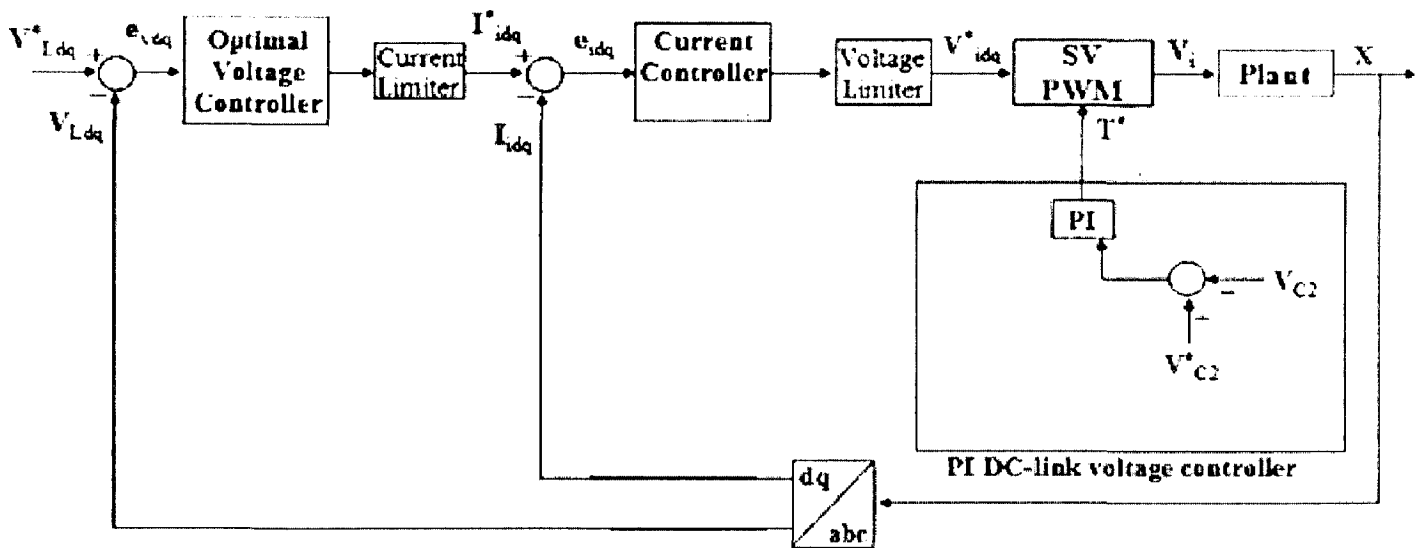
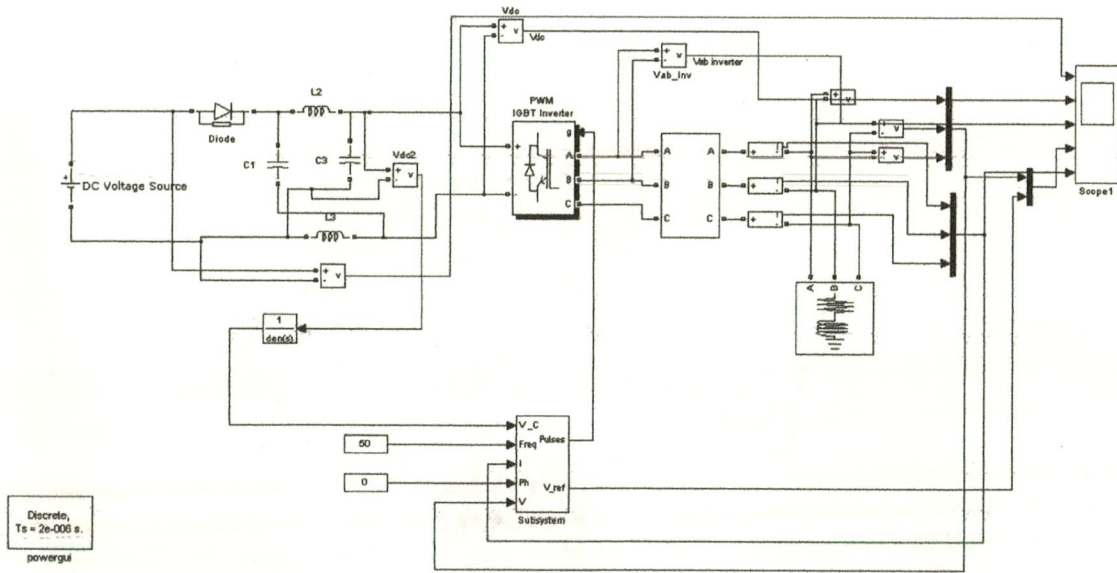


Fig 4.13 (a) Closed loop Control Scheme



### 4.4.1 MSVM with DC Supply



**Fig.4.13(b). Closed Loop MSVM Simulink Model**

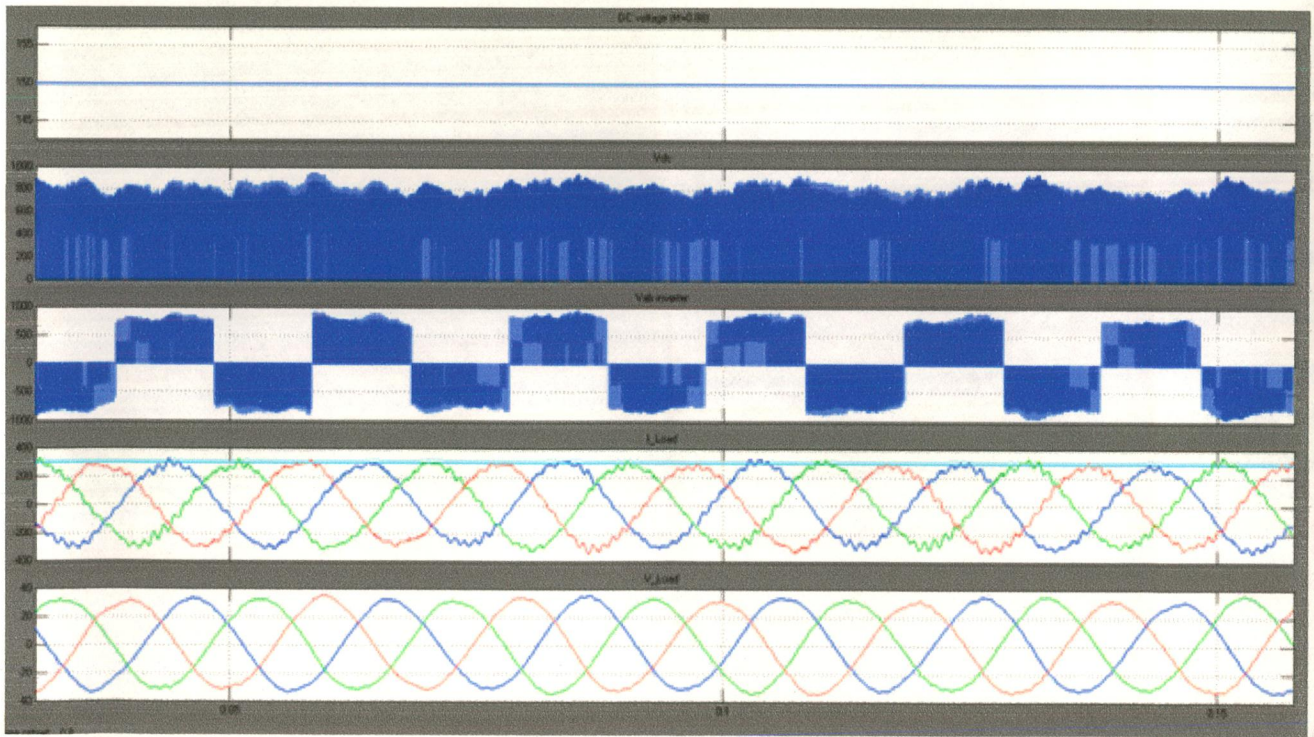


**Fig4.14. DC Source Voltage, DC Link Voltage, Inverter output, Load Voltage, Load Current at Steady state.**



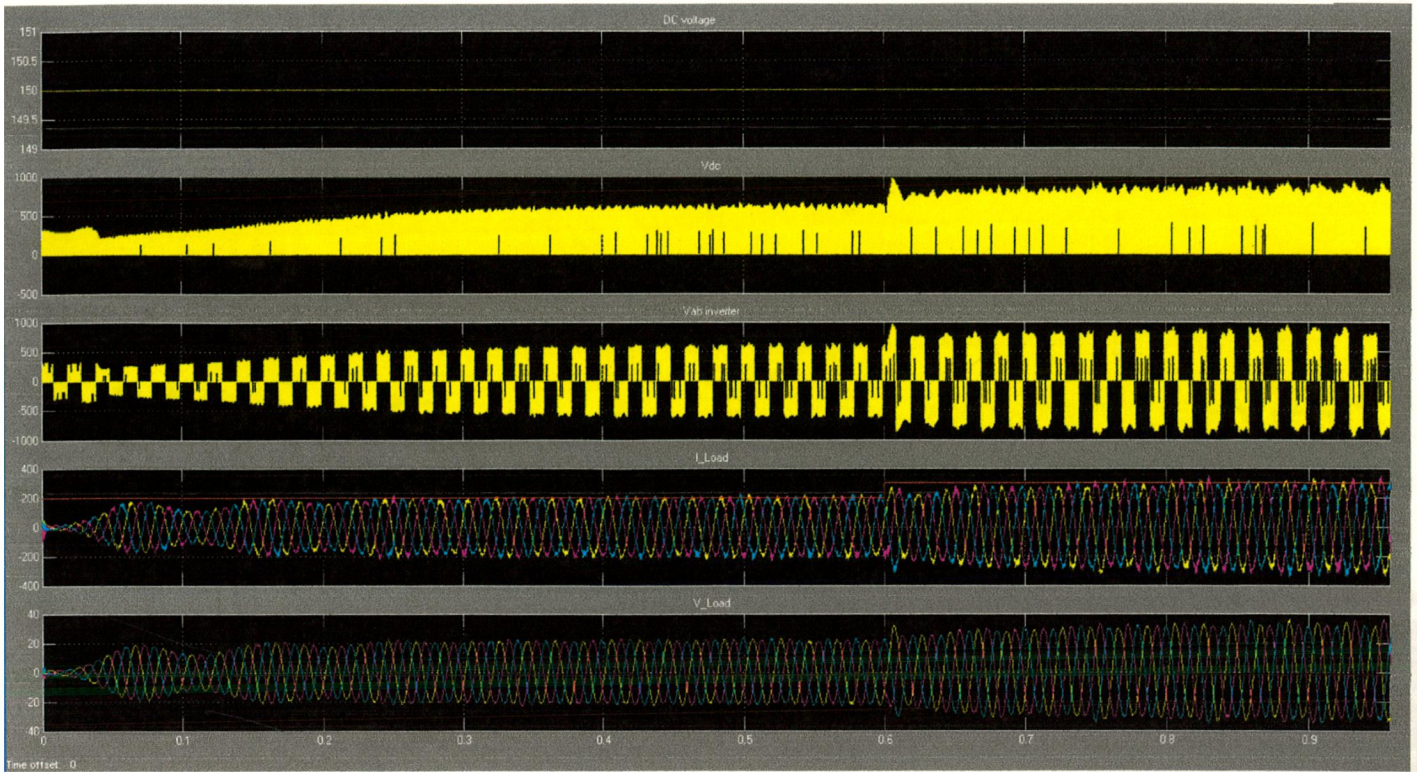


**Fig.4.15 DC Source Voltage, DC Link Voltage, Inverter output, Load Voltage, Load Current when reference capacitor AC output voltage is changed.**

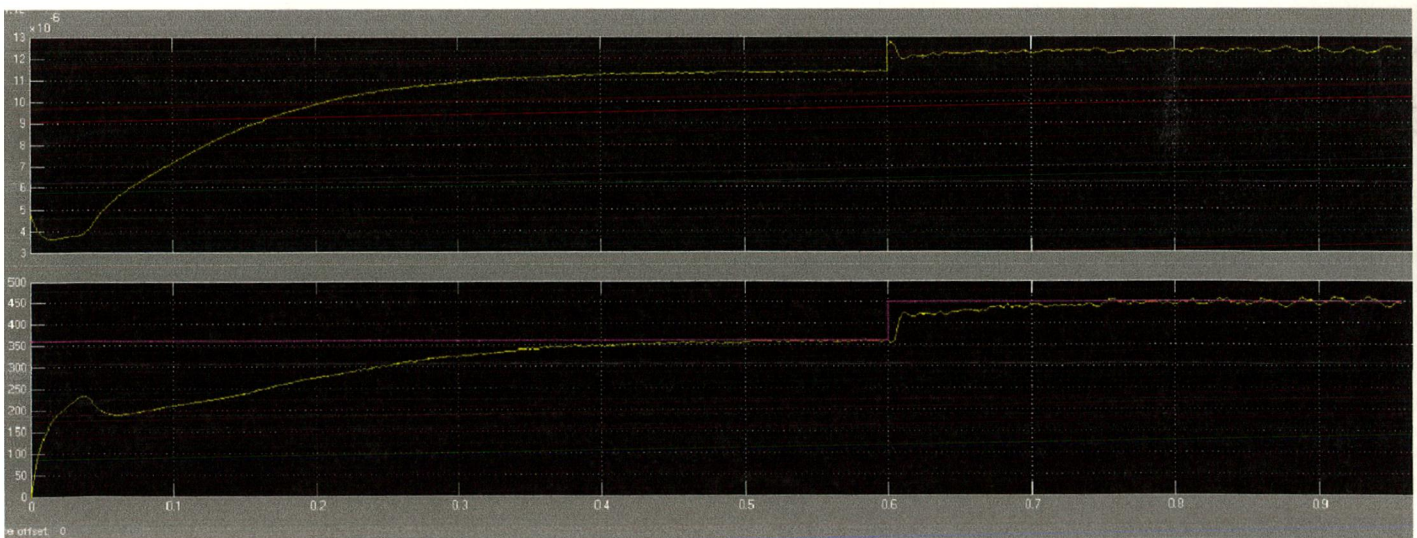


**Fig.4.16 Shoot Through Time and Capacitor Voltage**



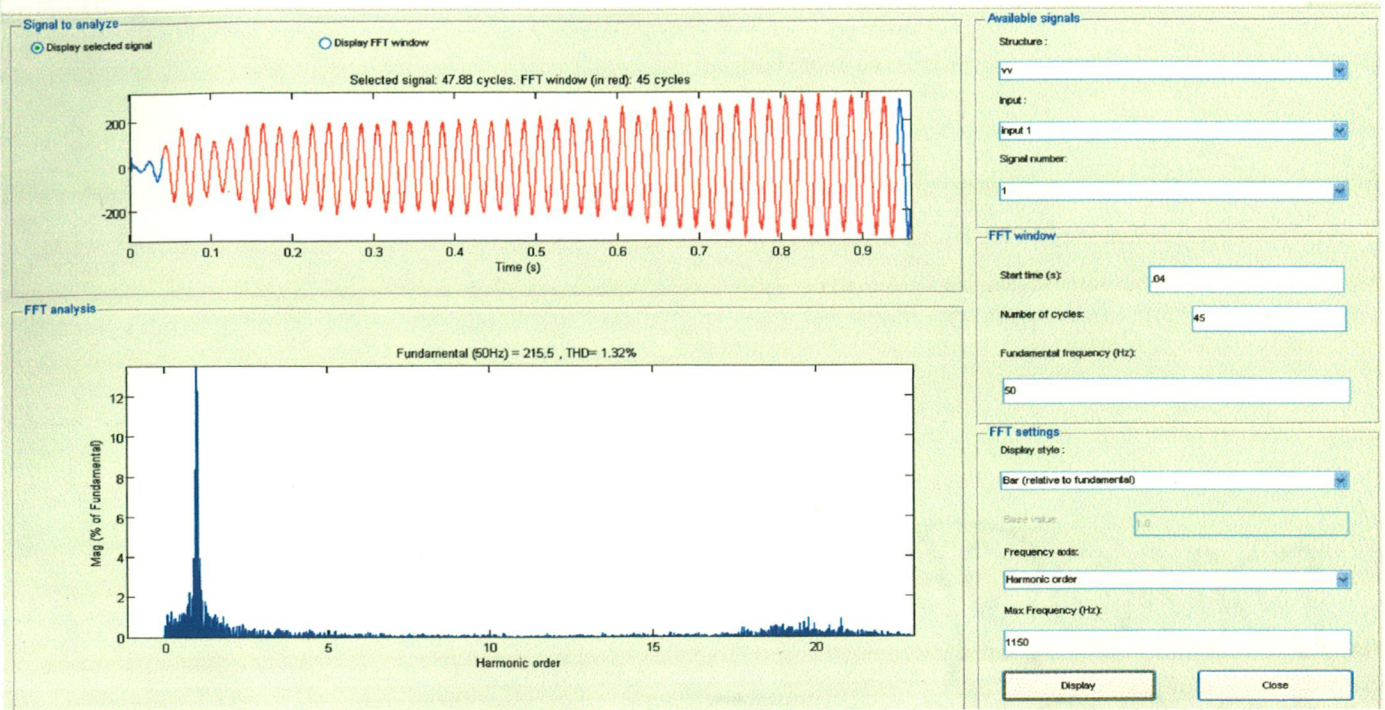


**Fig.4.17 The FFT analysis of the load voltage THD 1.32**

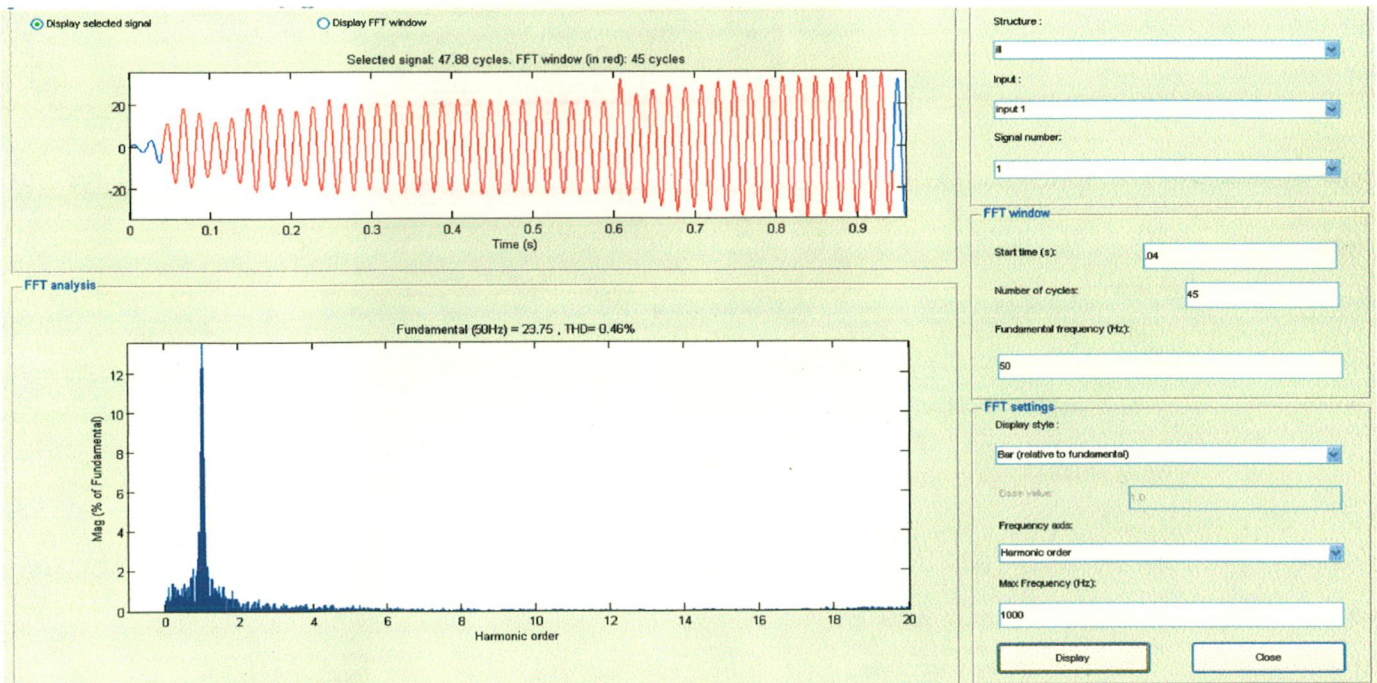


**Fig.4.18 The FFT analysis of the load current THD 0.46**

## 4.4.2 MSVM PHOTO VOLTAIC CELL

Solar cars use the photo voltaic cells as the energy source. The solar energy will be converted into electric energy. The output power depends on many factors of the photovoltaic cell. The photo voltaic cell is modeled and used along with the Z-Source Inverter. The photo voltaic cell model is shown below.

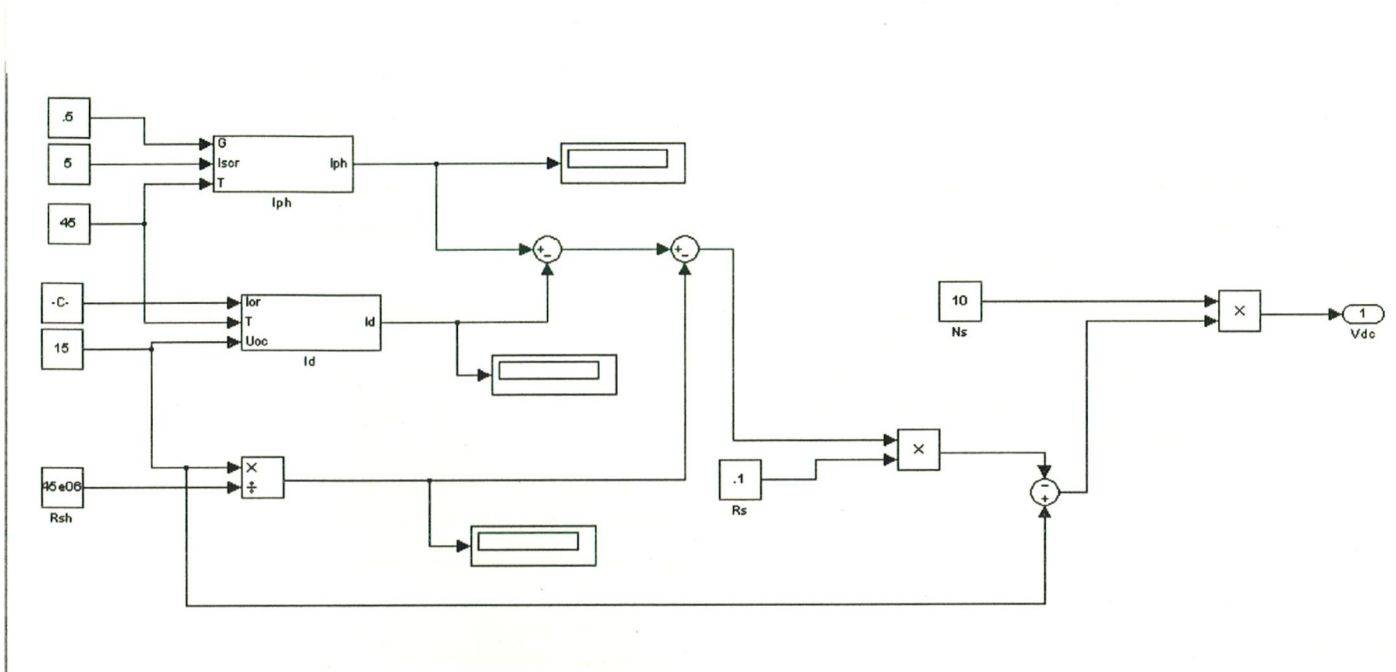


Fig.4.19 Photo Voltaic Cell Model

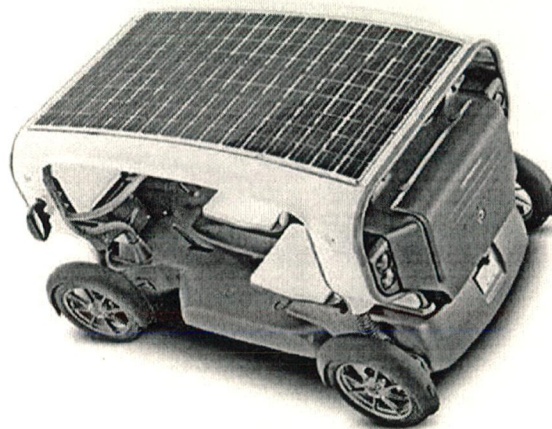
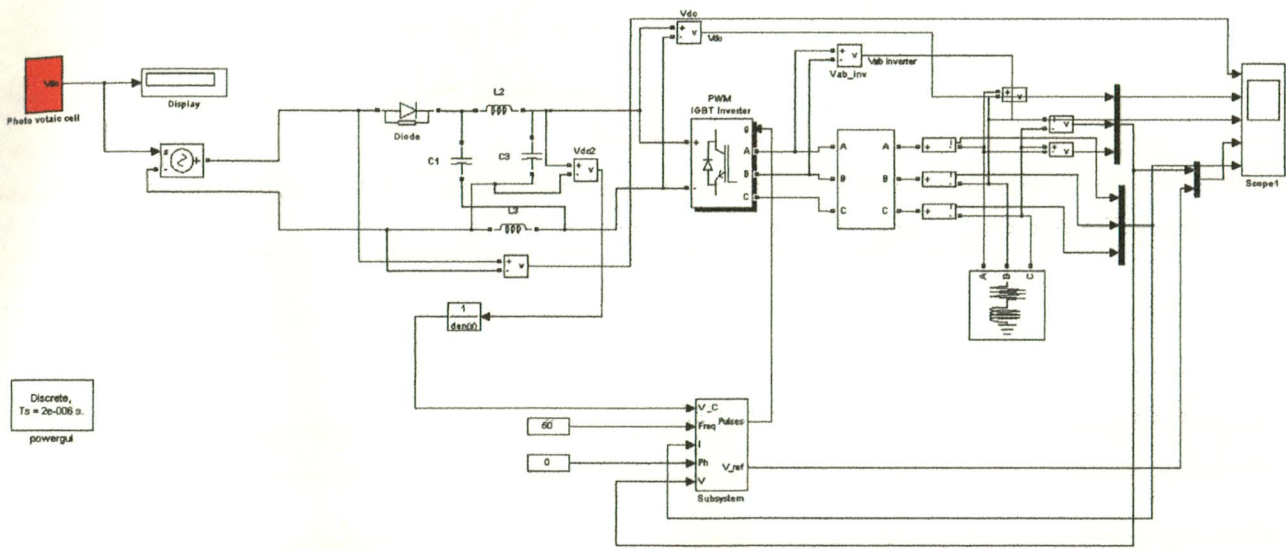
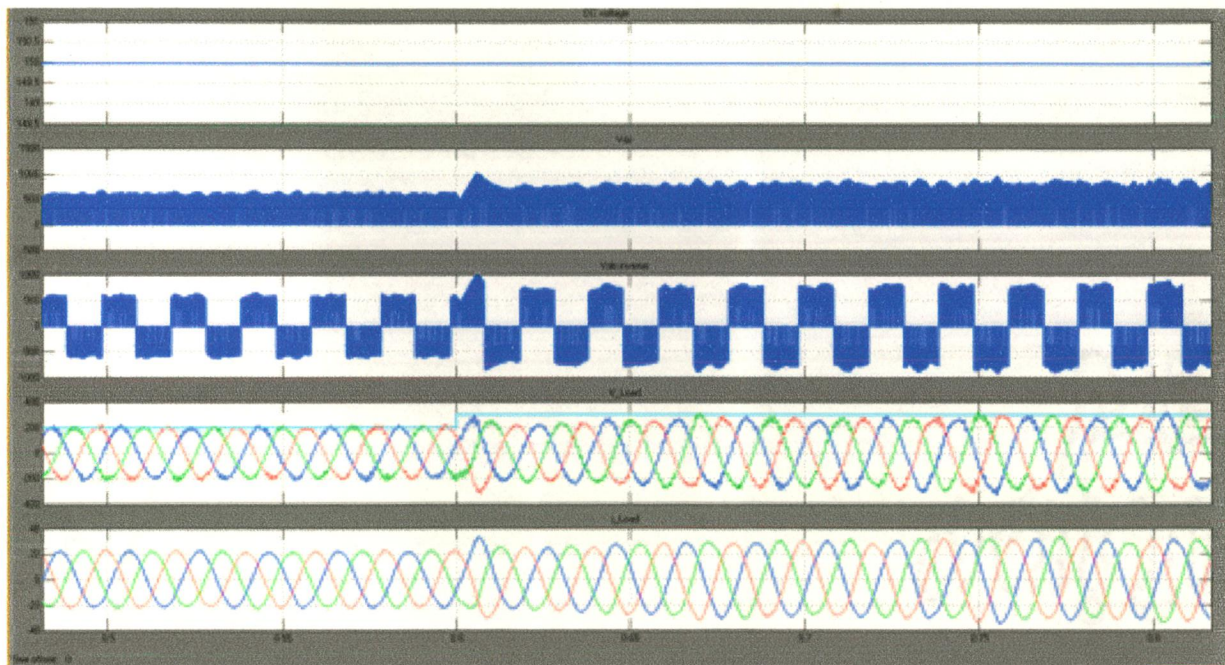


Fig.4.20 Image of Solar Car





**Fig.4.21 Closed Loop MSVM With Photo Voltaic Cell**



**Fig.4.22 Photovoltaic Cell Output, DC Link Voltage, Inverter Output, Load Voltage, Load Current**



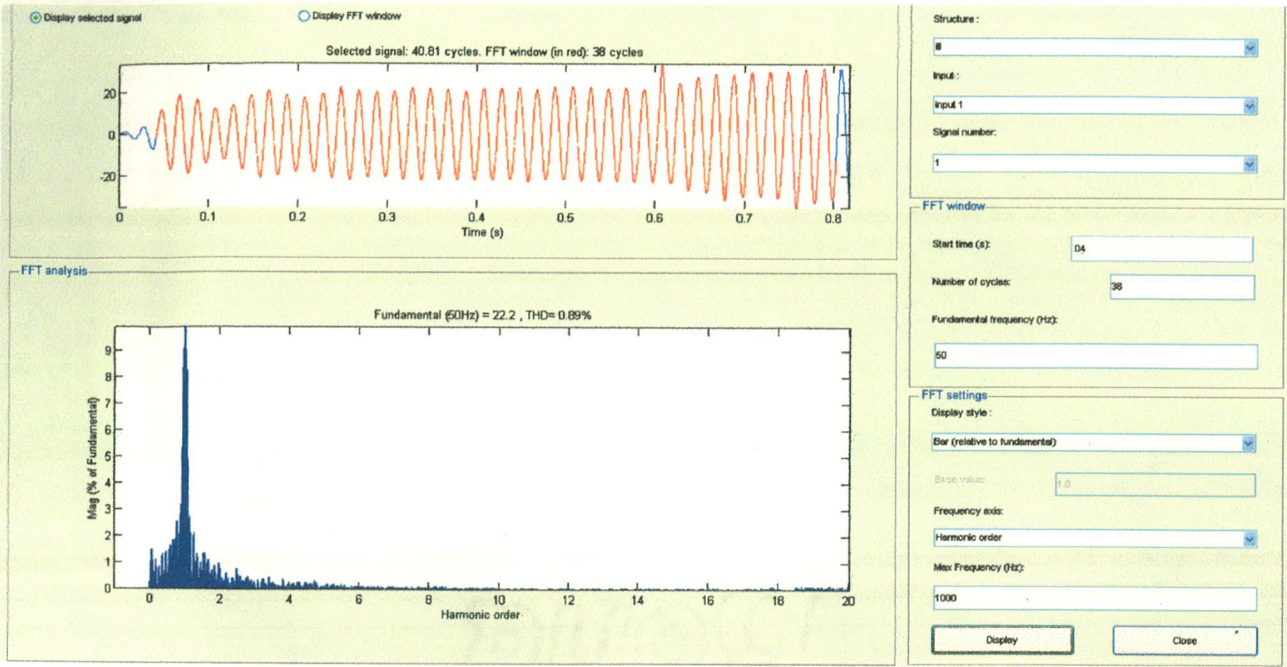


**Fig.4.23 The FFT analysis of the load current THD 0.89**

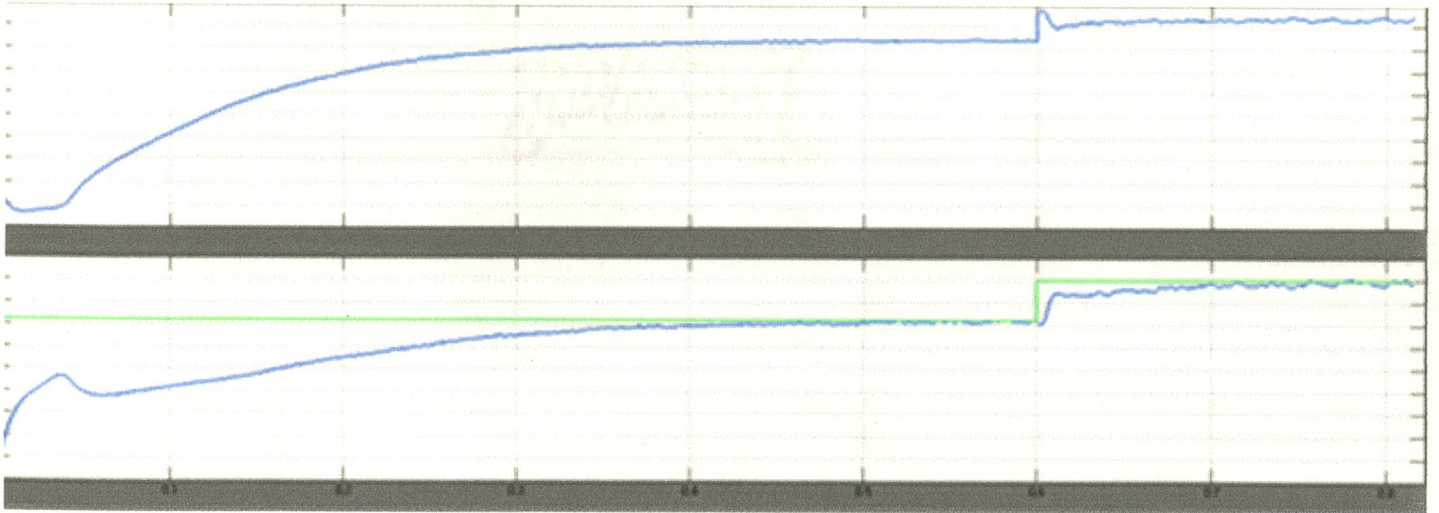


**Fig.4.24 Shoot Through Time and Capacitor Voltage**

### 4.4.3 MSVM with Fuel Cell

Fuel Cell cars use the Fuel cells as the energy source. The Chemical energy will be converted into electric energy. The output power depends on many factors of the Fuel Cell and the many input factors such as Fuel supply rate, Air flow rate. The Fuel Cell is model available in Simulink is used along with the Z-Source Inverter. The PEMFC type of fuel cell is used with a open circuit voltage of 64 V.

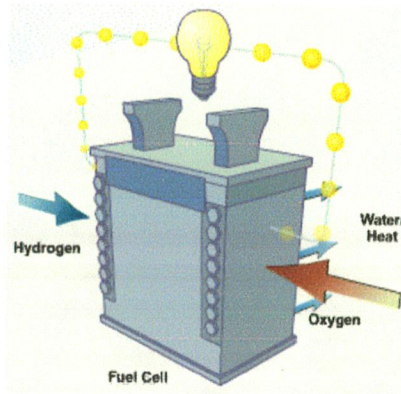


Fig.4.25 Image of Fuel Cell

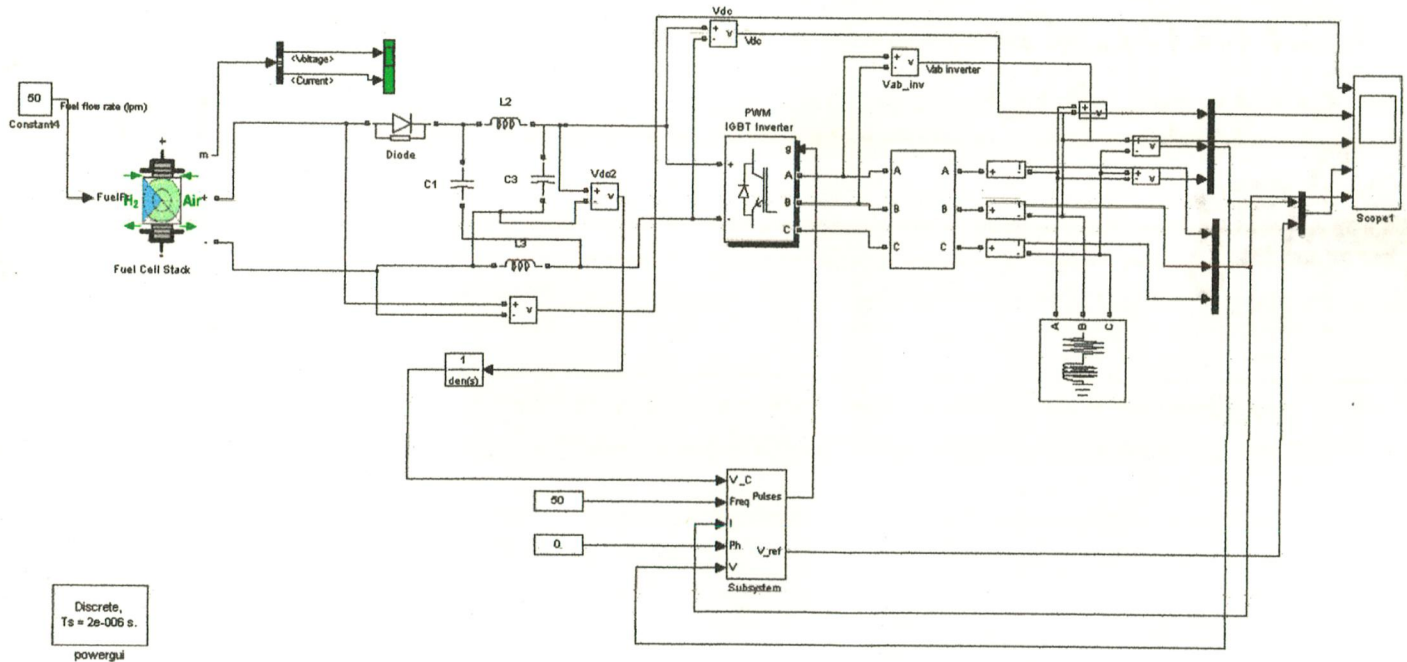
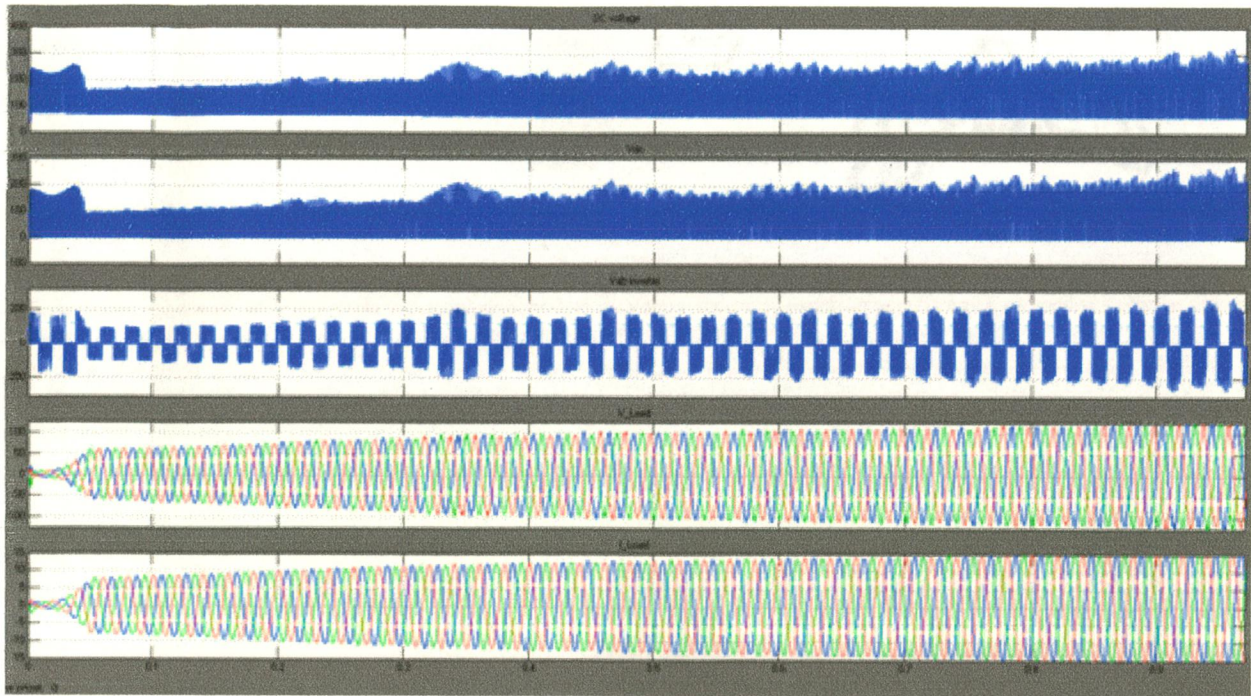


Fig.4.26 MSVM Simulation of ZSI with Fuel Cell

In Closed loop simulation the capacitor reference is 150 V, AC peak reference is 110V. The RL load is used. The fuel flow rate is fixed at 50 lpm.





**Fig.4.27 Fuel Cell Output Voltage, DC Link Voltage, Inverter Output Voltage, Load Line Voltages, Load Currents.**

### 4.3 Conclusion

The Maximum Boost control technique is simulated at various loads and third harmonic injection is also investigated. The Space Vector Modulation is modified to use for Z-Source Inverter and simulated also FFT analysis is carried out

# Hardware Development

---

In this chapter design procedure of the hardware developed for the implementation of Z-Source Inverter has been described.

The snubber circuit and other hardware requirements have been described briefly.

### **HARDWARE DEVELOPMENT:**

The system has been developed for open loop control containing following blocks:

1. Power circuit.
2. Pulse amplification and isolation circuit.
3. Power supplies.
4. Snubber circuit.

### **5.1 POWER CIRCUIT:**

Figure 5.1 shows the power circuit of Z-Source Inverter. IGBTs are used in power circuit consists of an inbuilt anti parallel diode. No forced commutation is required for IGBT because they are self commutating devices. The ant parallel diode is used across the IGBT. The high frequency inductors used across in the power circuit. The ferrite core is used for the design of the inductors. The inductors are designed for 15KHz. The inductors size is comparatively small because of the high frequency operation. The value of inductors must be same for the operation of the Z-Source inverter. Heat sinks are used for the cooling purpose. As the prototype is for lab experiments the size of the heat sinks is normal.

The power circuit mainly consists of Capacitor and Inductor. Electrolytic capacitors are used in the prototype. Care must be taken to avoid the inductance of the cables or else the the inductance comes into picture and the operation of ZSI will be gets affected.



**Fig 5.1 The Z-Source Inverter Developed**

### **5.1.1 Inductor Design**

During traditional operation mode, when there is no shoot-through, the capacitor voltage is always equal to the input voltage; therefore, there is no voltage across the inductor and only a pure dc current going through the inductors. The purpose of the inductors is to limit the current ripple through the devices during boost mode with shoot-through. During shoot-through, the inductor current increases linearly, and the voltage across the inductor is equal to the voltage across the capacitor; during non-shoot-through modes (six active modes and the two traditional zero modes), the inductor current decreases linearly and the voltage across the inductor is the difference between the input voltage and the capacitor voltage. The average current through the inductor is

$$\bar{I}_L = \frac{P}{V_{in}}$$

where  $P$  is the total power and  $V_{in}$  is the input voltage.

To minimize the size and weight of the inductors, the two inductors are built together on one core. For a single coil on one core, the flux through the core is

$$\phi = PNi$$

where  $P$  is a constant related to the core material and dimension,  $N$  is the number of turns of the coil, and  $i$  is the current through the coil. The inductance of the coil is

$$\Delta V_C = \frac{I_{av} T_\theta}{C} .$$

For the two inductors in the Z-source inverter, because of the symmetry of the circuit, the current through the inductors is always exactly the same. For two coils on one core with exactly the same current,  $i$ , the flux through the core is

$$\phi = 2PNi.$$

The resulting inductance of each coil when supplying exactly the same current to the two coils is

$$L = \frac{N\phi}{i} = 2PN^2 .$$

### 5.1.2 Capacitor Selection

The purpose of the capacitor is to absorb the current ripple and maintain a fairly constant voltage so as to keep the output voltage sinusoidal. During shoot-through, the capacitor charges the inductors, and the current through the capacitor equals the current through the inductor. Therefore, the voltage ripple across the capacitor can be roughly calculated by

$$\Delta V_C = \frac{I_{av} T_\theta}{C} .$$

where  $I_{av}$  is the average current through the inductor,  $T_\theta$  is the shoot-through period per switching cycle, and  $C$  is the capacitance of the capacitor.

### 5.2. PULSE AMPLIFICATION & ISOLATION CIRCUIT:

The pulse amplification and isolation circuit for IGBT is shown in figure. The opto-coupler (MCT-2E) provides the necessary isolation between the low voltage isolation circuit and high voltage power circuit. The pulse amplification is provided by the output amplifier transistor 2n2222. when the input gating signal is at +5v level, the transistor saturates, the LED conducts and the light emitted by it falls on the base of the photo transistor thus formatting its base drive.

The output transistor thus receives no base drive and therefore remains in the cut-off state and a +12v pulse appears across its collector terminal.

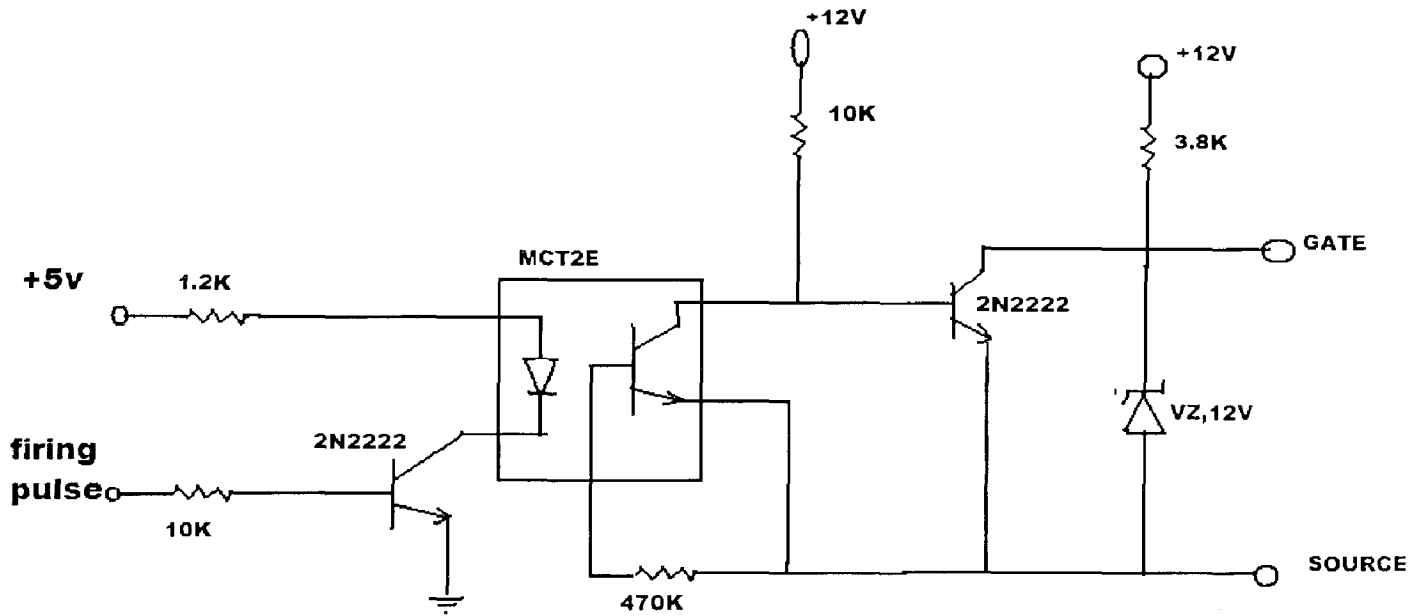


**Fig 5.2 Pulse amplification and isolation Circuit**

When the input gating signal reaches the ground level, the input switching transistor goes into the cut-off state and LED remains off, thus emitting no light and therefore a photo transistor of the opto coupler receives no base drive and therefore remains in the cut-off state. Due to this output falls to ground level. In this way, the circuit provides proper amplification and isolation.

**Specifications of devices(for each circuit):**

1. Opto-coupler MCT-2E: 1 in No
2. Output amplifier transistor (2N2222): 2 no.
3. Resistances 10k:2 no, 1.2k:1 no, 470k ,3.8 k.
4. Zener diode (+12v): 1 in No copper clad sheet for making 6 circuits

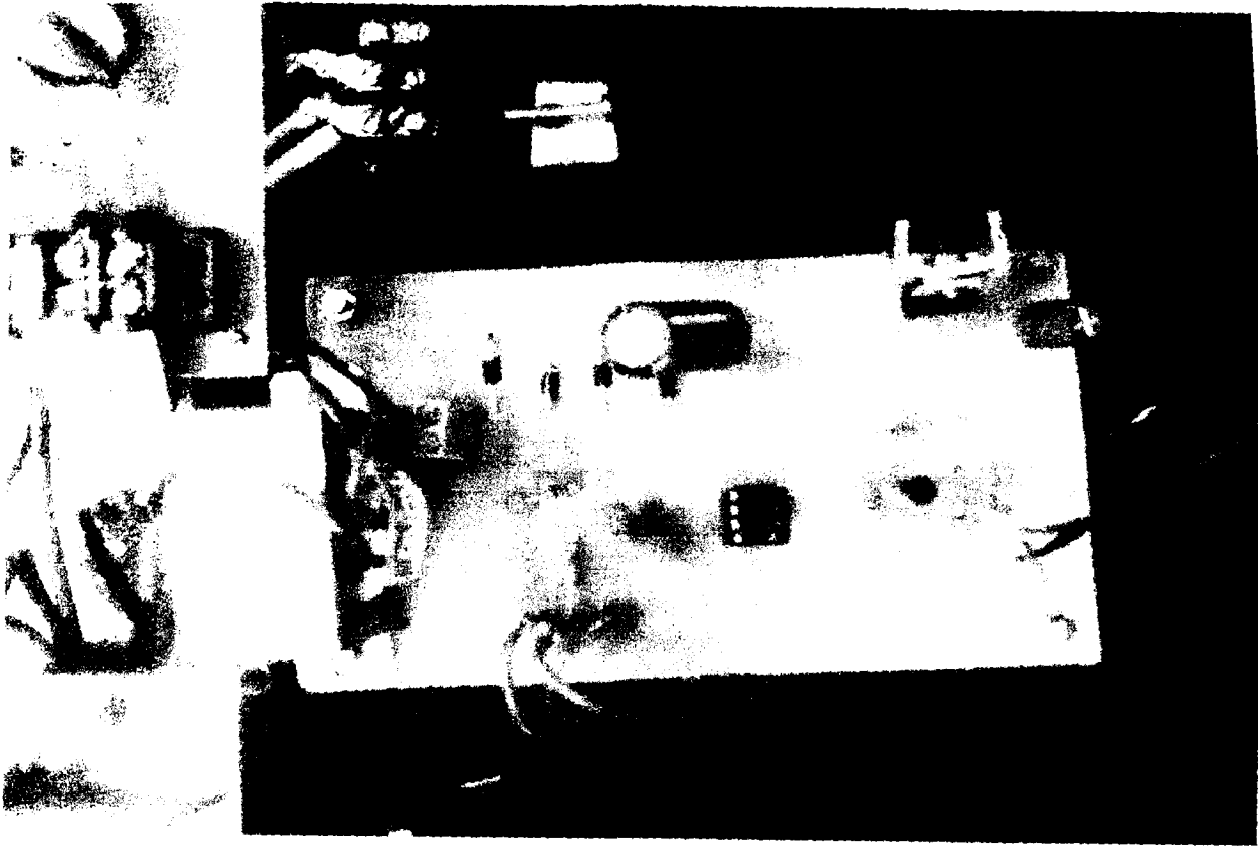


**Fig 5.3 Pulse amplification and isolation Circuit**

Six such pulse isolation and amplification circuits are made.

**5.3. POWER SUPPLIES:**

DC regulated supplies (+12v, +5v) are required for providing biasing to various circuits like pulse amplification and isolation circuits etc. using IC's 7812 for +12v and 7805 for +5 v.

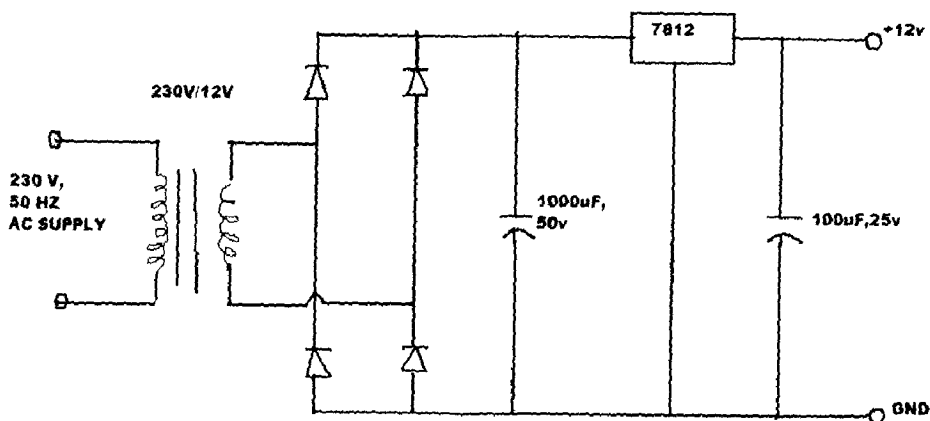


**Fig 5.4. +12V Power Supply**



Primary side of 230v/12v single phase transformer is fed through an single phase 230v, 50hz supply. Secondary side is connected to a diode bridge.

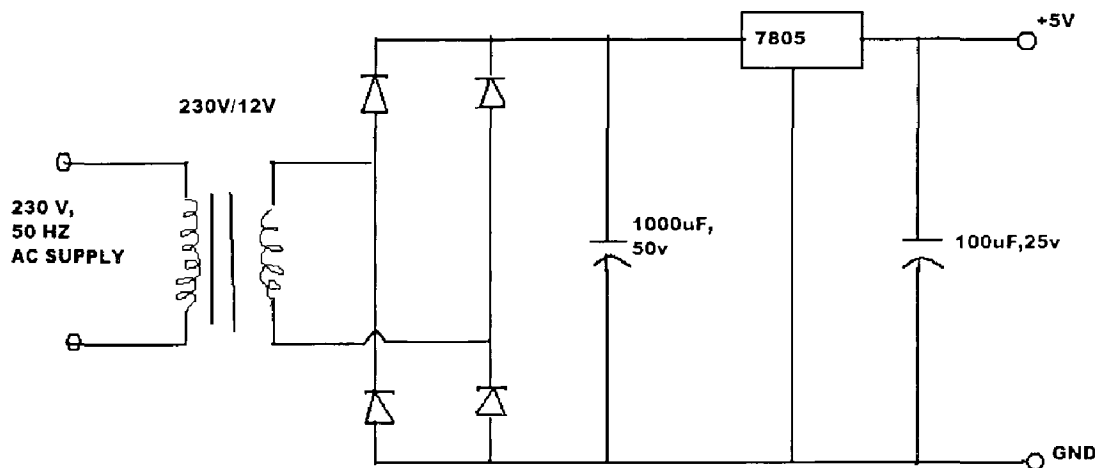


**Fig 5.5. +5V Power Supply**

**Specifications(for each circuit):**

1. IC 7805 : 1 no
2. IC 7812: 6 no.
3. Capacitors 1000uf, 50v :7 no.
4. Capacitors 100uf, 250: 7 no.
5. Diodes IN4007 : 28 No.
6. Single-phase transformers 230v/12v : 7 No.

**Six +12 V power supplies are made and one +5 V is made in the Lab.**

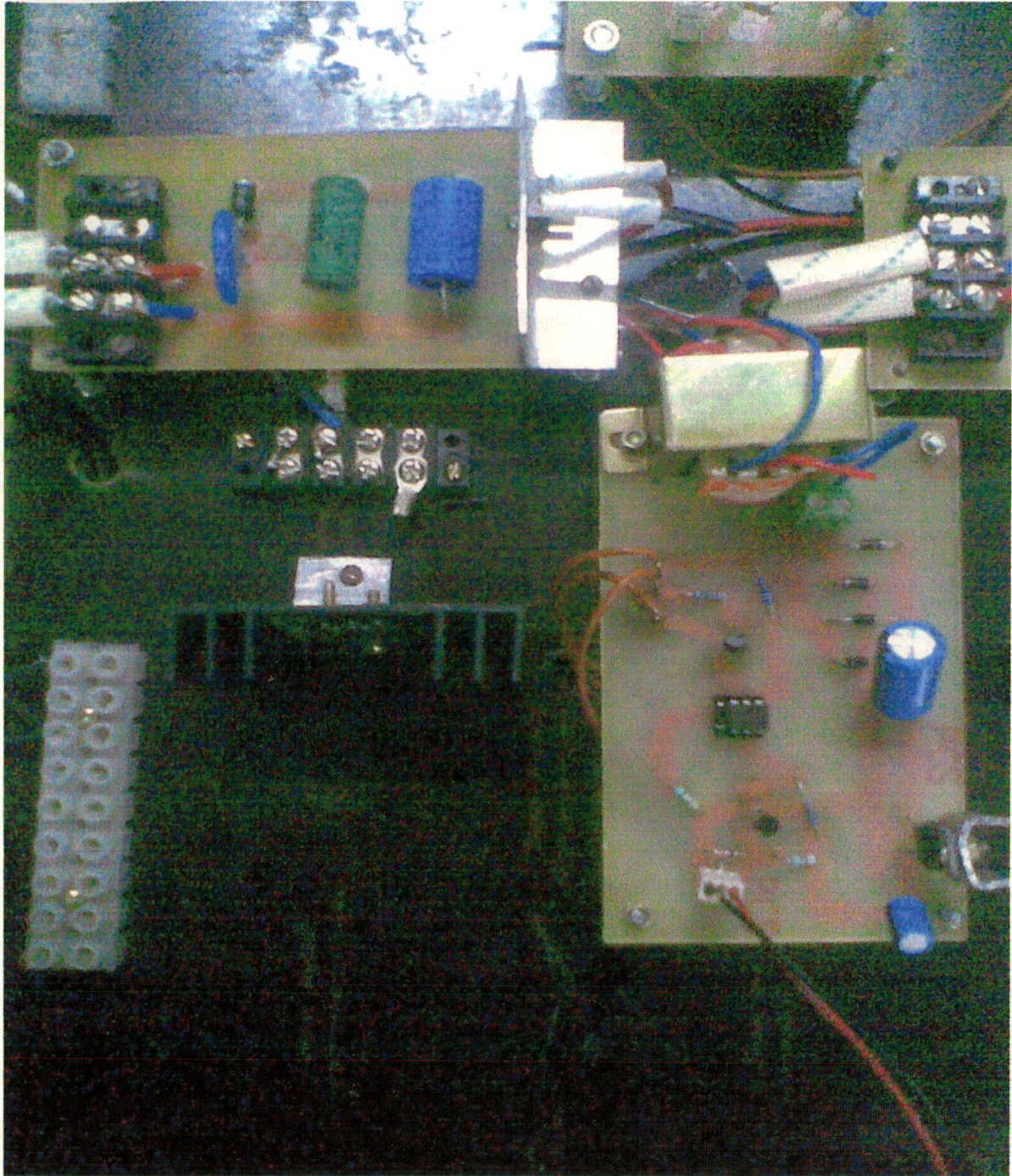


**Fig 5.6. IGBT Switch**

#### **5.4. SNUBBER CIRCUIT**

RC snubber circuit has been used for protection of the main switching device from  $dV/dT$  switching. Snubbers are therefore needed to protect the switch from transients. An additional protective metal oxide varistor is used across each device to provide the protection against over voltages across the devices.

1. Resistance 3k,10w.



- 2. Capacitor 0.01uf/250 v.
- 3. MOV (metal oxide varistor) :510v
- 4. Diode IN 5408

Six Snubber circuits are developed each for one snubber circuit.

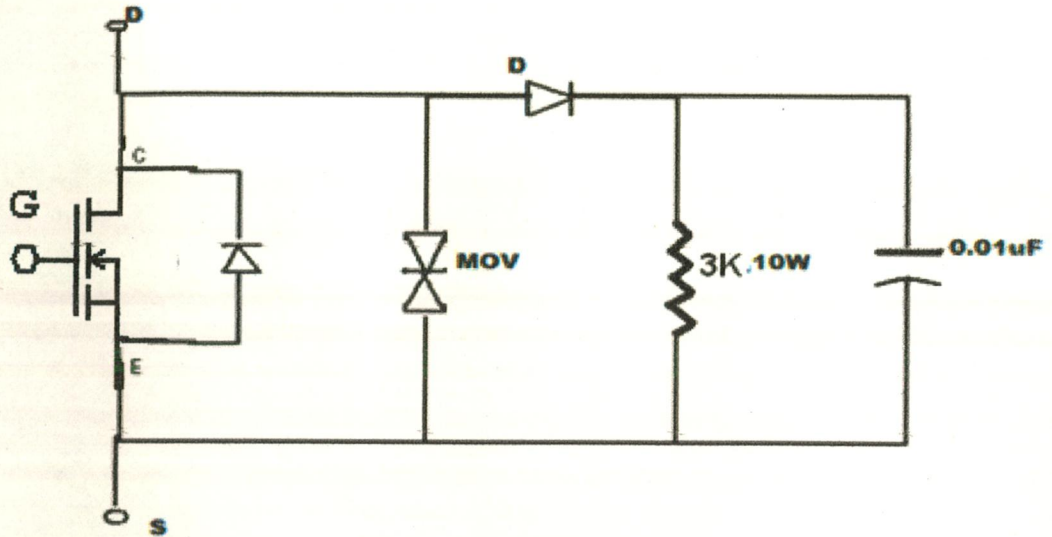


Fig 5.7. Snubber Circuit



Fig 5.8. Snubber Circuit

## 5.5 Switching Devices

In the hardware IGBT are used, the fast recovery diode is used in anti parallel with the IGBT.

### 5.5.1 IGBT

The IGBT IRG4PH40U manufactured by international Rectifiers is used in the project  
The technical specifications of the IGBT are as follows

#### Absolute Maximum Ratings

	Parameter	Max.	Units
$V_{CES}$	Collector-to-Emitter Breakdown Voltage	1200	V
$I_C @ T_C = 25^\circ\text{C}$	Continuous Collector Current	41	A
$I_C @ T_C = 100^\circ\text{C}$	Continuous Collector Current	21	
$I_{CM}$	Pulsed Collector Current $\text{\textcircled{D}}$	82	
$I_{LM}$	Clamped Inductive Load Current $\text{\textcircled{D}}$	82	
$V_{GE}$	Gate-to-Emitter Voltage	$\pm 20$	V
$E_{ARV}$	Reverse Voltage Avalanche Energy $\text{\textcircled{D}}$	270	mJ
$P_D @ T_C = 25^\circ\text{C}$	Maximum Power Dissipation	160	W
$P_D @ T_C = 100^\circ\text{C}$	Maximum Power Dissipation	65	
$T_J$ $T_{STG}$	Operating Junction and Storage Temperature Range	-55 to + 150	$^\circ\text{C}$
	Soldering Temperature, for 10 seconds	300 (0.063 in. (1.6mm) from case )	
	Mounting torque, 6-32 or M3 screw.	10 lbf•in (1.1N•m)	

### 5.5.2 Fast Recovery Diode across the IGBT

The MUR1660CT is used across the IGBT.

The technical specifications of the Fast recovery rectifier are as follows

#### MAXIMUM RATINGS

Rating	Symbol	MUR			Unit
		1620CT	1640CT	1660CT	
Peak Repetitive Reverse Voltage Working Peak Reverse Voltage DC Blocking Voltage	$V_{RRM}$ $V_{RWM}$ $V_R$	200	400	600	Volts
Average Rectified Forward Current Total Device, (Rated $V_R$ ), $T_C = 150^\circ\text{C}$	Per Leg Total Device $I_{F(AV)}$	8.0 16			Amps
Peak Rectified Forward Current (Rated $V_R$ , Square Wave, 20 kHz), $T_C = 150^\circ\text{C}$	Per Diode Leg $I_{FM}$	16			Amps
Nonrepetitive Peak Surge Current (Surge applied at rated load conditions halfwave, single phase, 60 Hz)	$I_{FSM}$	100			Amps
Operating Junction Temperature and Storage Temperature	$T_J, T_{stg}$	- 65 to +175			$^\circ\text{C}$

## 5.6 Digital Control

For implementing the control algorithm of the Z-Source Inverter DSP Processor TMS320F2812 based eZdsp is used because of the ease of implementation and high speed of execution (150 MIPS). In this eZdsp we can generate the code for the specified DSP processor from the simulink model. So here it is not required to write the code which is a laborious process.

### TMS320F2812 eZdsp BOARD

Here the DSP controller TMS320F2812 is used. The technical specifications of the DSP controller TMS320F2812 are

Specification	Rating
Instruction Cycle (at 150 MIPS)	6.67 ns
3.3-V On-Chip Flash (16-bit word)	128K
Single-Access RAM (SARAM) (16-bit word)	18K
12-Bit ADC Channels	16
Digital I/O Pins (Shared)	56
Packaging	179-ball GHH and ZHH 176-pin PGF

**Table 5.1 Specifications of TMS320F2812**

#### 5.6.1 Overview of the eZdsp F2812

The eZdsp<sup>TM</sup> F2812 is a stand-alone card, allowing evaluators to examine the TMS320F2812 digital signal processor (DSP) to determine if it meets their application requirements. Furthermore, the module is an excellent platform to develop and run software for the TMS320F2812 processor.

The eZdsp F2812 is shipped with a TMS320F2812 DSP. The eZdsp F2812 allows full speed verification of F2812 code. Two expansion connectors are provided for any necessary

evaluation circuitry not provided on the as shipped configuration. To simplify code development and shorten debugging time, a C2000 Tools Code Composer driver is provided. In addition, an onboard JTAG connector provides interface to emulators, operating with other debuggers to provide assembly language and 'C' high level language debug.

### **5.6.2. Key Features of the eZdsp F2812**

The eZdsp F2812 has the following features:

- 1) TMS320F2812 Digital Signal Processor
- 2) 150 MIPS operating speed
- 3) 18K words on-chip RAM
- 4) 128K words on-chip Flash memory
- 5) 64K words off-chip SRAM memory
- 6) 30 MHz clock
- 7) 2 Expansion Connectors (analog, I/O)
- 8) Onboard IEEE 1149.1 JTAG Controller
- 9) 5-volt only operation with supplied AC adapter
- 10) TI F28xx Code Composer Studio tools driver
- 11) On board IEEE 1149.1 JTAG emulation connector

### **5.6.3. Functional Overview of the eZdsp F2812**

Fig.3.8 shows a block diagram of the basic configuration for the eZdsp F2812. The major interfaces of the eZdsp are the JTAG interface, and expansion interface

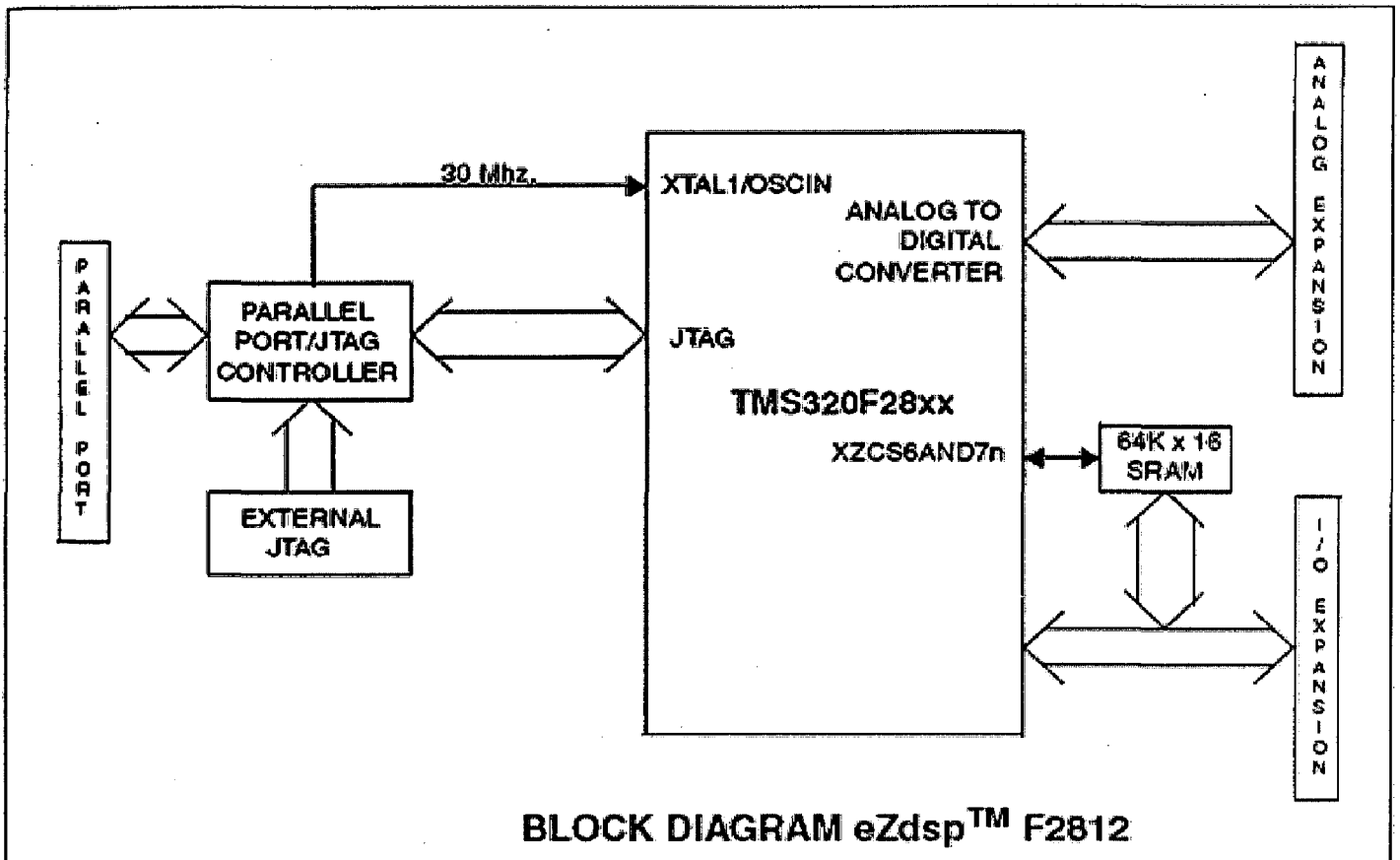
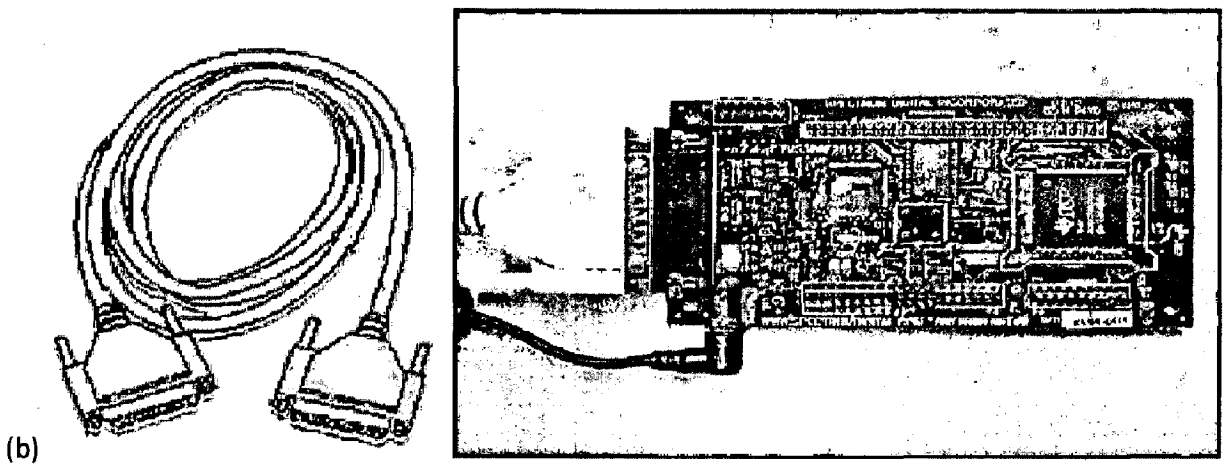


Figure 5.9 Block Diagram of eZdsp F2812

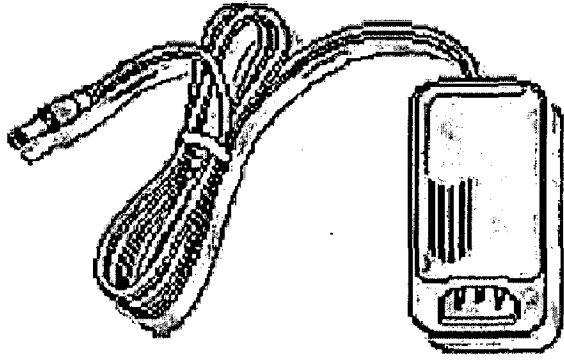
The eZdsp board supplied by the spectrum digital contains the following

- 1) eZdsp card
- 2) +5V power supply
- 3) TMS320C2000 Code Composer Studio CD ROM
- 4) TMS320F2812 eZdsp Driver CD ROM
- 5) Printer parallel port



**Parallel Port**

**(a) eZdsp Board**



**(c) +5V Power Supply**

**Figure 5.10 (a) eZdsp board (b) Parallel port (c) Power supply**

Using the parallel port the eZdsp board will be connected with the Computer. The eZdsp can be programmed with the Code Composer Studio in C language. But we can use Link for Code Composer Studio and Real-Time Workshop, Real-Time Workshop Embedded Coder to directly program the eZdsp board.

**5.6.4 CODE COMPOSER STUDIO**

Code Composer Studio (CCStudio) Integrated Development Environment (IDE) is a key element of the eXpress DSP Software and Development Tools strategy from Texas Instruments. CCStudio delivers all of the host tools and runtime software support for your TMS320 DSP and OMAP based real-time embedded applications.



CCStudio's easy to use IDE allows DSP designers of all experience levels to move quickly through each phase of the application development process including design, code and build, debug, analyze and tune. The familiar tools and interfaces allow users to get started faster and become productive immediately.

The IDE includes DSP/BIOS support, real-time analysis capabilities, debugger and optimization tools, C/C++ Compiler, Assembler, Linker, integrated CodeWright editor, visual project manager, and a variety of simulators and emulation drivers. The CCStudio IDE provides easy to use tooling that spans the entire development process. The feature set is both rich and deep so that developers can take advantage of time-saving, stress relieving productivity tools that get their applications to market quicker and take advantage of sophisticated debug tooling allowing them to find and fix real time issues. The tuning and optimization features enable developers to produce highly efficient applications taking full advantage of the device capabilities.

#### **SYSTEM HARDWARE AND SOFTWARE REQUIREMENTS**

These operating platform requirements are necessary to install the Code Composer Studio (CCS) integrated Development Environment and support the printer port. The requirements for the operating platform are:

##### **Minimum Configuration**

- a) 233 Mhz. or faster Pentium or compatible
- b) 600MB of free hard disk space
- c) Microsoft Windows 98SE, ME, N5-4 (SP 6 or higher) 2000(SP1 or higher), or XP
- d) 64MB of RAM
- e) SVGA (640x480) color display

#### **5.6.5 Link for Code Composer Studio**

Link for Code Composer Studio connects MATLAB and simulink with the Code Composer Studio embedded software development environment from texas instruments(TI). Link for code composer studio allows user to debug and verify embedded code running on TI DSPs using MTLAB scripts and Simulunk Models. User can use Link for Code Composer

Studio with Real Time Work Shop to generate complete Code Composer Studio projects, including application C code and linker command files.

Link for Code Composer Studio enables user to build, verify, and debug the embedded software application on a TI DSP at algorithmic and system level from MATLAB and Simulink. User can create complete projects in Code Composer Studio using the code generated from Simulink models by Real Time Workshop Embedded Coder.

The required software's are

**Simulink**

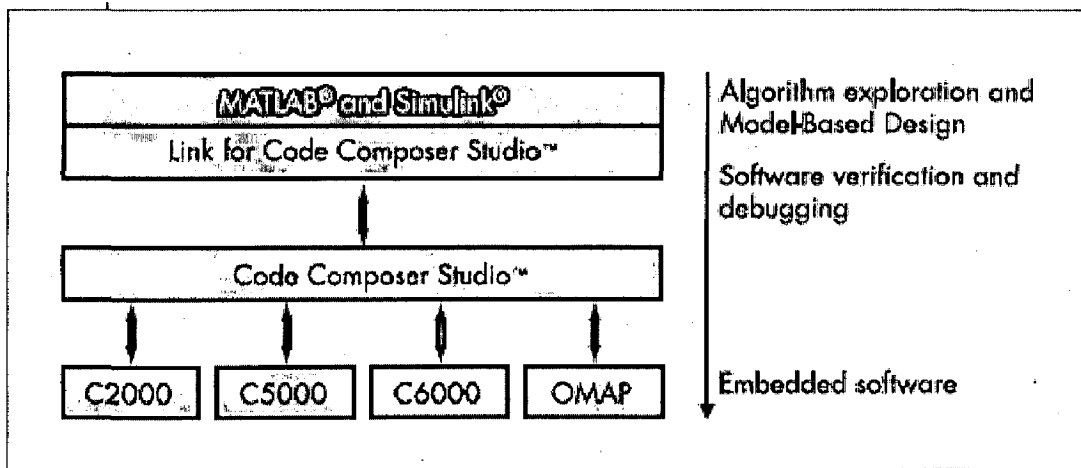
Required for using RTDX and models

**Real-Time Workshop**

Required for generating Code Composer Studio projects from Simulink Models

**Real-Time Workshop Embedded Coder**

Required for PIL simulation from Simulink.



**TMS320F2812 with matlab Simulink**

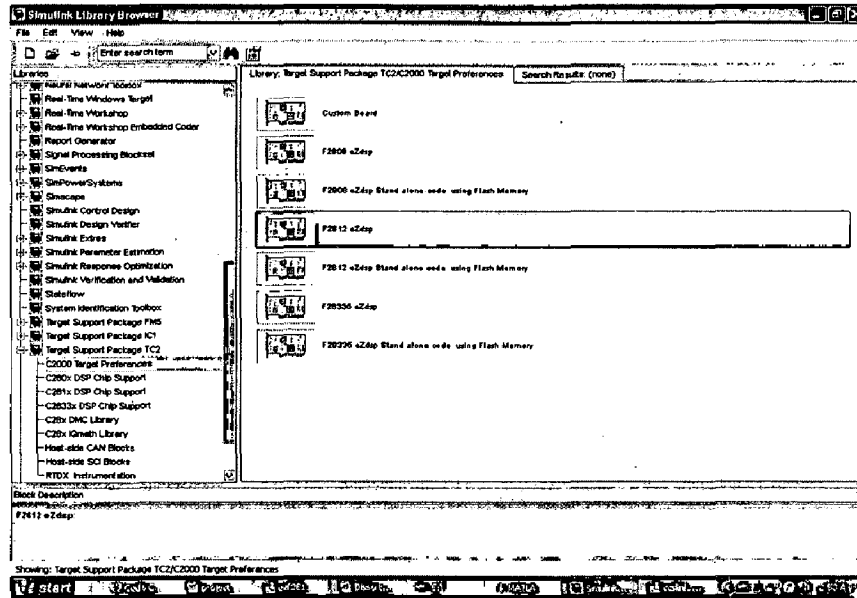


**Figure 5.11 Simulink Tool for Development of Simulink Model**

## DIGITAL CONTROL IMPLEMENTED

The z-Source Inverter control algorithm is implemented on the eZdsp board. In this process first The simulink model of the control scheme is developed which is shown in the below figure Fig.5.13. Then from the simulink model the RealtimeTarget will generate the C-Code of the control Model. Then the Simulink CCS(Code Composer Studio) Link will Connect to the Code Composer Studio Software and the project will be developed which can be dumped into the DSP Processor. This entire process will be done by the 'Incremental Build' option available in the Matlab Simulink.

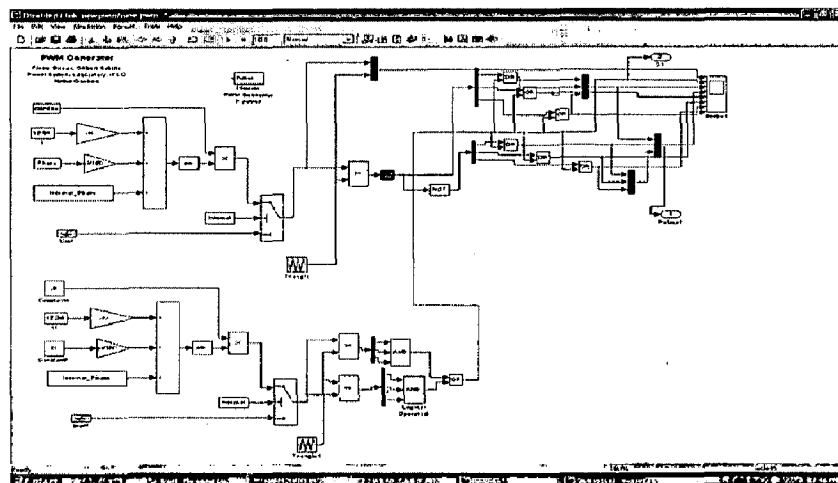


**Fig.5.13 Simulink Model of Open Loop Control of Z-Source Inverter**

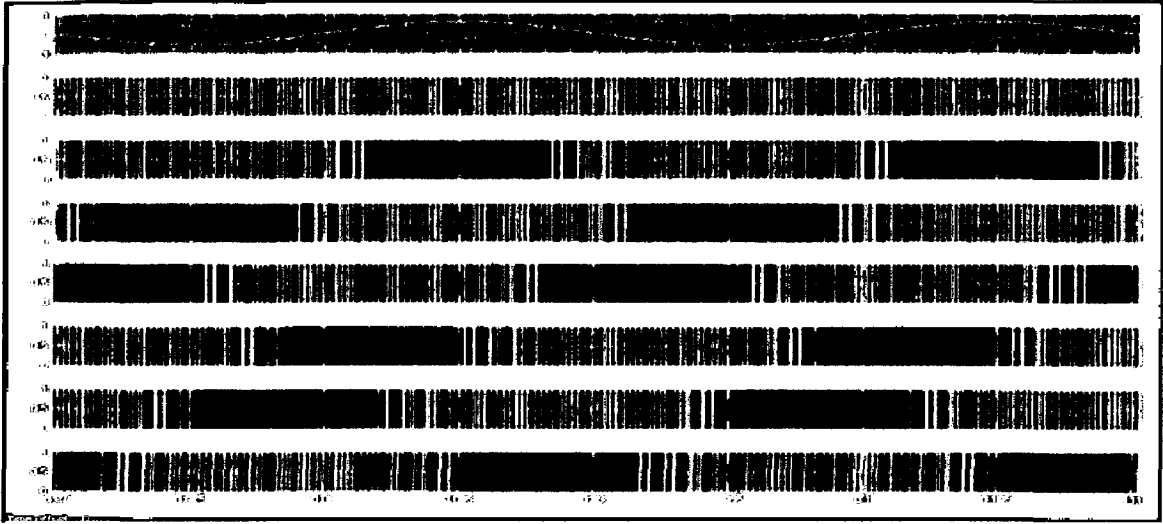


**Fig.5.14 The Pulses Generated**

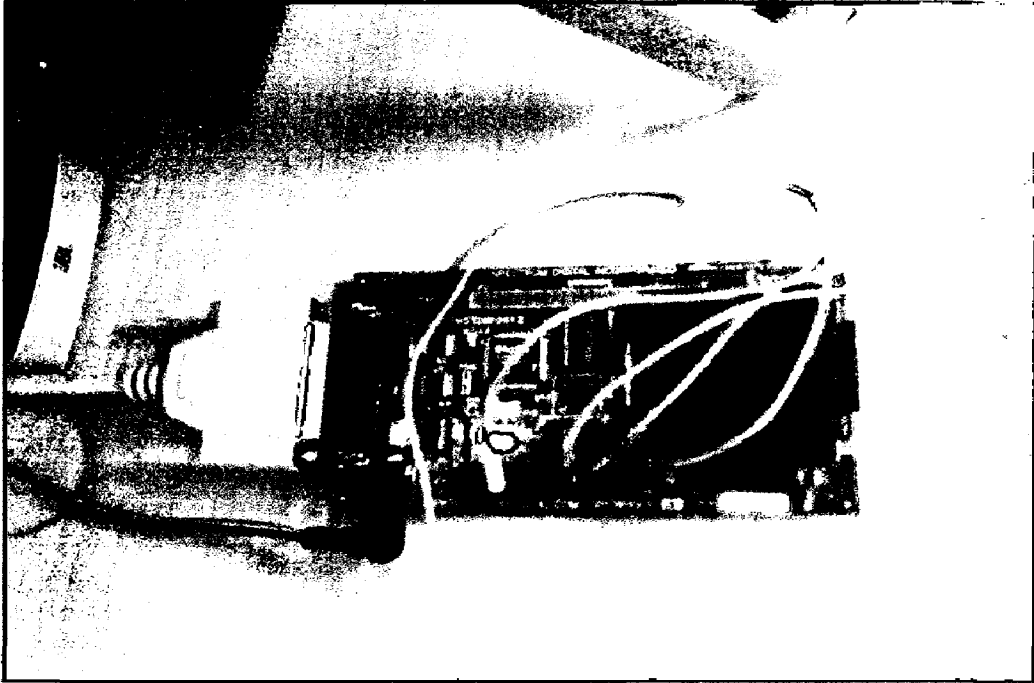
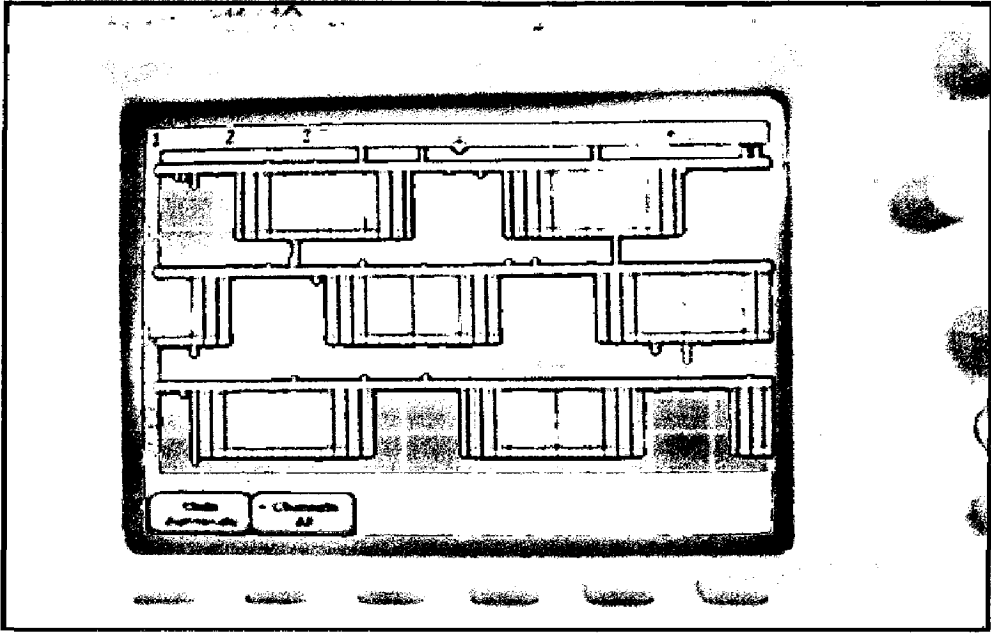
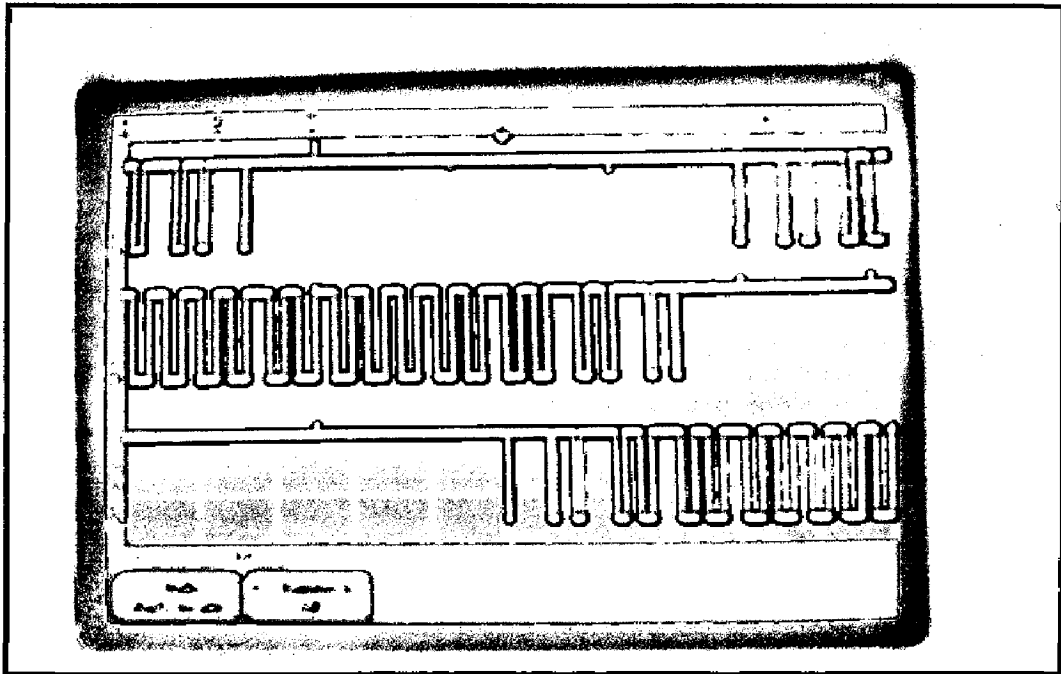


**Fig 5.15 eZdsp kit**



(a)



(b)

**Fig 5.16 Pulses Generated (a) and (b)**

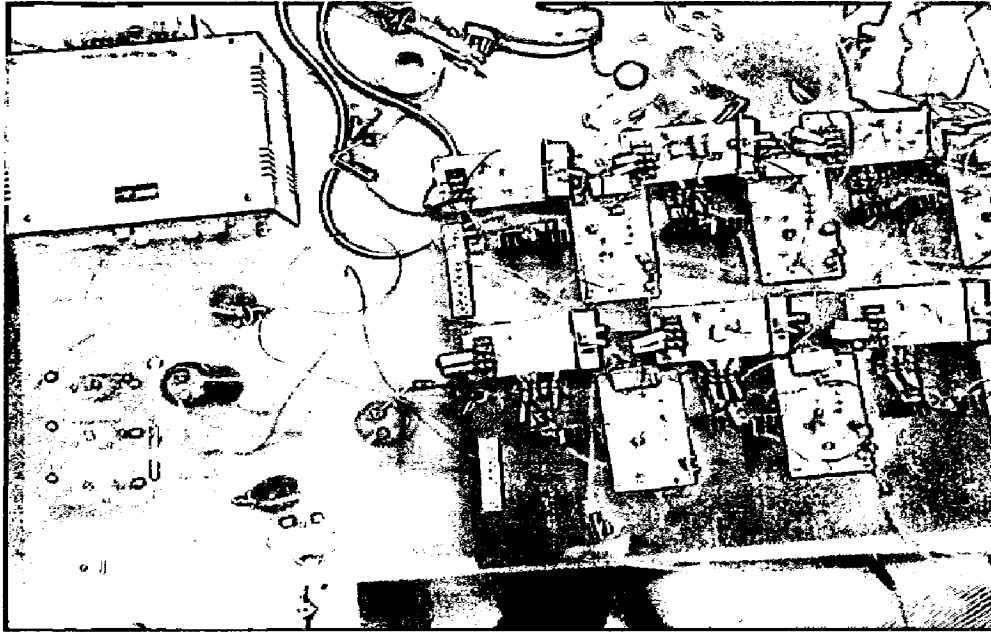


**Fig 5.17 Power Circuit**

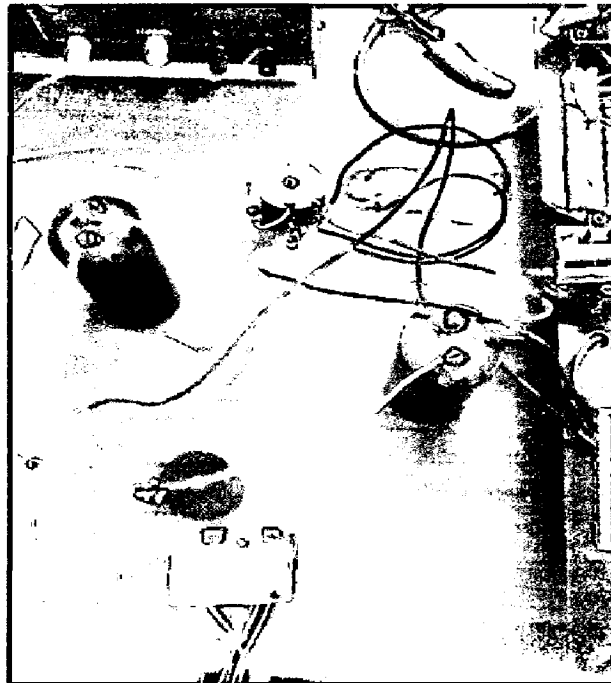


**Fig 5.18 Impedance Network**

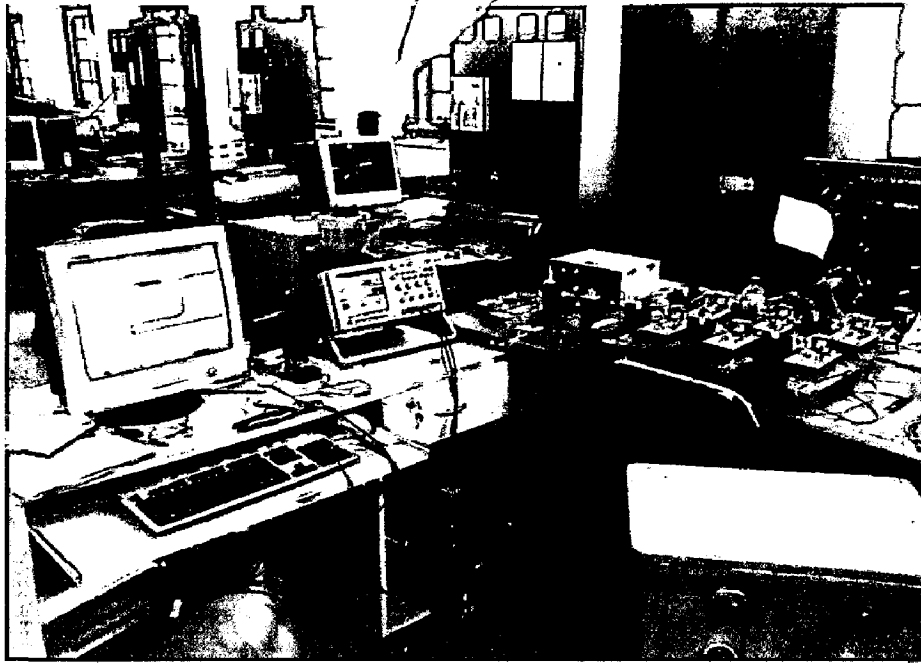


**Fig 5.19 Hardware setup**

## **5.7 Conclusion**

The hardware is developed in the laboratory for testing purpose. The control is implemented on the TMS320F2812 DSP processor based eZdsp.

### Conclusions and Scope for Future Work

---

The Z-Source Inverter can Boost the voltages without additional stage, which increase the system efficiency and reduces the cost. The Voltage Boost operation is possible because of the Impedance network present in the Z-Source Inverter. Different controlling methods are given like Boost Control, Constant Boost Control. The SVM technique has been modified to use for the Z-Source Inverter. Closed loop voltage control is used in this work. Both the Capacitor voltage and AC Voltage, AC output Currents are taken as reference.

The Modified Space Vector Modulation is simulated in closed loop control with various sources like Photo Voltaic Cell, Fuel Cell. The FFT analysis of output voltages and currents is carried out.

Hardware is developed in the laboratory. The control scheme is implemented on TMS320F2812 DSP processor based eZdsp.

The PI Controller is used in this control scheme. Because of PI controller wide range of Voltage control is not possible. The neural network trained controllers can be developed to tune the PI controller online.



## References

1. Fang. Z. Peng, "Z-source inverter" *Proc. of IEEE IAS 2002*, pp.775 - 781.
2. Fang. Z. Peng, "Z-source inverter" *IEEE Transactions on Industry Applications*, **39**(2), March–April 2003, pp. 504–510.
3. Fang. Z. Peng, Xiaoming Yuan, Xupeng Fang, and Zhaoming Qian, "Z-source inverter for adjustable speed drives," *IEEE Power Electronics Letters*, **1**(2), June 2003, pp. 33–35.
4. Fang. Z. Peng, "Z-source inverter for adjustable speed drives," IEEE/PESC Aachen, 2004, pp. 249–254.
5. Fang. Z. Peng, Miaosen Shen, and Zhaoming Qian, "Maximum boost control of the Z-source inverter," IEEE/PESC Aachen, 2004, pp. 255–260.
6. Miaosen Shen, Alan Joseph, Jin Wang, Fang Z. Peng, and Donald J. Adams, "Comparison of traditional inverter and Z-Source inverter for fuel cell vehicles," IEEE WPET 2004, pp. 125–132
7. Fang. Z. Peng, Miaosen Shen, and Zhaoming Qian, "Maximum boost control of the Z-source inverter," published in *IEEE transactions on Power Electronics*, **20**(4), 2005.
8. Miaosen Shen, Alan Joseph, Jin Wang, Fang Z. Peng, and Donald J. Adams, "Comparison of traditional inverters and Z-source inverter," to be presented at IEEE PESC 2005.
9. Y. Huang, M. Shen, F. Z. Peng, and J. Wang, "Z-source inverter for residential photovoltaic system," *IEEE Trans. Power Electron.*, vol. 21, no. 6, pp. 1176-1782, Nov. 2006.
- 11) . Fang Z. Peng, Miaosen Shen, and Zhaoming Qian "Maximum Constant Boost Control" published in *IEEE transactions on Power Electronics*, **20**(4), 2006.
12. Q. Zeng and L. Chang, "Improved current controller based on SVPWM for three-phase grid-connected voltage source inverters" in *Proc. IEEE Power Electron. Spec. Conf.*, Jun. 2005, pp. 2912-2917.
- 12) F. Z. Peng, M. Shen, K. Holland, "Application of Z-source inverter for traction drive of fuel cell-battery hybrid electric vehicles," *IEEE Trans. Power Electron.*, vol. 22, no. 3, pp. 1054 1061, May 2007.
- 13). M. Shen, A. Joseph, Jin Wang, F. Z. Peng and D. J. Adams, "Comparison of the traditional inverters and Z-source inverter for fuel cell vehicles," *IEEE Trans. Power Electron.*, vol.22, no.4, pp. 1453-1463, Jul. 2007.
- 14) M. Shen, J. Wang, A. Joseph, F. Z. Peng, L. M. Tolbert, and D. J. Adams, "Constant boost control of the Z-source inverter to minimize current ripple and voltage stress," *IEEE Trans. Ind. Appl.*, vol. 42, no. 3, pp. 770–778, May/June. 2006.

15. X. Ding, Z. Qian, S. Yang, B. Cui, and F. Z. Peng, "A Direct Peak DC-link Boost Voltage Control Strategy in Z-Source Inverter" in *Proc. IEEE Applied Power Electron. Conf.*, Feb. 2007, pp. 648-653.
16. X. Ding, Z. Qian, S. Yang, B. Cui, and F. Z. Peng, "A PID Control Strategy for DC-link Boost Voltage in Z-Source Inverter," in *Proc. IEEE Applied Power Electron. Conf.*, Feb. 2007, pp. 1145-1148.
17. Q. Tran, T. Chun, J. Ahn, and H. Lee, "Algorithms for controlling both the dc boost and ac output voltage of Z-source inverter," *IEEE Trans. Ind. Electron.*, vol. 54, no.5, pp. 2745-2750, Oct. 2007.
18. Jin-Woo Jung, *Member, IEEE*, and Ali Keyhani, "Control of a Fuel Cell Based Z-Source Converter" in *IEEE Transactions on Energy Conversion*, Vol. 22, No. 2, June 2007
16. EMI Experimental Comparison of PWM Inverters Between Hard- and Soft-Switching Techniques by Y. Tang, H. Zhu, B. Song, J. S. Lai Virginia Polytechnic Institute & State University and C. Chen Scientific Research Lab. Ford Motor Company 7803-4398 1998 IEEE
17. Packaging and Performance of an IGBT-Based Hybrid Electric Vehicle Philip T. Krein, Timothy G. Roethemeytx, Robert A. W t e , Brandon R Masterson, Proceedings of IEEE conference on Powerelectronics in Transportation 2002
18. K. Wang, C. Y. Lin, L. Zhu, D. Qu, F. C. Lee, J. S. Lai Bi-directional DC to DC Converters for Fuel Cell Systems ,proceedings of Power electronics in Transportation conference 1998, IEEE Catalogue No. 98TH8349
19. Miaosen Shen, and Fang Z. Peng, "Operation Modes and Characteristics of the Z-Source Inverter with Small Inductance," IEEE IAS 2005, pp. 1253-1260
20. J. Liu, J. Hu, and L. Xu;" A Modified Space Vector PWM for Z-Source Inverter - Modeling and Design" in *Proc. of International Conference on Electrical Machines and Systems*, 2005. Volume 2, pp.1242 – 1247, 27-29 Sept. 2005.
21. C.J.Gajanayake, D.M.Vilahgamuwa, and P.Loh, " Modeling and design of multi loop controller for Z-Source inverter for Distributed Generation", In *Proc.IEEE Power Electronics Specialists Conference*, 2006,pp. 1353-1359,June, 2006.

## **BIBLIOGRAPHY:**

- 1 .Pulse width modulation for power converters By D. Grahame Holmes, T. A. Lipo
2. Power electronics and motor drives By Bimal K. Bose
3. Power electronics handbook By M. H. Rashid
4. Battery reference book By Thomas Roy Crompton
5. The Electric Vehicle Hand-book By Harry Cooke Cushing, Frank Whitney Smith
6. Fuel cells Hand Book EG&G Technical Services, Inc.
7. Modern electric, hybrid electric, and fuel cell vehicles By Mehrdad Ehsani, Sebastien E. Gay

# Appendix

## Data Sheet Of Photo Voltaic cell

Parameters	Values
Solar irradiation in $W/m^2$	0.5
Short Circuit current	5A
Operating Temperature	45°C
Reverse saturation Current	19.963 $\mu$ A
Open circuit voltage	15V
S.C Temperature coefficient	0.0017A/°C
Reference Temperature	301.18°K
Curve fitting constant(A)	1.92
Ideality factor	0.8
Boltzmann Constant(joule/ <sup>0</sup> KT)	1.38*10 <sup>-23</sup>
Band gap for silicon	1.12ev
Charge of electron(C)	1.69*10 <sup>-19</sup>
Series resistance	0.1 $\Omega$
Shunt resistance	45 M $\Omega$
No. of cells connected	10

# Block Parameters: Fuel Cell Stack



Fuel Cell Stack (mask) (link)

Implements a generic hydrogen fuel cell model which allows the simulation for the following types of cells:

- Proton Exchange Membrane Fuel Cell (PEMFC)
- Solid Oxide Fuel Cell (SOFC)
- Alkaline Fuel Cell (AFC)

Parameters

Signal variation

Fuel Cell Dynamics

Preset model: PEMFC - 6 kW - 45 Vdc

Model detail Level: Detailed

Open circuit voltage (V)

65

Nominal operating point [ $I_{nom}(A)$ ,  $V_{nom}(V)$ ]

[133.3, 45]

Maximum operating point [ $I_{end}(A)$ ,  $V_{end}(V)$ ]

[225, 37]

Number of cells

65

Nominal stack efficiency (%)

55

Operating temperature (celcius)

65

Nominal Air flow rate (lpm)

300

Nominal supply pressure [Fuel (bar), Air (bar)]

[1.5, 1]

Nominal composition (%) [H2 O2 H2O(Air)]

[99.95, 21, 1]

Plot V-I characteristic

View Cell parameters

OK

Cancel

Help

Apply

## **Simulation Circuit Details**

### **1) Maximum Boost Control Technique Simulation**

**C=1.3mF**

**L=1mH**

**Filter Capacitance = 200 $\mu$ F**

**Filter Inductance = 2mH**

**Input DC Voltage = 145 V**

**Under Load Condition**

**Active Power = 8e3**

**Inductive Reactive Power = 6e3**

**Modulation Index = 0.812**

### **2) Maximum Boost Control Technique Simulation With Third Harmonic Injection.**

**C=1.3mF**

**L=1mH**

**Filter Capacitance = 200 $\mu$ F**

**Filter Inductance = 2mH**

**Input DC Voltage = 250 V**

**Load Resistance = 5  $\Omega$**

### **3) MSVM with DC Supply**

**C=22 $\mu$ F**

**L=3.5mH**

**Filter Capacitance = 250 $\mu$ F**

**Filter Inductance = 2mH**

**Input DC Voltage = 145 V**

**Active Power = 8e3**

**Inductive Reactive Power = 6e3**

### **4) MSVM with Photo Voltaic Cell**

**C=22 $\mu$ F**

**L=3.5mH**

**Filter Capacitance = 15 $\mu$ F**

**Filter Inductance = 3mH**

**Input DC Voltage = 145 V**

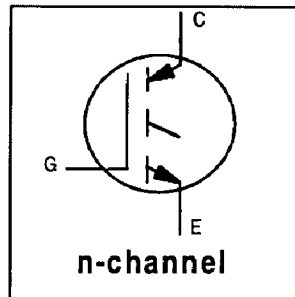
**Active Power = 8e3**

**Inductive Reactive Power = 6e3**



### Features

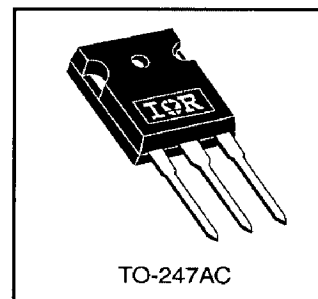
- UltraFast: Optimized for high operating frequencies up to 40 kHz in hard switching, >200 kHz in resonant mode.
- New IGBT design provides tighter parameter distribution and higher efficiency than previous generations
- Optimized for power conversion; SMPS, UPS and welding
- Industry standard TO-247AC package



$V_{CES} = 1200V$
$V_{CE(on)} \text{ typ.} = 2.43V$
@ $V_{GE} = 15V, I_C = 21A$

### Benefits

- Higher switching frequency capability than competitive IGBTs
- Highest efficiency available
- Much lower conduction losses than MOSFETs
- More efficient than short circuit rated IGBTs



### Absolute Maximum Ratings

	Parameter	Max.	Units
$V_{CES}$	Collector-to-Emitter Breakdown Voltage	1200	V
$I_C @ T_C = 25^\circ C$	Continuous Collector Current	41	A
$I_C @ T_C = 100^\circ C$	Continuous Collector Current	21	
$I_{CM}$	Pulsed Collector Current ①	82	
$I_{LM}$	Clamped Inductive Load Current ②	82	
$V_{GE}$	Gate-to-Emitter Voltage	$\pm 20$	V
$E_{ARV}$	Reverse Voltage Avalanche Energy ③	270	mJ
$P_D @ T_C = 25^\circ C$	Maximum Power Dissipation	160	W
$P_D @ T_C = 100^\circ C$	Maximum Power Dissipation	65	
$T_J$	Operating Junction and	-55 to +150	°C
$T_{STG}$	Storage Temperature Range		
	Soldering Temperature, for 10 seconds	300 (0.063 in. (1.6mm) from case )	
	Mounting torque, 6-32 or M3 screw.	10 lbf•in (1.1N•m)	

### Thermal Resistance

	Parameter	Typ.	Max.	Units
$R_{\theta JC}$	Junction-to-Case	—	0.77	°C/W
$R_{\theta CS}$	Case-to-Sink, Flat, Greased Surface	0.24	—	
$R_{\theta JA}$	Junction-to-Ambient, typical socket mount	—	40	
Wt	Weight	6 (0.21)	—	g (oz)

## Electrical Characteristics @ $T_J = 25^\circ\text{C}$ (unless otherwise specified)

	Parameter	Min.	Typ.	Max.	Units	Conditions
$V_{(BR)CES}$	Collector-to-Emitter Breakdown Voltage	1200	—	—	V	$V_{GE} = 0V, I_C = 250\mu A$
$V_{(BR)ECS}$	Emitter-to-Collector Breakdown Voltage ④	18	—	—	V	$V_{GE} = 0V, I_C = 1.0A$
$\Delta V_{(BR)CES}/\Delta T_J$	Temperature Coeff. of Breakdown Voltage	—	0.43	—	V/°C	$V_{GE} = 0V, I_C = 1.0mA$
$V_{CE(ON)}$	Collector-to-Emitter Saturation Voltage	—	2.43	3.1	V	$I_C = 21A$ $V_{GE} = 15V$ See Fig.2, 5
		—	2.97	—		
		—	2.47	—		
$V_{GE(th)}$	Gate Threshold Voltage	3.0	—	6.0		$V_{CE} = V_{GE}, I_C = 250\mu A$
$\Delta V_{GE(th)}/\Delta T_J$	Temperature Coeff. of Threshold Voltage	—	-11	—	mV/°C	$V_{CE} = V_{GE}, I_C = 250\mu A$
$g_{fe}$	Forward Transconductance ⑤	16	24	—	S	$V_{CE} = 100V, I_C = 21A$
$I_{CES}$	Zero Gate Voltage Collector Current	—	—	250	$\mu A$	$V_{GE} = 0V, V_{CE} = 1200V$
		—	—	2.0		$V_{GE} = 0V, V_{CE} = 10V, T_J = 25^\circ\text{C}$
		—	—	5000		$V_{GE} = 0V, V_{CE} = 1200V, T_J = 150^\circ\text{C}$
$I_{GES}$	Gate-to-Emitter Leakage Current	—	—	$\pm 100$	nA	$V_{GE} = \pm 20V$

## Switching Characteristics @ $T_J = 25^\circ\text{C}$ (unless otherwise specified)

	Parameter	Min.	Typ.	Max.	Units	Conditions
$Q_g$	Total Gate Charge (turn-on)	—	86	130	nC	$I_C = 21A$ $V_{CC} = 400V$ $V_{GE} = 15V$ See Fig. 8
$Q_{ge}$	Gate - Emitter Charge (turn-on)	—	13	20		
$Q_{gc}$	Gate - Collector Charge (turn-on)	—	29	44		
$t_{d(on)}$	Turn-On Delay Time	—	24	—	ns	$T_J = 25^\circ\text{C}$ $I_C = 21A, V_{CC} = 960V$ $V_{GE} = 15V, R_G = 10\Omega$ Energy losses include "tail" See Fig. 9, 10, 14
$t_r$	Rise Time	—	24	—		
$t_{d(off)}$	Turn-Off Delay Time	—	220	330		
$t_f$	Fall Time	—	180	270		
$E_{on}$	Turn-On Switching Loss	—	1.04	—	mJ	See Fig. 9, 10, 14
$E_{off}$	Turn-Off Switching Loss	—	3.40	—		
$E_{ts}$	Total Switching Loss	—	4.44	5.2	mJ	$T_J = 150^\circ\text{C}$ , $I_C = 21A, V_{CC} = 960V$ $V_{GE} = 15V, R_G = 10\Omega$ Energy losses include "tail" See Fig. 11, 14
$t_{d(on)}$	Turn-On Delay Time	—	24	—		
$t_r$	Rise Time	—	25	—		
$t_{d(off)}$	Turn-Off Delay Time	—	310	—		
$t_f$	Fall Time	—	380	—	nH	Measured 5mm from package
$E_{ts}$	Total Switching Loss	—	7.39	—		
$L_E$	Internal Emitter Inductance	—	13	—	pF	$V_{GE} = 0V$ $V_{CC} = 30V$ $f = 1.0MHz$ See Fig. 7
$C_{ies}$	Input Capacitance	—	1800	—		
$C_{oes}$	Output Capacitance	—	120	—		
$C_{res}$	Reverse Transfer Capacitance	—	18	—		

### Notes:

- ① Repetitive rating;  $V_{GE} = 20V$ , pulse width limited by max. junction temperature. ( See fig. 13b )
- ②  $V_{CC} = 80\%(V_{CES})$ ,  $V_{GE} = 20V$ ,  $L = 10\mu H$ ,  $R_G = 10\Omega$ , (See fig. 13a)
- ③ Repetitive rating; pulse width limited by maximum junction temperature.
- ④ Pulse width  $\leq 80\mu s$ ; duty factor  $\leq 0.1\%$ .
- ⑤ Pulse width  $5.0\mu s$ , single shot.

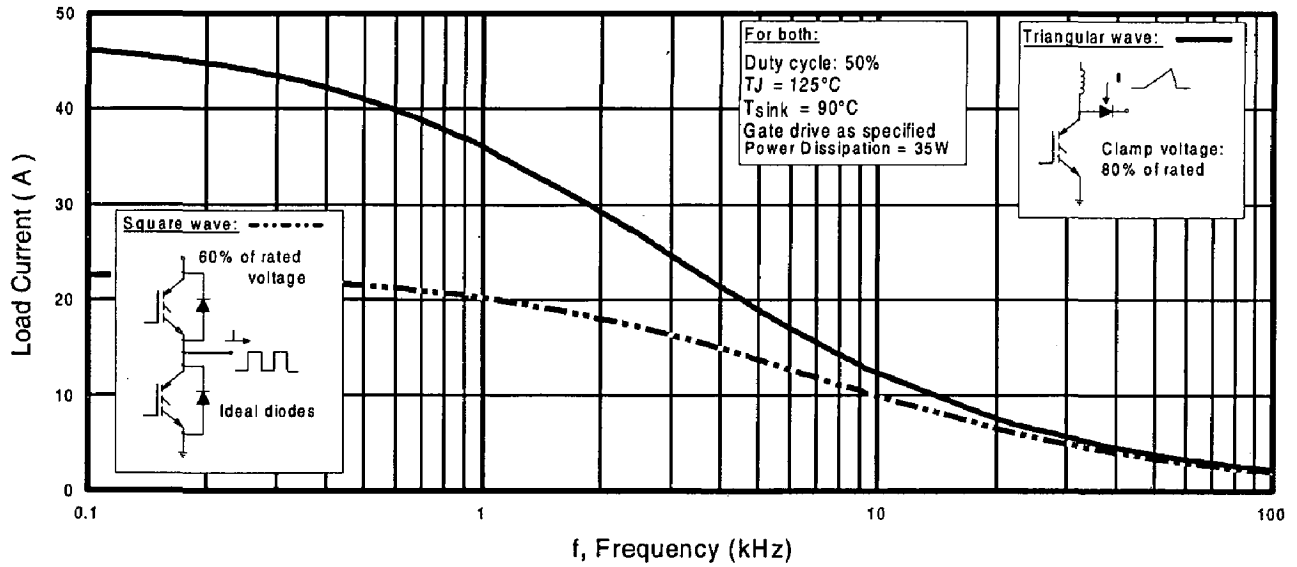


Fig. 1 - Typical Load Current vs. Frequency  
(Load Current =  $I_{\text{RMS}}$  of fundamental)

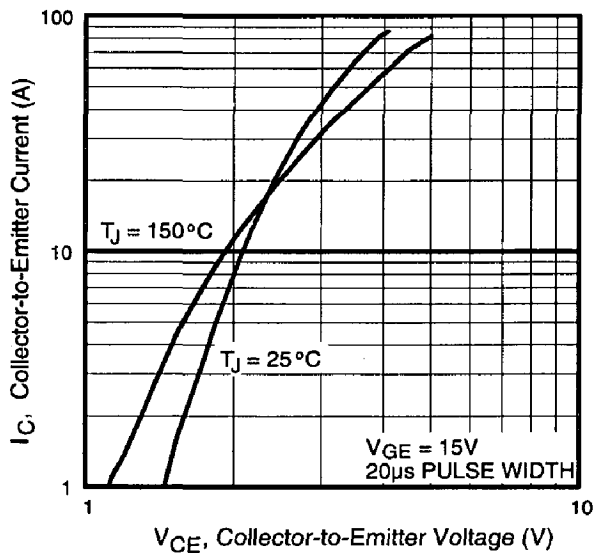


Fig. 2 - Typical Output Characteristics

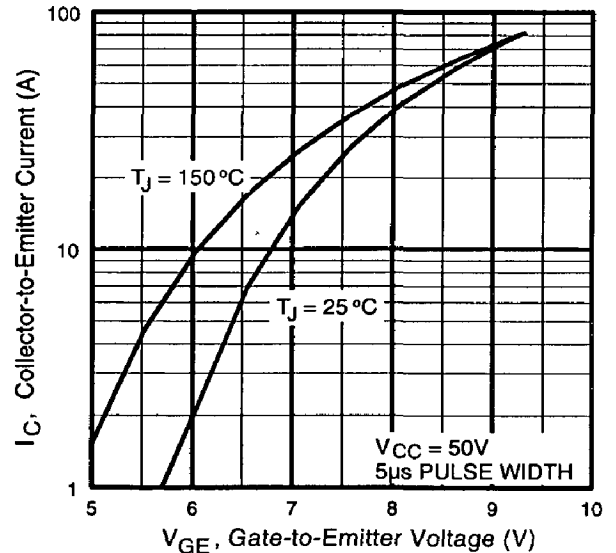


Fig. 3 - Typical Transfer Characteristics

# IRG4PH40U

International  
**IRF** Rectifier

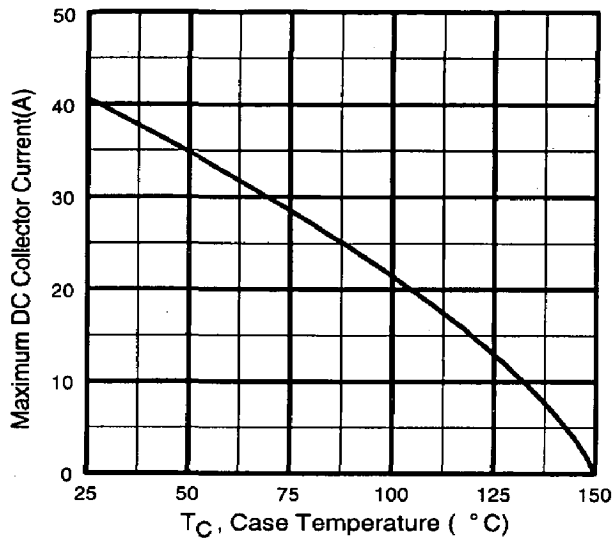


Fig. 4 - Maximum Collector Current vs. Case Temperature

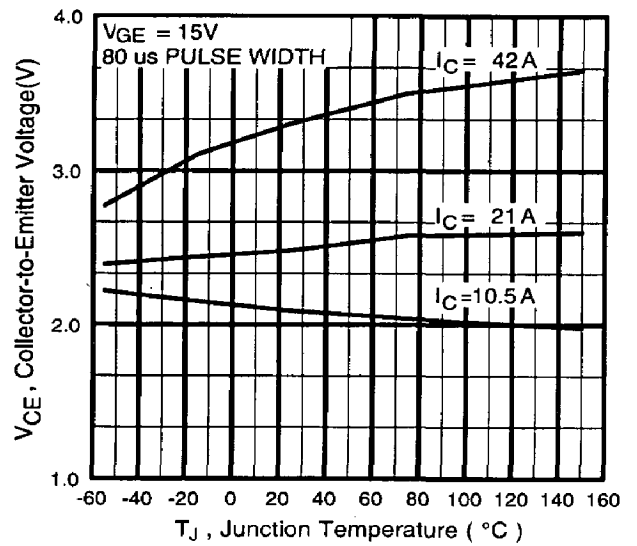


Fig. 5 - Typical Collector-to-Emitter Voltage vs. Junction Temperature

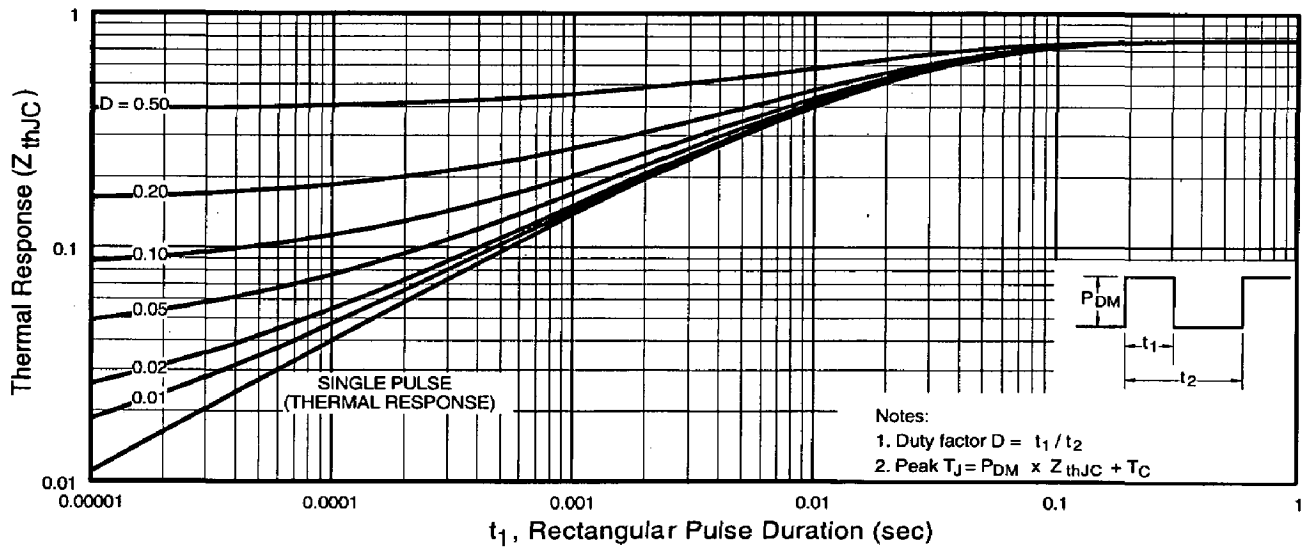


Fig. 6 - Maximum Effective Transient Thermal Impedance, Junction-to-Case

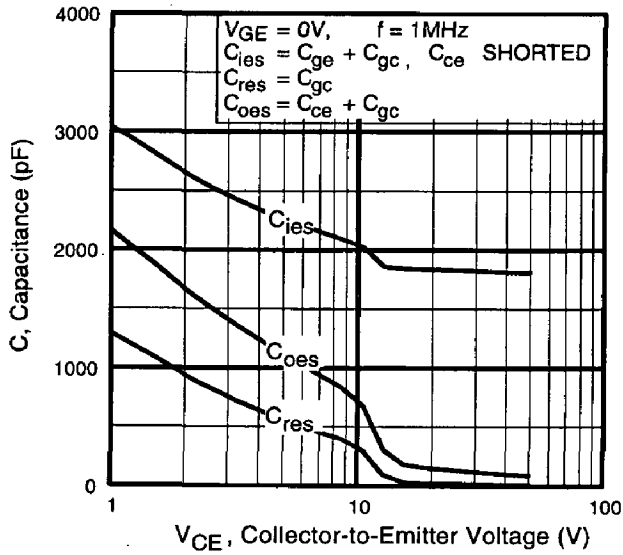


Fig. 7 - Typical Capacitance vs. Collector-to-Emitter Voltage

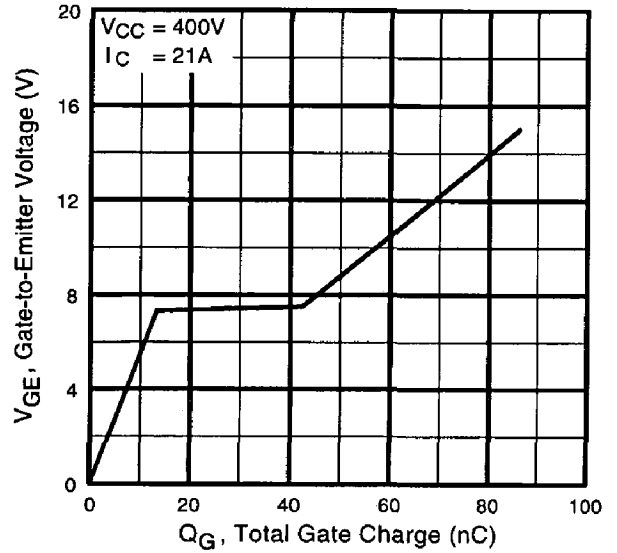


Fig. 8 - Typical Gate Charge vs. Gate-to-Emitter Voltage

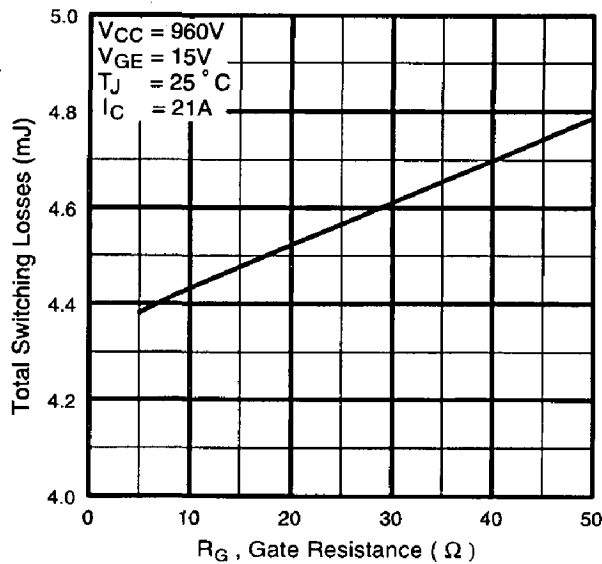


Fig. 9 - Typical Switching Losses vs. Gate Resistance

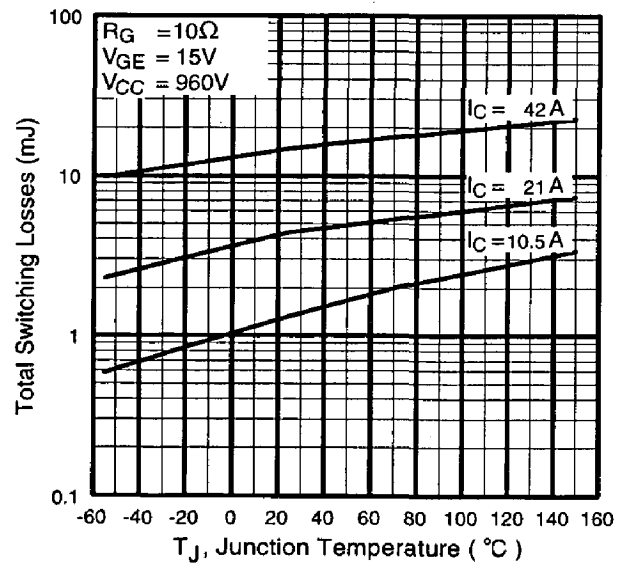
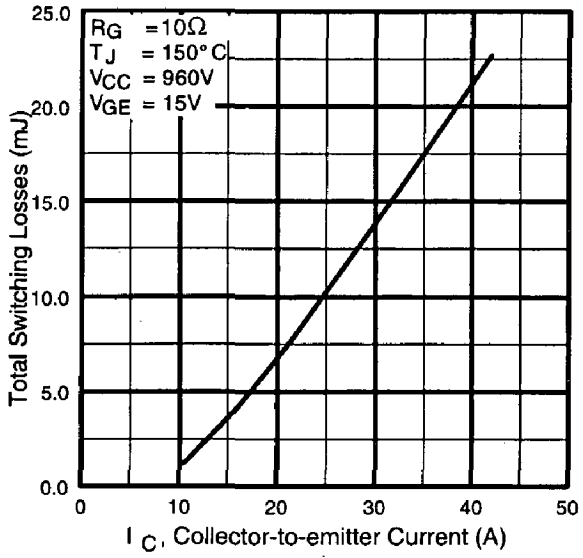


Fig. 10 - Typical Switching Losses vs. Junction Temperature

# IRG4PH40U

International  
**IR** Rectifier



**Fig. 11** - Typical Switching Losses vs. Collector-to-Emitter Current

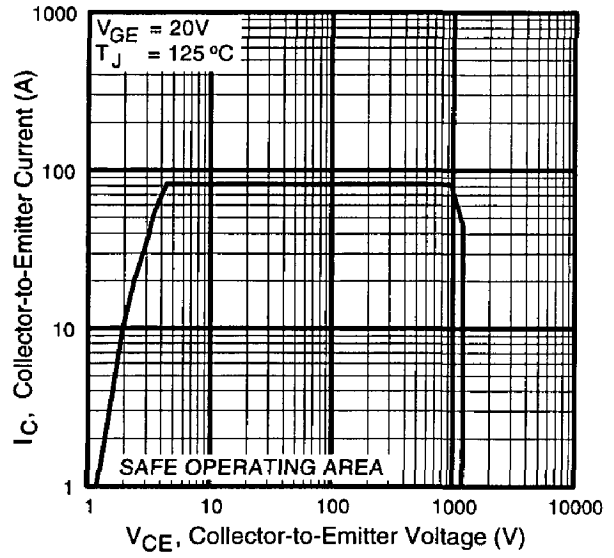


**Fig. 12** - Turn-Off SOA





# MUR1620CT THRU MUR1660CT

## 16.0 AMPS. Switchmode Power Rectifiers



Voltage Range  
200 to 600 Volts  
Current  
16.0 Ampere

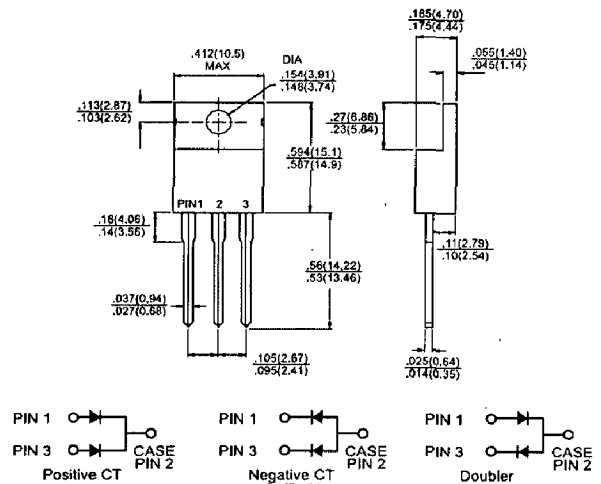
### Features

- ◇ Ultrafast 35 and 60 Nanosecond Recovery times
- ◇ 175°C Operating Junction Temperature
- ◇ Popular TO-220 Package
- ◇ Epoxy meets UL94, V<sub>0</sub> @ 1/8"
- ◇ High temperature glass passivated junction
- ◇ High voltage capability to 600 volts
- ◇ Low leakage specified @ 150°C case temperature
- ◇ Current derating @ both case and ambient temperatures

### Mechanical Data

- ◇ Case: Epoxy, molded
- ◇ Lead temperature for soldering purposes: 260°C Max. for 10 seconds
- ◇ Finish: all external surfaces corrosion resistant and terminal leads are readily solderable
- ◇ Shipped 50 units per plastic tube
- ◇ Weight: 1.9 grams (approximately)

### TO-220



Dimensions in inches and (millimeters)

### MAXIMUM RATINGS

Type Number	Symbol	MUR 1620CT	MUR 1640CT	MUR 1660CT	Units
Peak Repetitive Reverse Voltage	V <sub>RRM</sub>				
Working Peak Reverse Voltage	V <sub>RWM</sub>	200	400	600	V
DC Blocking Voltage	V <sub>R</sub>				
Average Rectified Forward Current Per Leg	I <sub>F(AV)</sub>		8.0		Amps
Total Device, (Rated V <sub>R</sub> ), T <sub>c</sub> =150°C			16		
Peak Rectified Forward Current (Rated V <sub>R</sub> , Square Wave, 20 KHz), T <sub>c</sub> =150°C	I <sub>FM</sub>		16		Amps
Nonrepetitive Peak Surge Current (Surge Applied at Rated Load Conditions Halfwave, Single Phase, 60 Hz)	I <sub>FSM</sub>		100		Amps
Operating Junction Temperature and Storage Temperature	T <sub>J</sub> , T <sub>STG</sub>	-65 to + 175			°C

### THERMAL CHARACTERISTICS, PER DIODE LEG

Typical Thermal Resistance, Junction to Case, Mounted on 2" x 3" x 0.25 Al-Plate.	R <sub>θjc</sub>	3.0	2.0	°C/W
-----------------------------------------------------------------------------------	------------------	-----	-----	------

### ELECTRICAL CHARACTERISTICS, PER DIODE LEG

Maximum Instantaneous Forward Voltage (Note 1) (I <sub>F</sub> =8.0 Amps, T <sub>c</sub> =25°C) (I <sub>F</sub> =8.0 Amps, T <sub>c</sub> =150°C)	V <sub>F</sub>	0.975 0.895	1.30 1.300	1.50 1.20	V
Maximum Instantaneous Reverse Current at Rated DC Blocking Voltage @ T <sub>A</sub> =25°C @ T <sub>A</sub> =125°C	I <sub>R</sub>	5.0 250	10 500		uA uA
Maximum Reverse Recovery Time (I <sub>F</sub> =0.5 Amp, I <sub>R</sub> =1.0 Amp, I <sub>RR</sub> =0.25 Amp)	T <sub>rr</sub>	25	50		nS

Note: 1. Pulse Test: Pulse Width = 300 us, Duty Cycle ≤ 2.0%.



## RATINGS AND CHARACTERISTIC CURVES (MUR1620CT THRU MUR1660CT)

FIG.1- CURRENT DERATING, CASE, PER LEG

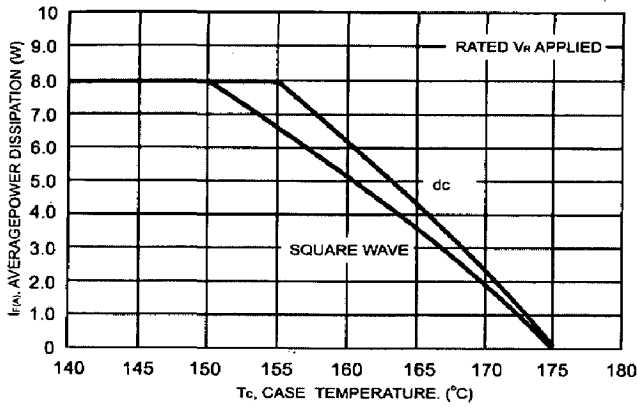
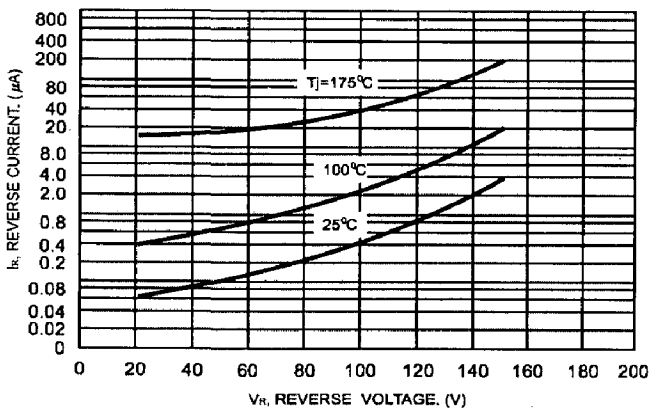


FIG.2- TYPICAL REVERSE CURRENT, PER LEG



\*The curves shown are typical for highest voltage device in the voltage grouping. Typical reverse current for lower voltage selections can be estimated from these same curves if V<sub>R</sub> is sufficiently below rated V<sub>R</sub>.

FIG.4- TYPICAL CAPACITANCE, PER LEG

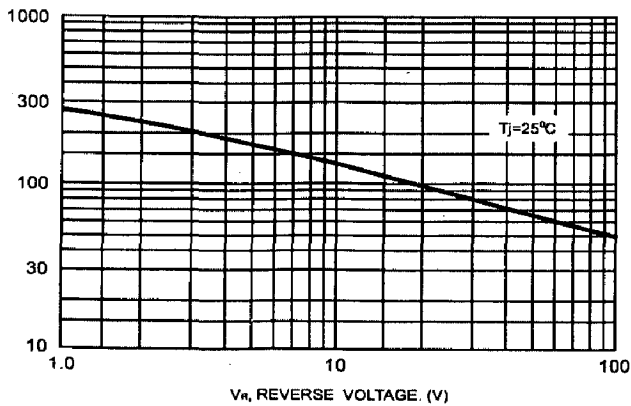


FIG.3- TYPICAL FORWARD VOLTAGE, PER LEG

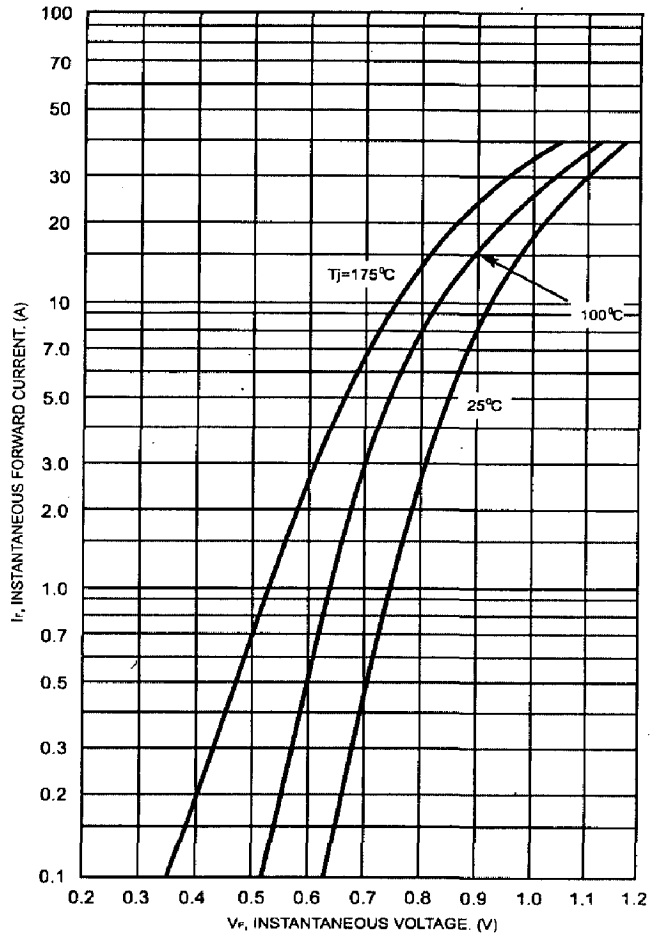
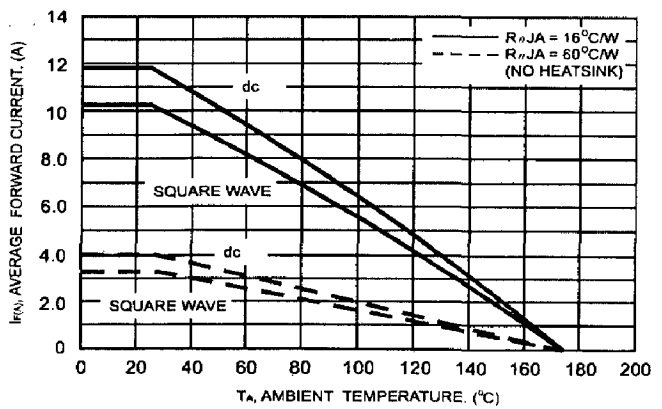
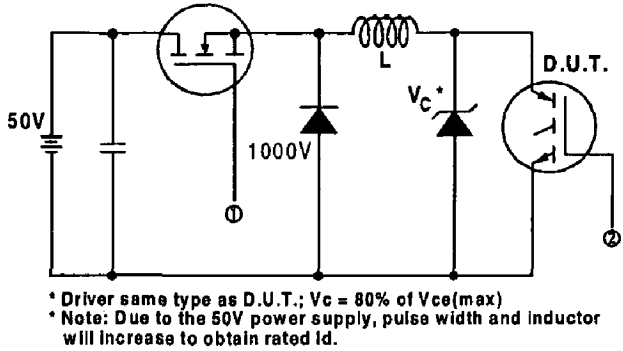
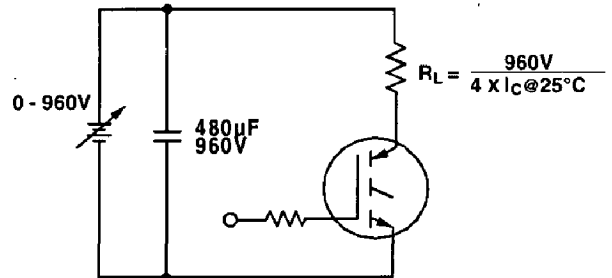


FIG.5- CURRENT DERATING, AMBIENT, PER LEG





**Fig. 13a** - Clamped Inductive Load Test Circuit



**Fig. 13b** - Pulsed Collector Current Test Circuit

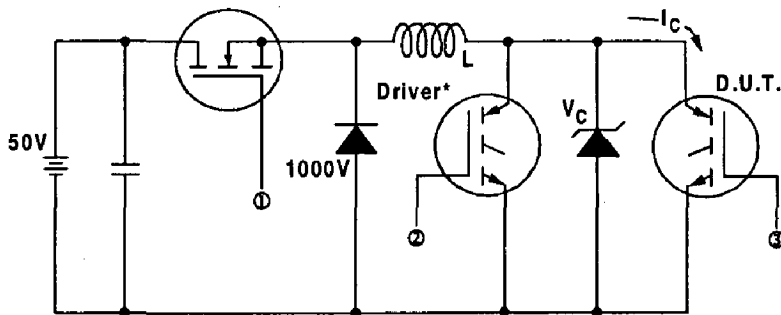


**Fig. 14a** - Switching Loss Test Circuit

\* Driver same type as D.U.T.,  $V_c = 960V$

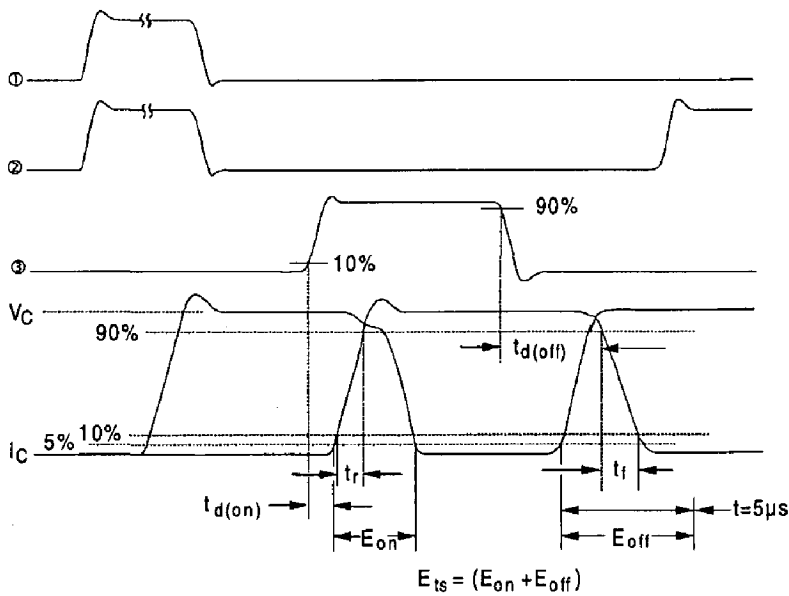
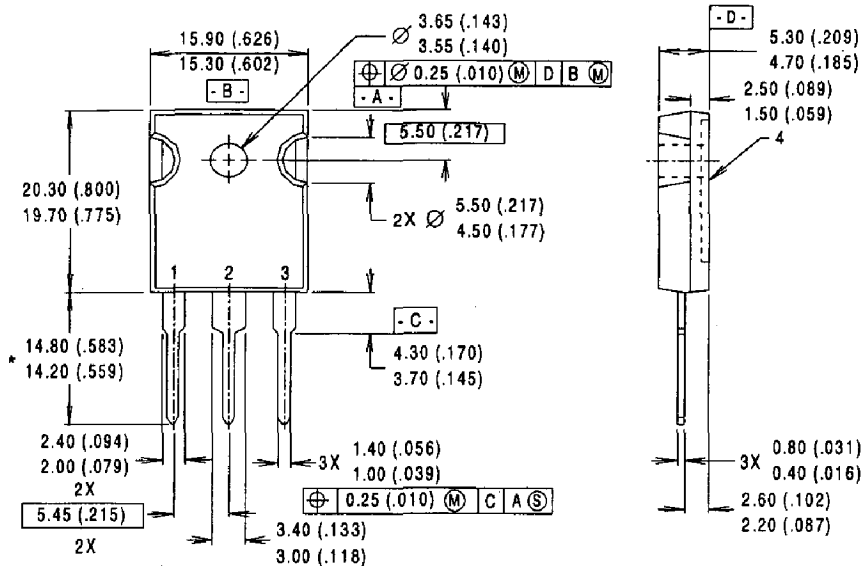


**Fig. 14b** - Switching Loss Waveforms

# IRG4PH40U

International  
**IR** Rectifier

## Case Outline and Dimensions — TO-247AC



### NOTES:

- 1 DIMENSIONS & TOLERANCING PER ANSI Y14.5M, 1982.
- 2 CONTROLLING DIMENSION : INCH.
- 3 DIMENSIONS ARE SHOWN MILLIMETERS (INCHES).
- 4 CONFORMS TO JEDEC OUTLINE TO-247AC.

### LEAD ASSIGNMENTS

- 1 - GATE
- 2 - COLLECTOR
- 3 - EMITTER
- 4 - COLLECTOR

\* LONGER LEADED (20mm) VERSION AVAILABLE (TO-247AD) TO ORDER ADD "E" SUFFIX TO PART NUMBER

**CONFORMS TO JEDEC OUTLINE TO-247AC (TO-3P)**  
Dimensions in Millimeters and (Inches)

International  
**IR** Rectifier

**IR WORLD HEADQUARTERS:** 233 Kansas St., El Segundo, California 90245, USA Tel: (310) 252-7105  
**IR EUROPEAN REGIONAL CENTRE:** 439/445 Godstone Rd, Whyteleafe, Surrey CR3 OBL, UK Tel: ++ 44 (0)20 8645 8000  
**IR CANADA:** 15 Lincoln Court, Brampton, Ontario L6T3Z2, Tel: (905) 453 2200  
**IR GERMANY:** Saalburgstrasse 157, 61350 Bad Homburg Tel: ++ 49 (0) 6172 96590  
**IR ITALY:** Via Liguria 49, 10071 Borgaro, Torino Tel: ++ 39 011 451 0111  
**IR JAPAN:** K&H Bldg., 2F, 30-4 Nishi-Ikebukuro 3-Chome, Toshima-Ku, Tokyo 171 Tel: 81 (0)3 3983 0086  
**IR SOUTHEAST ASIA:** 1 Kim Seng Promenade, Great World City West Tower, 13-11, Singapore 237994 Tel: ++ 65 (0)838 4630  
**IR TAIWAN:** 16 Fl. Suite D. 207, Sec. 2, Tun Haw South Road, Taipei, 10673 Tel: 886-(0)2 2377 9936  
*Data and specifications subject to change without notice. 7/00*